UQAC
UNIVERSITÉ DU QUÉBEC
À CHICOUTIMI

THESIS PRESENTED TO

UNIVERSITY OF QUEBEC AT CHICOUTIMI

IN PARTIAL FULFILLMENT OF THE REQUIREMENT FOR

THE DEGREE OF DOCTOR OF PHILOSOPHY IN ENGINEERING

PRESENTED BY

Khaled Youssef

RECONFIGURABLE CABLE DRIVEN PARALLEL MECHANISM

QUÉBEC, CANADA

Dedicated to the memory of my father

RÉSUMÉ

En raison de la croissance de la demande de produits personnalisés et de la nécessité de réduire les coûts de fabrication tout en augmentant la qualité des produits et en augmentant la personnalisation des produits fabriqués en plus d'assurer la sécurité des travailleurs, les concepteurs se sont appuyés sur des mécanismes robotiques afin d'atteindre ces objectifs. Récemment, les mécanismes parallèles entraînés par câble (MPEC) ont attiré beaucoup d'attention en raison de leurs nombreux avantages par rapport aux mécanismes parallèles conventionnels, tels que l'espace de travail considérablement grand et la capacité dynamique. De plus, ce mécanisme a une masse plus faible par rapport à d'autres mécanismes parallèles en raison de ses câbles de masse négligeable comparativement aux liens rigides. Dans de nombreuses applications, il est nécessaire que l'humain interagisse avec les machines et les robots pour réaliser des tâches avec précision et rapidité. Par conséquent, un nouveau domaine de recherche scientifique a été introduit, à savoir l'interaction humain-robot, où les opérateurs peuvent partager le même espace de travail avec des robots et des machines telles que les mécanismes entraînés par des câbles. L'une des principales exigences en raison de cette interaction que les robots doivent répondre aux actions humaines d'une manière sécuritaire et collaboratif. En conséquence, de nombreux problèmes ont été soulevés tels que la commande et la stabilité dues au contact physique entre l'humain et le robot. Aussi, l'un des enjeux les plus importants est de garantir un espace sans collision (pour éviter les collisions entre des câbles et un opérateur et éviter les collisions entre les câbles entre eux). Le but de ce projet de recherche est de modéliser, concevoir, analyser et mettre en œuvre un mécanisme parallèle reconfigurable à six degrés de liberté entraîné par huit câbles. La principale contribution de ces travaux de recherche est de développer un modèle non linéaire et résolvez le problème de cinématique direct et inverse d'un CDPM entièrement contraint étant donné que les points d'attache sur les rails se déplacent verticalement (les mécanismes entraînés par des câbles conventionnels ont des points d'attache fixes sur les rails) tout en contrôlant les longueurs des câbles. Dans une deuxième étape, l'idée de la reconfiguration est ensuite utilisée pour éviter les interférences entre les câbles et entre les câbles et les membres d'un opérateur en temps réel en déplaçant un point de fixation du câble sur le cadre pour augmenter la distance la plus courte entre eux tout en gardant la trajectoire de l'effecteur terminal inchangée. Troisièmement, la nouvelle approche proposée a été évaluée et testée en créant une trajectoire d'interférence câble-câble et câble-humain simulée, détectant et évitant ainsi les collisions câble-câble et câble-humain en utilisant la reconfiguration en temps réel proposée tout en conservant la trajectoire effectrice finale. Enfin la dernière étape des travaux de recherche consiste à étudiez l'effet du déplacement des points d'attache sur l'espace de travail réalisable du CDPM.

ABSTRACT

Due to the fast growth in industry and in order to reduce manufacturing budget, increase the quality of products and increase the accuracy of manufactured products in addition to assure the safety of workers, people relied on mechanisms for such purposes. Recently, cable driven parallel mechanisms (CDPMs) have attracted much attention due to their many advantages over conventional parallel mechanisms, such as the significantly large workspace and the dynamics capacity. In addition, it has lower mass compared to other parallel mechanisms because of its negligible mass cables compared to the rigid links. In many applications it is required that human interact with machines and robots to achieve tasks precisely and accurately. Therefore, a new domain of scientific research has been introduced, that is human robot interaction, where operators can share the same workspace with robots and machines such as cable driven mechanisms. One of the main requirements due to this interaction that robots should respond to human actions in accurate, harmless way. In addition, the trajectory of the end effector is coming now from the operator and it is very essential that the initial trajectory is kept unchanged to perform tasks such assembly, operating or pick and place while avoiding the cables to interfere with each other or collide with the operator. Accordingly, many issues have been raised such as control, vibrations and stability due the contact between human and robot. Also, one of the most important issues is to guarantee collision free space (to avoid collision between cables and operator and to avoid collisions between cables itself). The aim of this research project is to model, design, analysis and implement reconfigurable six degrees of freedom parallel mechanism driven by eight cables. The main contribution of this work will be as follow. First, develop a nonlinear model and solve the forward and inverse kinematics issue of a fully constrained CDPM given that the attachment points on the rails are moving vertically (conventional cable driven mechanisms have fixed attachment points on the rails) while controlling the cable lengths. Second, the new idea of reconfiguration is then used to avoid interference between cables and between cables and operator limbs in real time by moving one cable's attachment point on the frame to increase the shortest distance between them while keeping the trajectory of the end effector unchanged. Third, the new proposed approach was tested by creating a simulated intended cable-cable and cable-human interference trajectory, hence detecting and avoiding cable-cable and cable-human collision using the proposed real time reconfiguration while maintaining the initial end effector trajectory. Fourth, study the effect of relocating the attachment points on the constant-orientation wrench feasible workspace of the CDPM.

ACKNOWLEDGEMENTS

In the name of Allah, most gracious and most merciful. First, I would like to express my sincere grateful and appreciation to my supervisor, Prof. Martin Otis. Without his guidance, support and patience, this research study would have not been completed until the end. I still remember, and will always do, his first words to me that "whenever I seek his help, it will always be a YES". I have seen these words turned to actions during the last three and half years.

I would like also to thank Prof. Philippe Cardou for his help and availability during the year that I spent at Laval University. I would also like to thank members of robotics laboratory at Laval University especially Simon Foucault.

Lastly, I express my gratitude to my family: my brother Ashraf, my sister Donia and my mother Laila for their support and presence. I would like also to thank my wife Hanan, my little three children Mohamed, Youssef and Mohanad for being the most quiet children I have ever seen (☺). Finally, a special message for my father: "I have become the man that you have always dreamed about…till we meet again"

CONTENTS

LIST OF TABLES

LIST OF FIGURES

CHAPTER 1

1. Introduction

1.1. Motivation

Manipulators may be divided into two main categories according to their linkages arrangement, serial [1] and parallel [2]. Serial manipulators are open chain mechanisms that consist of linkages which are connected in series by joints (Figure 1(a)) where these joints usually allow relative translation (prismatic) or relative rotation (revolute) in planar types of mechanisms. In spatial mechanisms, the actuators consists of universal and spherical joints. The most important advantage of serial manipulators is that it has a larger volume of workspace compared to parallel ones. On the contrary, serial manipulators have many disadvantages such as its inertial limiting acceleration and lower accuracy [3]. The acceleration problem arise due to the structural design of serial manipulators where the very first actuator has to support and actuate the whole mechanism as well as the end effector which usually perform the desired action such as carrying an object from one location to another. Therefore, the higher acceleration of the actuator will produce a bigger momentum due to the motion of each link. The lower accuracy occurs due to the series accumulation errors of the actuators due to its serial connection [3].

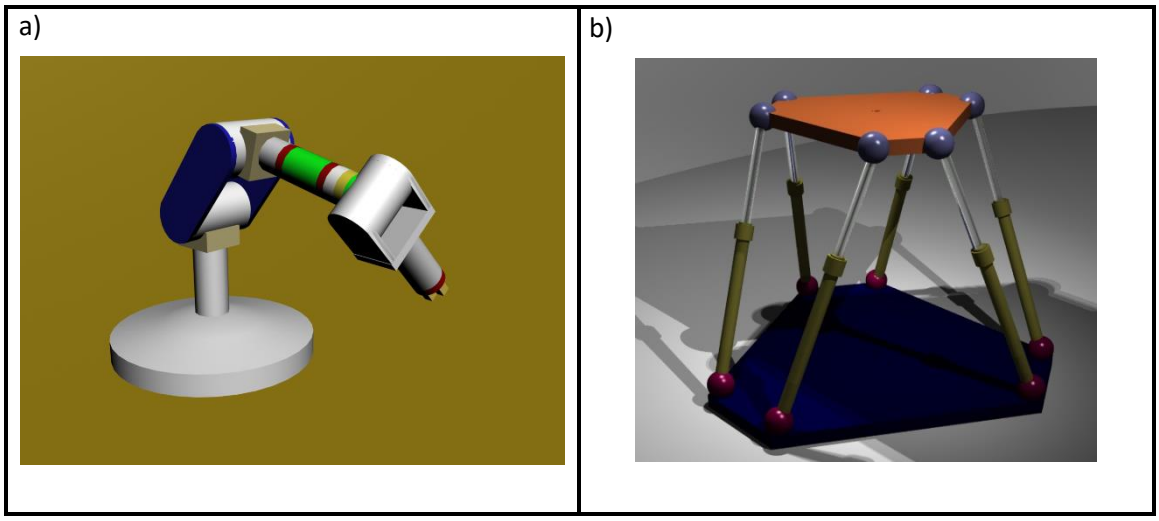

Figure 1 a) Serial manipulator [4][1] ; b) Parallel manipulators [5][2]

On the other hand, parallel manipulators (Figure 1(b)) are closed chain mechanisms where the mobile end effector is joined to the fixed base through several links that work independently from each other and work in a parallel manner. Parallel manipulators have many advantages over serial ones. The closed chain kinematics of parallel manipulators can result in greater structural rigidity, and hence greater accuracy than open chain robots [1]. These advantages are the result of the structural design of the parallel manipulators where the actuators are placed in a parallel arrangement rather than serial and usually attached on the base, therefore all of the actuators can support the end effector and the whole mechanism simultaneously. Moreover, the higher accuracy is coming from independent actuators (i.e. not in an accumulative form) therefore; the errors are not accumulative like serial mechanisms but a mean of each actuator errors.

[1] Public domain
[2] CC BY 2.5

1.2. Cable-driven parallel mechanism

In late 1980s, a new category of parallel robots has been presented which are Cable-driven parallel mechanisms [6] (CDPMs) (Figure 2). CDPM's concept is based on manipulating the end effector's pose (position and orientation) by means of taut cables that can be extended or shortened with rotational motors where these motors are firmly attached to fixed rails. In addition to its advantages as parallel manipulator, it is also characterized by its significant large workspace besides its dynamics capacity over conventional parallel robots [7]. Over and above it has lower mass compared to other parallel robots due to the fact that the actuating links are replaced by massless cables.

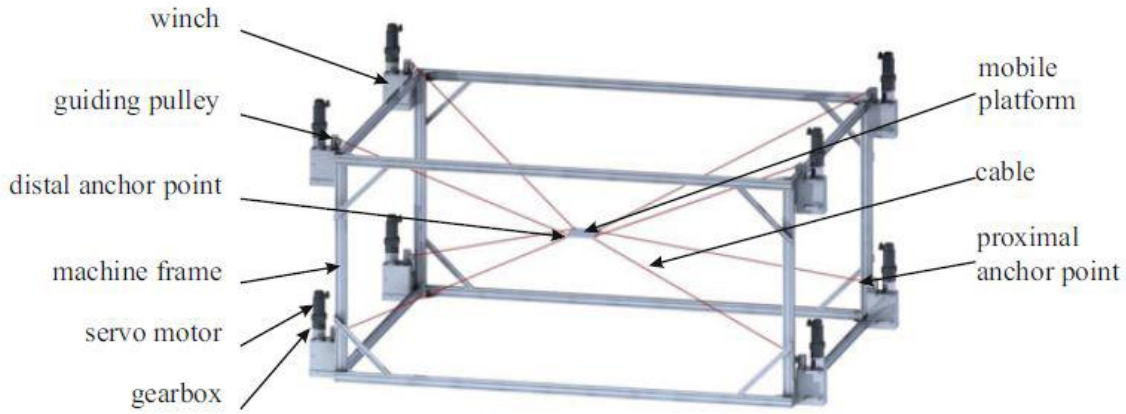

Figure 2 Fully constrained CDPM "Courtesy of Andreas Pott" [8] [3]

Due to its higher capabilities over conventional robots, CDPM have been used in many applications such as industry locations to lift and transport heavy parts from one location to another [9], haptic machines [10] and locomotion interfaces [11], air vehicle simulator [12] and also for construction a high-speed manipulators [13].

[3] Permission has been granted by the author and is attached in Appendix B [1]

CDPM has been classified according to the number of cables and degree of freedom of the end effector [14]. In the first category, the mechanism is fully constrained if the number of cables is greater than the degrees of freedom of the end effector. In the second category, the mechanism is under constrained if the number of cables is equal to or less than the degrees of freedom of the end effector [15].

Since CDPM has been presented, a wide variety of scientific research projects has been conducted to resolve issues and challenges related to such unique mechanism. Researcher in this field addressed many problems such as dynamic trajectory planning [16] kinematics study [17], cables tension distribution [18], workspace analysis [19], vibration analysis [20], control of the cables [11,21] and collisions of the cables with itself [22], with the environment, or with the mobile platform [23].

1.2.1. Inverse and forward kinematics

The inverse kinematics problem of CDPM is defined as determining the cable lengths given the pose (position and orientation) of the end effector. Due to the easiness of this problem in parallel manipulators compared to serial ones, it had been studied and solved in many research studies. Roberts [24] studied kinematics, statics, and fault tolerance [25] of cable suspended robots. The author illustrated some examples to demonstrate his approach for solving full inverse kinematics of CDPM with eight cables. Zi et al. [26] studied the dynamic modeling and active control of a cable-suspended parallel robot based on the inverse kinematics analysis using Lagrange's equations. The authors proved the effectiveness of the proposed method by comparing experimental and simulation results.

In addition, the control system was simple and fast which was applicable for online applications.

In contrary to the invers kinematics, the forward kinematics of CDPM is determining the position and orientation of the movable end effector given the lengths of the actuated cables. Forward kinematics is a very important step in designing a manipulator especially in a case of closed loop position and velocity control of parallel mechanisms. Forward kinematics of CDPM; unlike serial manipulators; has no known closed form solution for the most general CDPM [27]. The fully constrained mechanism is similar in geometry and construction to the Stewart Gough mechanism (SGm) where the difference is SGm consists of a fixed base plate and upper mobile platform where both parts are connected together with 6 extensible solid legs. Due to this similarity, the approaches used to solve the forward kinematics of SGm [28] is applicable to fully constrained CDPM. Husty [29] introduced a method for solving the forward kinematics problem of 6-6 SGm with a minimal set of constrained equations obtained by kinematic mapping to produce a univariate polynomial of 40th degree. In this method, the parallel manipulator kinematics is formulated as polynomial equations system where the number of equations is equal to the number of unknowns. As the author mentioned, solving the most general case (6-6 Stewart platform), the rational representation comprised a univariate equation of degree 40 and 4 real solutions were computed. Obviously, this approach is not suitable for real time applications due to computational burden and multiple solutions. Pott [17] presented an algorithm for solving real time forward kinematics of CDPM using a combination of interval techniques and an iterative solver where the author validated his approach by applying it experimentally on a seven cables parallel robot. Liwen et al. [30] solved the forward kinematics of six cables

parallel robot (fully constrained) by finding the end effector pose using minimum potential energy principle. Ghasemi et. al. [27] solved the forward kinematics using multilayer perceptron (Artificial Neural Network) method. The authors demonstrated higher modeling accuracy compared to other approaches however, they did not include any study about the required convergence time for such lengthy computations since the convergence time is very important for high-speed applications in real-time.

1.2.2. Vibration

Similarly, to all mechanisms, vibrations is a main issue that has been investigated when studying CDPMs. Regardless which applications is performed using CDPM, the end effector should not be exposed to vibrations to insure smooth motion. In addition, vibrations should be reduced or eliminated especially in haptic devices [25,31] where human share the same workspace with robot in order to maintain human's safety. Dagalakis et al. [16] studied the stiffness characterization of a parallel link robot crane with six cables. The authors concluded that stiffness is changing linearly with the change of the suspended weight as well as the lengths of the cables. Xiumin et al. [20] investigated the vibration analysis of fully constrained cable driven parallel manipulator where a mathematical model was developed and solved using MATLAB and MSC ADAMS. The authors concluded that axial and transversal vibrations occurs in the elastic cables due to external disturbances. In addition, they studied the vibrations of the end effector (due to the vibration of cables) in terms of the natural frequencies and the modal kinetic energy and

concluded that transversal vibration of cables caused 1.4% vibration of the end effector while vibration in the axial direction caused 98.6% of the end effector vibration.

1.2.3. Collisions

One of the issues that have been studied when designing a CDPM is collisions of the cables with itself, with the environment, or with the operator sharing the same workspace with manipulator. According to Lahouar [32], collision avoidance has been well studied for serial mechanisms, however, for parallel mechanisms the problem is still not well developed. Lahouar et al. [32] studied collision free path planning for four cables driven parallel robot in order to avoid collisions of the end effector or the cables with an obstacle and to avoid collisions of the cables with itself. However, the authors admitted that the chosen way (in case of presence of an obstacle) with this approach is not always the shortest way. Pinto et al. [33] studied a visual-guided approach for motion control and path planning for four degrees of freedom robot that is manipulated by four cables. This research based on visual interpretation of the robot position, the target and obstacle locations by means of camera that is fixed on the top of the workspace and accordingly the authors designed a control system by means of Kalman filter in order to determine a collision free trajectory.

1.2.4. Workspace analysis

On of the most essential issues in designing CDPM, is workspace analysis. Since cables, can only pull and not push, workspace is defined as all set of end effector poses where all the cables are to remain taut [34]. Many studies were presented to discuss the issue of finding the optimal cable tension distributions in CDPM using different approaches. Pott [35] listed almost all the well known methods to solve for cable tension distributions with a well organised comparison in terms of real time capabilities, workspace coverage, continuity and computational operations. Borgstrom et al. [36] presented a new linear programming formulation to solve for cables tension distribution of fully constrained CDPM by introducing of a slack variables to the equations. The validity of the suggested approach was confirmed by comparing theoretical to experimental results on 6-DOF driven by nine cables and 2-DOF driven by four cables mechanisms. The authors showed that by adding the slack variable to the linear programming formulation, lead to fast generation of a feasible solution. Pham et al. [37] studied the dynamic analysis of fully constrained planar 3-DOF mechanism driven by four cables. Two different simulation were performed where the authors concluded that stable optimal torque solutions were obtained using well-developed linear programming. In addition, there are many other methods to solve for optimal cable tension distributions in CDPM rather than linear programming such as quadratic programming [38], gradient-based optimization method [39], minimizing p-norm [40], closed-form solution [41], however, in this project research, the focus will be on linear programming.

1.3. Problem statement and objectives

Combining human sense and intelligence with machine strength and durability within the same workspace is the main demand behind using human robot interaction (HRI) devices in industry. Such mechanisms may respond to a human action such as force or motion and accordingly fulfil complicated tasks with flexibility and responsiveness that cannot be done with human bare hands such as moving heavy parts from one location to another, assembly complex parts or machining and so on. It has been studied and suggested that physically personified interactions robots are favoured by human operators rather than virtual and remote tele - conference interactions [42]. In addition, this robotic interactivity helps to decrease of physical effort which may reduce the operator's musculoskeletal disorders (MSDs) that may result, particularly those at the end or in career extensions [43]. Inside the closed-loop control of robots, it is possible to use an admittance model or an impedance model. The admittance model accepts a force as input and generates a position (or velocity) which is the set point for a position (or velocity) feedback controller [44]. On the other hand, the impedance model accepts position as input and generates a force to be controlled [44]. When admittance control systems are used to control such robots (with HRI), two main problems have been raised due to this interaction, which are stability and vibration. Stability has been studied in many research studies, however vibration problems are still a challenge especially when robot is actuated by direct force from human arm [45].

Parallel cable driven mechanisms have been used recently in industry for its particular advantages, however, they are still need more investigation regarding operator’s safety

while sharing the same workspace. One of the main issues in designing such mechanisms is to avoid collisions between cables and itself or cables with the environment and platform.

Lahouar [32] identified two methods for designing collision free path-planning for cable-driven parallel robots. First, global methods where it consists of two stages by representing a model of the free space of the robot by means of grid sampling or random sampling and then by means of artificial intelligence approach, one can find a path in the predefined model. It was mentioned that the global methods get high computational burden and hence are not appropriate for real time computation. Second, local methods depends on the idea that the robot has no previous data about its environment and as it moves to reach its destination, the robot notice obstacles by means of sensors and try to avoid it until it reaches its final position. This method is suitable for real time path planning, however it has some drawbacks such as local minima.

It was noticed in the literature review that most approaches in parallel mechanisms, collision avoidance depends mainly on finding a path before the robot start its motion and/or change the robot trajectory while in motion to avoid collisions until it reaches its final position.

Moreover, since it is possible to use an interference point as a virtual reel by crossing cables together as suggested in Wischnitzer et al. [46], it is also possible to maintain the desired trajectory. However, the non-linear behavior of friction at the interference point reduces the accuracy of the rendered force and torque at the end effector. Friction, by its static and dynamic natures (stick and slip: jerky movement), add vibration and position of the interference is still unknown in a stick-slip motion. The challenge is to keep the desired trajectory without reducing the rendered force and torque by a compromise on the size of

the workspace. In order to maintain and continue the desired trajectory, this research project proposes moving the spool (motorized reel) position and hence the interference location. Therefore, our suggested solution considers a linear displacement of the reel position with the compromise of adapting the geometry and the workspace of the CDPM. One of the contribution of the present work is that the initial trajectory is unchanged. In a collaborative physical human-robot interaction, or in a haptic application [47], the trajectory comes from the user input and should not be constrained by cable interference to let the user perform its work or task using the CDPM. Otherwise, the trajectory is changed since the user is constrained by a force to avoid folding cables as suggested be Meziane et al. [47]. Therefore, moving the reel position to avoid cable interference enables transparent manipulation.

This research project proposes a new approach to avoid collisions between cables and between cables and an operator sharing the same workspace in cable driven parallel mechanism. The main objective of this research study is to model, design and analysis a fully constrained reconfigurable six degrees of freedom parallel mechanism driven by eight cables dedicated to human robot interaction applications. This study will be divided into three main objectives: 1) Model a reconfigurable fully constrained CDPM and solve it forward and inverse kinematics given the attachment points on the rails are moving vertically, 2) Using the idea of reconfiguration to detect and avoid cable-cable and cable-human collisions be relocating the attachment points to increase the shortest distance between cables while maintaining the initial trajectory of the end effector unchanged and 3) to study the effect of the on-line reconfiguration on the constant-orientation wrench feasible workspace of the CDPM.

The first part, contributes to the fundamental understanding of systematic modeling and simulation of cable driven mechanism using multibody dynamics method as presented by Haug [48]. The nonlinear over determined mathematical formulations can then be solved using least-squares method such as Levenberg and Marquardt. By solving the nonlinear model, the forward kinematics of the mechanism can be determined given that the attachment points on the rails are moving up and down (in conventional CDPM, attachment points are firmly fixed on specific positions on the rails). The Forward kinematics is a very important step in closed loop position control of parallel mechanisms. The inverse kinematics is also solved given the relocation of the attachment points by obtaining the vector loop-closure equation for all the cables. Linear programming optimization tool in MATLAB was used to solve the vector loop-closure equation for each pose of the end effector. The proposed algorithm can be used also to determine the required positions of the attachment points on the rails given the eight cable lengths.

The second part of this study is focussed on collisions detection and avoidance of cable-cable and cable-human, which is detected by an algorithm to measure the shortest distance between all the cables and between human limbs and cables in real time situations. A cable-cable or cable-human limbs collision can be treated as two-line interference in 3D, where a collision is detected when these two lines get close to each other to a certain threshold value. In this study, the cables will be assumed to be massless and straight lines (without sagging), and collision between cables can be geometrically computed as will be discussed. Once a collision is detected between two cables or between a cable and human limbs, the attachment points of the corresponding cables on the fixed rails will relocate vertically up or down until collision risk is released. The third part is focused on the effect of the online

reconfiguration on the constant-orientation wrench feasible workspace (WFW) of the mechanism. The WFW is mapped by satisfying the cables' tension distribution equations by testing a 3D grid of points lying within the physical limits of the mechanism. The external wrench in this study is set to 25 N acting in the negative Z direction, which represents the weight of the mobile platform. In addition, the allowed upper and lower tensions induced within the eight cables were set to 120 N and 20 N respectively. It is also possible to set specific upper and/or lower values for each cable separately. The feasible workspace was mapped for every change occurring in any of the attachment points on the rails.

1.4. Scope of the thesis

The scope of this thesis is divided into three main topics. First, modeling of fully constrained 6-DOF CDPM driven by eight cables using non-linear multibody dynamics and solving its forward and inverse kinematics given that the attachment points on the rails are moving vertically up and down. Second, the online reconfiguration concept is then used to avoid interference between cables and between cables and operator limbs in real time by moving one cable's attachment point on the frame to increase the shortest distance between them while keeping the trajectory of the end effector unchanged. Third, to study the effect of relocating the attachment points on the workspace of the mechanism. In order to address the objectives of this research project, the discussions and results of this thesis are presented in the following paragraph:

Chapter 2 is dedicated to the background of cable collision detection and avoidance in CDPM, the suggested methods and discussion of the results for each method. A comparison is presented to compare between our suggested approach and recent studies in terms of degrees of freedom, number of cables, workspace analysis and trajectory preservation.

Chapter 3 presents the modeling of a six degrees of freedom fully constrained CDPM driven by eight cables. The modelling describes the kinematic constraints due to the translational joints, the driving constraints and the vector loop-closure equation. In this chapter, the forward kinematics is solved using as Levenberg and Marquard method given that the attachment points on the rails are moving vertically unlike conventional CDPM. In addition, the inverse kinematics is presented by solving the vector loop-closure equation using linear programming. In addition, the cables tension distribution equation is presented

as well as the suggested method to solve it in order to assure a positive tension in each cable.

Chapter 4 presents in details the formulation to measure the shortest distance between two cables in real time applications. One of the main contributions of this thesis will be discussed in chapter 4, which is cable-cable collision detection and avoidance. An algorithm of the suggested approach is presented and the results of different trajectories simulation will be discussed to proof the validation of the reconfiguration theory.

Chapter 5 discusses the use of the reconfigurable idea to detect and avoid interference between cables and a virtual human limb in real-time application, where the virtual human represents an operator sharing the same workspace with the moving parts of the mechanism. In this chapter, the representation of the human skeleton is discussed and three different trajectories is simulated where the virtual human is inserted within a colliding distance with cables. The generated algorithm is presented and explained and the results from the three simulations are presented and enlightened in details.

Chapter 6 is devoted to present different types of workspaces for general cable driven mechanisms and the different methods used for mapping the wrench closure and feasible workspace. In addition, the formulation and method of computation of the workspace of the suggested reconfigurable CDPM is presented and the results of real-time change in workspace due to the reconfiguration is discussed.

Finally, chapter 7 is dedicated for concluding remarks on this research project and emphasize on the validity of the suggested approach. Recommendations and suggestions are presented for future work.

CHAPTER 2

2. Literature review

2.1. Introduction

In this chapter, a general review about cable-driven parallel mechanisms (CDPMs) is presented such as related terminologies and basic concepts that are used specifically in the study of CDPM kinematics and dynamics. In addition, a literature review of recent and up to date work relevant to cables interference detection and avoidance in CDPM is presented as well as suggested methods to solve for cables tension distribution equation.

Unlike, rigid bodies' mechanism, CDPM has a unique governing kinematics and dynamics equations such as the relation between the DOF and the required number of cables to control the mobile platform and how to compute the workspace, which depends mainly on the cables tension distribution equation. It was presented and suggested in previous studies that cables in CDPM should be attached to the end effector in a crossed configuration manner for a better controllability. Therefore, new challenges were arise to detect and avoid cables collision with itself or with the environment.

Section 2.2 is dedicated to present general formulation and terminologies to describe CDPM kinematics and dynamics equations and section 2.3 will focus on presenting previous research studies about cables interference detection and avoidance.

2.2. Cable driven parallel mechanisms

In spite of their several advantages, there are a number of challenges related to CDPM design and analysis. The reasons behind replacing the traditional rigid links in CDPM by flexible wires were to reduce the number of stiff moving parts and accordingly increase the mechanism's payload ratio, acceleration, velocity as well as easing its assembly process comparing to conventional mechanisms such as serial industrial robot and parallel robot for instance Gough-Stewart [49]. However, since cables can only pull and not push, a constraint has been imposed to be fulfilled where cables must always be maintained in tension, otherwise, too much sagging effects will cause uncontrollable consequence on the end effector and cause an undesired tension level in the cables system [50]. Due to these uniqueness properties, the modeling and analysis equations that govern the kinematics and dynamics of conventional rigid link mechanisms cannot be applied to CDPM directly. In addition, due to the cables tension constraints and in order to fully control the end effector, the number of cables (n) should be greater than the number of degrees of freedom (DOF) of the end effector such that $n \geq DOF + 1$. In this case the mechanism is called fully constrained [51]. On the other hand, if $n \leq DOF$, then the mechanism is called under constrained. In this regard, degree of redundancy in CDPM is defined as the excess number of cables than the minimum required to control the end effector [52]. In mathematical expression, degree of redundancy is equal ($n - DOF$), however CDPM is not kinematically and statically redundant [52]. Figure 3 shows a schematic of typical CDPM with different degrees of redundancy in which the mechanism shown in (a) is a suspended planar (SCDPM) under constrained three DOF driven by two cables (two fully constraints DOF and the other one depends on the gravity and is not fully controllable). Figure 3 (b) shows

a spatial fully constrained six DOF mechanism driven by eight cables where the degree of redundancy is one since the mechanism has one more cable in excess.

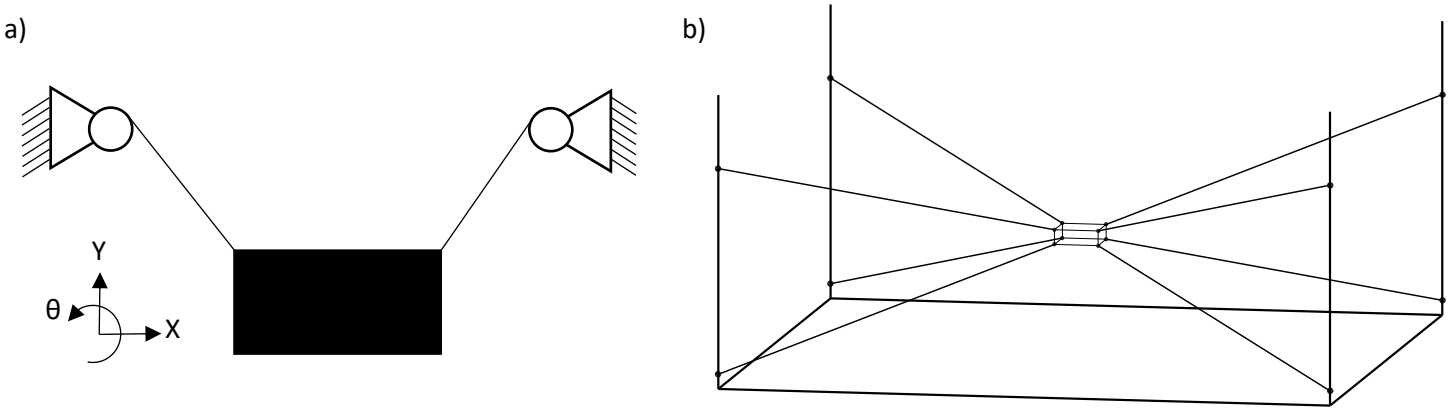

Figure 3 CDPM schematic a) planar under constrained CDPM, b) spatial fully constrained CDPM

Usually, the cables are rolled along winches (motorized reel or spool) where these winches are attached to a fixed frame on the ground (Figure 4); therefore, the only moving parts are the end effector and the cables, which are relatively massless, compared to the end effector.

Figure 4 Six DOF-eight cables CDPM
Photo © Laboratoire de robotique, Université Laval[4]

[4] Permission has been granted by the author and is attached in Appendix B [2]

Since the actuators are fixed on the ground and the payload weight is divided between them, it makes the cable driven mechanisms needs smaller motors in power compared to serial mechanism where the motor at the base support the overall limbs. Consequently, they are applicable to be used in applications that requires holding very heavy masses such as pick and place in Figure 5. Unlike conventional rigid mechanisms, CDPMs can be constructed in extremely large scale [53,54] such as the five-hundred-meter aperture spherical radio telescope (labelled as FAST) [55,56] that is designed in China (Figure 6). Moreover, it can be used in application that requires vey high speed and acceleration such as the skycam camera that is used for live broadcast in sports and entertainment where its velocity can reach up to 45 km/h [57] as shown in Figure 7.

Figure 5 Cogiro project [58][5]

[5] Permission has been granted by the author and is attached in Appendix B [3]

Figure 6 Five-hundred-meter aperture spherical radio telescope (FAST) project-produced by the FAST team [59][6]

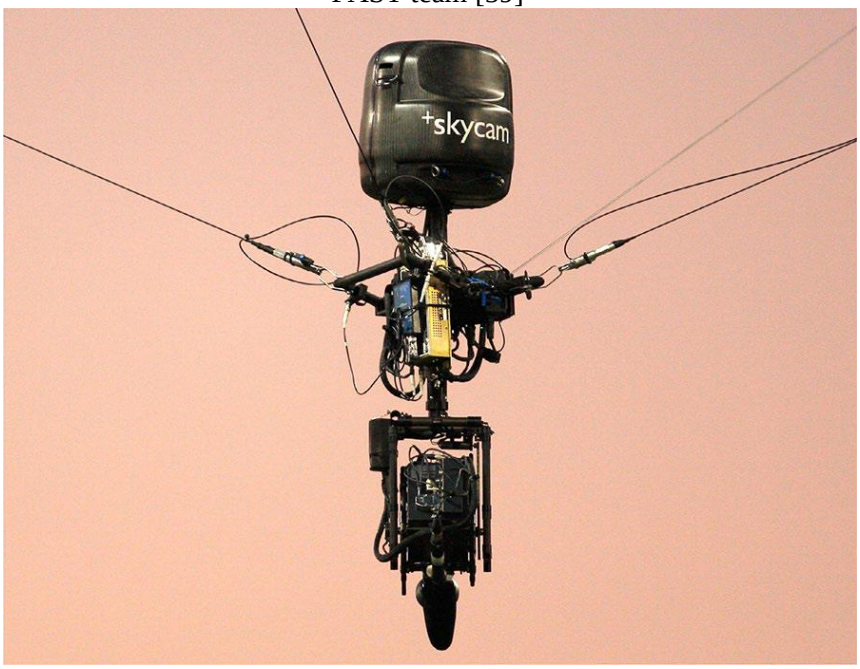

Figure 7 Skycam commercial product [60][7]

[6] Permission has been granted by the author and is attached in Appendix B [4]

[7] CC BY-SA 3.0

Dynamics analysis in mechanisms is vital to understand the governing relationship between the mechanism joint forces and/or torques and the output accelerations. Dynamics in rigid bodies' mechanisms is mainly to build the relation between forces/torques acting on a rigid body and its kinematics (displacement, velocity and acceleration). The forward dynamics is defined as given forces and/or torques and compute output accelerations [61]. On the other hand, inverse dynamics is defined as given accelerations and compute the required output forces and/or torques [62]. Commonly, in order to obtain any mechanism's dynamic equations, there are two approaches that can be used. First, the most famous Newton-Euler equations and second, the Lagrange's equation. The Newton-Euler approach is originally derived from Newton's law of motion to describe a dynamic system. The Lagrange approach depends on the principals of work and energy to describe a dynamic system, which makes it much easier and systematic than the Newton-Euler formulation since work and energy are scalar quantities. Dynamic modeling of CDPM is mainly focused on the cables while the end effector is usually modelled as rigid body. To simplify the modeling process, previous research studies consider the cables as massless non-elastic line segments. Other research studies model the cables with mass quantity, damping and longitudinal flexibility, which create more complicated dynamic model. Bedoustani et al. [63] studied the effect of adding elastic and damping effect of the cables by deriving the kinematic and dynamic equations of a three DOF cable driven mechanism with one degree of redundancy. Newton-Euler formulation approach was used to derive the non-linear dynamic model of the mechanism. The authors compared the results of the mechanism dynamics with and without the cable elasticity and showed the effect of the non-linear model on the rise time of the system. The elasticity produced larger delay time in the

dynamic response, which makes the closed loop control of the manipulator much complicated. Khosravi et al. [64] presented a dynamic and control analysis with elastic cables model for fully constrained CDPM. Lagrange's formulation method was used to model the dynamic system of the mechanism while the cables were modelled as axial springs. The authors concluded that the proposed control algorithm using simple PD is capable of stabilizing the system with elastic model of the cables where the closed-loop system was analyzed using Laypunov second method [65].

CDPMs can mainly be controlled by two methods, which are through the mobile platform position or force control [66]. In the first method, the cables lengths are required for a given pose (position and orientation) of the end effector where inverse kinematics can be used to obtain the cable lengths. This method has a drawback since the cables may exert tension forces which are less than the minimum or larger than the maximum allowable values which will lead to either the cables will be slack or damaged. On the other hand, the force control method requires that the tension forces of the cables to be computed for a certain trajectory of the end effector which leads to the definition of the inverse dynamics of cable driven mechanisms. CDPM inverse dynamics is defined as an input: given the pose of the end effector, and an output: determine the positive cables tension [66]. The inverse dynamics in CDPM is extremely important since it is usually required in real-time force control and to compute the workspace of the mechanism, which depends on solving the cables tension distribution equation:

$$\widetilde{\boldsymbol{w}}\overrightarrow{\boldsymbol{t}_i} + \overrightarrow{\boldsymbol{w}_J} = \vec{\mathbf{0}}_6 \qquad 2\text{-}1$$

where $\widetilde{\boldsymbol{w}}$ is the structure matrix, $\overrightarrow{\boldsymbol{t}_i}$ is the cables tension vector and $\overrightarrow{\boldsymbol{w}_J}$ is the external wrench vector. For completeness, a brief review of the mechanism model is described here where the geometry of the mechanism is described by attachment points on the rails (A_i) and the anchor points on the end effector (B_i). By applying a vector loop as shown in Figure 8, the cable length (ρ_i) is defined as:

$$\vec{\boldsymbol{r}}_{ef} + \boldsymbol{R}\vec{\boldsymbol{r}}'_i - \vec{\boldsymbol{r}}_{A_i} \tag{2-2}$$

where $\vec{\boldsymbol{r}}_{ef}$ is the end effector position vector, $\boldsymbol{R}$ is the rotation matrix, $\vec{\boldsymbol{r}}'_i$ is the position vector of the anchor points on the end effector represented in the local coordinate frame and $\vec{\boldsymbol{r}}_{A_i}$ is the position vector of the attachment points on the rails. The structure matrix $\widetilde{\boldsymbol{w}}$ resulting from the force and torque equilibrium at the end effector for the cable tension distribution $\overrightarrow{\boldsymbol{t}_i}$ is given by:

$$\underbrace{\begin{bmatrix} \vec{\boldsymbol{u}}_i \\ \vec{\boldsymbol{r}}_i \vec{\boldsymbol{u}}_i \end{bmatrix}}_{\widetilde{\boldsymbol{w}}} [t_i] + \left[\overrightarrow{\boldsymbol{w}_J}\right] = \vec{\boldsymbol{0}}_6 \tag{2-3}$$

where,

$$\vec{\boldsymbol{u}}_i = \frac{\vec{\boldsymbol{r}}_{ef} + \boldsymbol{R}\vec{\boldsymbol{r}}'_i - \vec{\boldsymbol{r}}_{A_i}}{\left\|\vec{\boldsymbol{r}}_{ef} + \boldsymbol{R}\vec{\boldsymbol{r}}'_i - \vec{\boldsymbol{r}}_{A_i}\right\|} \tag{2-4}$$

and,

$$\vec{\boldsymbol{r}}_i = \boldsymbol{R}\vec{\boldsymbol{r}}'_i \tag{2-5}$$

For fully constrained CDPM, the actuation redundancy leads to infinite different positive cable force solutions which in general a desirable feature in robotics however it leads to a lengthy computational time for online applications [67].

Cables tension distribution equations may be computed using two optimization methods which are linear programming [68] and quadratic programming [69]. Linear programming has the advantage of low computational time which is required for real time applications, however in some reported research studies it showed discontinuities in the solution of cables tension distribution equation [70] . The issue of discontinuities can be avoided using quadratic programming, however it has been reported that in some cases it may suffer form worst case runtime [71,72] which makes it inappropriate for applications that requires on-line computation. However, using real-time operating system such as RT-Linux or QNX, quadratic programming solving tension distribution takes less than 1% of the sampling period at 500Hz on a 2GHz Intel processor.

The cables tension distribution problem is defined as finding a positive right null vector of the structure matrix ($\widetilde{\boldsymbol{W}}$) while satisfying equation (2-1) in order to completely restrain the CDPM [36]. In addition, the cables tension values must be above lower tension limit (t_{min}), to maintain the cables in continuous tension state. Also, the cables tension values must be below upper tension limit (t_{max}), to adhere the finite torque capability of the mechanism's actuators. The main goal of the optimisation methods is to minimise a physically meaningful objective function (f) while satisfying the inequality constraints [66].

The general formulation of the optimisation problem to find a feasible solution to the cables tension distribution equation may be expressed as follow [36]:

$$\begin{aligned} &\text{Minimize : } f \\ &\text{Subject to: } \quad \widetilde{\boldsymbol{w}}\overrightarrow{\boldsymbol{t}_i} + \overrightarrow{\boldsymbol{w}_J} = \vec{\mathbf{0}}_6 \\ &\text{and} \qquad\quad t_{min} < \vec{\boldsymbol{t}}_i < t_{max} \end{aligned} \tag{2-6}$$

Expressing the function *f* in equation (2-6) is the key definition to consider the problem is either linear programming optimization or quadratic programming optimization. If the function *f* is formulated as the sum of tensions along the cables, the problem is defined as linear programming (LP) and hence minimizing *f* at every pose of the end effector is to find the smallest possible summation of $\vec{\boldsymbol{t}}_i$ without violating both constraints in equation (2-6) [73]. In the other form, the function *f* is formulated as the 2-norm of the vector $\vec{\boldsymbol{t}}_i$ which is represented as:

$$f = \left\| \vec{\mathbf{0}} - \vec{\boldsymbol{t}}_i \right\| \tag{2-7}$$

which is the Euclidean distance between the origin $\vec{\boldsymbol{t}}_i = 0$ and point $\vec{\boldsymbol{t}}_i$ [74]. In this case, the problem is defined as quadratic programming (QP) and hence minimizing *f* at every pose of the end effector is to find the smallest possible summation of f without violating both constraints in equation (2-6).

2.3. Cables interference detection and avoidance

Since the mobile platform is being manipulated by cables such that all the cables will always remain inside the geometry of the mechanism (installation space) and may be within the workspace [75], a collision investigation should be performed when designing such mechanism to ensure a collision-free workspace [76]. A collision may occur between cables, between cables and the environment, between the platform and the environment as well as between cables and the platform, as mentioned by Nguyen [23]. Bordalba et al. [77] proposes the use of a randomized kinodynamic planning technique to synthesize dynamic motions for cable-suspended parallel robots. The authors presented a method to find a collision-free trajectory between two points with known positions and velocities while maintaining the cables in tension continually and at the same time adhering to the actuators and joints force capabilities. Bordalba et al. validated the proposed approach by experimental data on a specific cable driven mechanism design; they concluded that this approach is valid for other architecture designs. Makino et al. [78] introduced a new design of six degrees of freedom with eight cables driven mechanism by embedding a rotational mechanism inside the moving part (end effector) and the cables are attached to it. A control algorithm is created to avoid collisions of cables when detected by changing the configurations of the cables by rotating the end effector around the vertical axis while rotating the pulley with the same amount of angle but in the opposite direction. However, the authors did not present any study on the computational time needed for the proposed approach and if it is valid for real-time robotic applications. Otis et al. [79] presented a determination and management method for cable interference between two 6 DOF foot

platforms in a cable-driven locomotion interface. The presented method computes the cable interference geometrically for any constrained trajectory and, an algorithm determines which cable can be released from an active actuation state while maintaining all the other cables in tension. The authors also solved the tension discontinuity issue that arises from releasing a cable from an active actuation state by presenting a collision prediction scheme that is applied to redundant actuators. The limitation of the workspace is the main issue arising from folding two cables on each other. Perreault et al. [80] proposed a method to optimize the workspace space given a prescribed workspace by locating the reel position while considering interference regions between two cables and/or between a cable and the end effector edges. However, the authors suggested that a free interference trajectory can be planned using the predetermined regions, which makes this approach valid for only limited trajectories. Wischnitzer et al. [46] suggested a method to permit collisions between cables for the sake of expanding the workspace significantly compared with collision free workspace mechanisms. The presented method was based on formulating the inverse kinematics of a six degrees of freedom redundant robot with two colliding cables and solving numerically while maintaining a feasible and positive wrench closure. Experimental and theoretical results were presented, and they demonstrated workspace expansion compared with a collision free case. However, the authors did not present any study on the vibration issue resulting from colliding cables, especially in high-speed applications. Ismail et al. [81] presented a dynamic path planning [82] algorithm for an under constrained planar mechanism to find the shortest path between two points while maintaining the wrench feasible workspace and at the same time avoiding obstacles. The algorithm was originally created for a serial manipulator; however, it was adapted for the

proposed hybrid planar design. The authors did not discuss if the proposed approach is valid for spatial mechanisms. Pinto et al. [33] presented a four degrees of freedom wire driven mechanism called SPIDERobot, which was designed for industrial pick and place applications. A new approach is introduced to optimize the trajectory of the robot by means of visual interpretation of the workspace. The suggested method is based on visually locating the position of the robot, its destination and the obstacles. This method determines the trajectory while avoiding the collision of the cables with the environment. The authors concluded that the approach is valid and effective for under constrained cable mechanisms by presenting simulated models; however, they did not include any examples for fully constrained parallel mechanisms.

Zhou et al. [83] added a new classification for cable driven manipulators: The first type is the conventional cable driven mechanism where the base is fixed and the mobile platform is controlled by varying the cable lengths, and the second type has the cable lengths fixed and the base moved to manipulate the mobile platform. In his study [83], Zhou combined the two types of cable driven mechanisms. However, he only discussed a three degrees of freedom mechanism derived by four cables. The authors concluded that for a given trajectory, adding a mobile base extends the wrench closure workspace as well as optimizes the tension factor for a better wrench feasible workspace. In 2017, Anson et al. [84] conducted another study on adding a mobile base for cable driven mechanism. However, it was also a planar three degrees of freedom mechanism driven by four cables. The authors investigated the quality of the wrench closure workspace by a tension factor index approach by comparing a traditional cable driven mechanism with a mobile base one. Two configurations were used in the study. The first type has a rectangular base and each

attachment point is constrained to move along its own linear rails. In the second type, the attachment points were constrained to move along a circular base. The authors concluded that the circular base had the better wrench closure workspace where the mobile platform had the ability to reach any position and orientation within the installation workspace. Tourajizadeh et al. [85] presented an optimal regulation for an under constrained six degrees of freedom mechanism driven by six cables to maximize the dynamic load capacity of the mobile platform for a predefined path while avoiding cables interference. However, in case of a near collision between two cables, the orientation of the mobile platform is changed to avoid interference, which makes this approach not valid for some applications that require vertical movements, such as pick-and-place. Arsenault [86] studied the interference-free wrench feasible workspace of a 3 DOF translational tensegrity mechanism where this kind of parallel mechanisms consists of both cables and rigid links. The authors proposed a new design by replacing the rigid links by equivalent compression spring legs (ECSLs) to avoid interference between the mechanisms links, however, the author concluded that there is still a possibility that cables will collide with suggested ECSLs unlike the suggested approach in this research study to detect and eliminate cables interference.

Fabritius et al. [87] presented a cable-platform collision-free total orientation workspace of cable-driven parallel mechanism with different platform orientation sets. The suggested method computes the free collision workspace based on geometry data of the platform without commanding any assumptions or restrictions and can be applied for different sets of end effector orientations. However, it was reported that common free collision workspace computation methods generates restrictions on the moving platform trajectories

[46] and even worse it restricts the size of the workspace [22]. In the suggested approach in this thesis, a linear displacement of the attachment points on the rails is considered to avoid cables collision and maintain the end effector trajectory unchanged. Martin et al. [88] presented a geometric determination method to detect interference regions between cables and cylinder within the workspace of cable driven parallel robot. The suggested method consider a fixed cylinder objects inside the workspace but did not consider interference detection and avoidance between cables or between cables and movable objects inside the workspace. Bingyao et al. [89] studied the collision free wrench closure workspace of planar 3 DOF mechanism driven by three cables. The suggested approach is based on mapping the collision free area (CFA) where CFA is defined as the area where the end effector is not colliding with obstacles. The study did not present what limitation this method will affect the workspace and if it is applicable for other spatial configuration cable driven mechanisms. Lesellier et al. [90] addressed the problem of detecting and avoiding collision between cables and movable parts located on the top of the mobile platform of a cable driven parallel robot. The proposed method was based on determining the set of all positions of the cables within a prescribed workspace, which is the cable span, and hence describe the free collision workspace as all the positions of the movable device where there is no intersection with the cable span. Blanchet et al. [91] studied the cable-cable and cable-objects interference detection for a six DOF freedom mechanism driven by seven cables using two algorithm based on interval analysis. The authors suggested a non-crossed cable arrangement model. It has been reported in many previous and recent research studies [15,92] that crossed cable configuration has a larger workspace as well as its higher capability to exert much higher torques compared to non-crossed cables configuration.

Barbazza et al. [93] introduced the concept of on-line reconfiguration of cables anchor points on the end effector for a three DOF CDPM driven by four cables for pick and place applications. The authors presented an optimized trajectory planning with real-time reconfiguration for the aim of reducing movement time between initial location and final destination. However, the study did not present any analysis on the effect of online reconfiguration on the workspace and what alternative scenarios can be applied if the anchor points on the end effector reaches its mechanical limit. Fabritius et al. [94] computed the interference free workspace volume for a fully constrained CDPM for printing large 3D objects in a sequence of horizontal layers. The interference free workspace was defined as the set of poses of the mobile platform can reach without collision between cables and the printing part. Although the authors concluded that the suggested approach is not limited to 3D-priniting applications only, however, they deduced that the proposed method is suitable for layer-based additive manufacturing which may restrict this method for special applications only. Pott [95] introduced a method to determine the cable span of CDPM which is defined as all the space occupied by the cables when the end effector is moving within its workspace. The suggested method is based on triangulation of the shell surface of the volume occupied by cables. This approach can be used to study collision of cables with other objects as been concluded by the author. Rasheed et al. [96] presented a path planning algorithm for a three DOF point mass end effector driven by four cables. The suggested design introduced the concept of mobile CDPM where each of the four rails are carried by independent mobile base and each cable is attached to one rail. The proposed path-planning algorithm consist of two stages. First, to find a feasible and collision-free path for the mobile base that caries the four rails.

Second, the algorithm generates a trajectory between initial and final position for the end effector. The authors concluded that the path between initial and final positions is not necessary the shortest path. Obviously, the mobile base approach is not valid in applications where there is limited place for the mobile base to relocate. Bak et al. [97] presented an algorithm using rapidly exploring random trees (RRT) to find a collision-free path for a cable driven robot in messy environments. The RRT method depends mainly on finding a path between two positions by randomly generating and connecting a node to a closest available node while checking that the nodes lies outside of an obstacle. While the authors claims that the suggested method is fast in computation, however it did not include any results about workspace limitation due to cable-cable and cable-obstacles avoidance.

Table 1 is a summary about the pros and cons of previous research in the field of cables collision interference and avoidance.

Table 1 Comparison between current and previous studies in terms of degrees of freedom, number of cables, workspace and trajectory

	Current study				
	6	8	Yes	Yes	-Online computation. -Detect near cable collision and provide solution to avoid it. -Initial trajectory is unchanged. -Applicable for any architecture. -Present solution when reaching mechanical limit of the attachment points. -Workspace analysis due to reconfiguration. -Smooth transition in all cable tension values since no cable is released. -Spatial mechanism. -Cables interference detection and avoidance is presented and simulated.
Reference	Degrees of freedom	Number of cables	Workspace analysis	Trajectory preserved	Comments
Bordalba et al. (2018)	3	3	No	No	-Validated for specific architectures only.
Makino et al. (2016)	6	8	No	No	-End effector orientation is changed to avoid cable collision. -Did not present solutions if mechanical limit of rotating pulley is reached. -No workspace discussion due to reconfiguration.

Reference	Degrees of freedom	Number of cables	Workspace analysis	Trajectory preserved	Comments
Otis et al. (2009)	6	8	No	Yes	-Limited workspace due to release of one cable. -Approach may lead to generation of mechanical vibration and instability due to sudden increase in other cables' tension.
Perreault et al. (2010)	6	8	No	No	-Offline computation. -Computes all planes at which interference between two cables can occur but do not give solution to avoid cable collision. -Valid for predetermined trajectories only
Wischnitzer et al. (2008)	6	7	yes	no	-No vibration analysis due to collision permit. -Discuss the permit of two cables only without giving consequences in case of more than two-cable collision. -Neglect the friction at the point of contact between two cables.
Ismail et al. (2016)	2	2	no	no	-Planar mechanism. -Hybrid cable–serial robot. -Predetermined specific trajectories that avoid obstacles.
Pinto et al. (2017)	3	4	no	no	-Predetermined free collision trajectory depending on visual images of the workspace. -No wrench or feasible workspace analysis.

Reference	Degrees of freedom	Number of cables	Workspace analysis	Trajectory preserved	Comments
Anson et al. (2017)	3	4	yes	no	-Planar mechanism (2D) -Wrench closure workspace analysis due to reconfiguration -No study was conducted on cable interference avoidance.
Tourajizadeh et al. (2016)	6	6	No	No	-Orientation of the mobile platform is deviated to avoid cable interference.

To the best of our knowledge, no design strategy has been suggested in the literature for real-time reconfiguration of spatial six DOF cable driven parallel mechanism driven by eight cables. In most of the previous research studies, typically, the end effector's trajectory is adapted in order to avoid interference between two cables or between cables and the environment. This environment may be stationary or dynamic such as an operator sharing the same workspace with the moving parts of the mechanism. In some other suggested methods, the workspace may be limited in order to allow the end effector to perform a prescribed trajectory without collision between cables. In this thesis, a new approach is proposed to detect and avoid interference between cables and between cables and human while maintaining the trajectory of the end effector unchanged and without limiting the workspace. In addition, the cables tension are kept continuous and within a set of lower and upper limits.

2.4. Conclusion

This chapter elaborate on the general background of CDPM especially in the kinematics and dynamics analysis and related terminologies and basic concepts. A detailed classification of the CDPM according to the DOF and number of cables has been explained and differences between CDPM and conventional rigid bodies mechanisms is presented in terms of kinematics and dynamics equations. Different real applications have been shown to demonstrate the importance of CDPM in different aspects such as industry, entrainment and research. Moreover, a comparison between two methods to solve for cables tension distribution equation has been discussed which are linear programming and quadratic programming optimization.

In addition, an up to date review of the literature about cables interference detection and avoidance as well as interference between cables and other movable objects within the workspace of the mechanism has been presented. A comparison between the suggested approach in this research study and previous recent studies is conducted in terms of DOF, number of cables, workspace analysis and preservation of the initial trajectory.

CHAPTER 3

3. Theory on reconfigurable CDPM and cable tension distribution

3.1. Introduction

This chapter discusses the general symbolic representation of the reconfigurable six DOF CDPM using multibody dynamics approach as presented in [48]. One of the main contributions of this research project is outlined in details in this chapter which is, to solve the forward and inverse kinematics given that the attachment points on the fixed rails are moving vertically unlike conventional CDPM where the attachment points are firmly fixed at specific locations.

In this chapter, the kinematic and driving constraints are derived and the total kinematic constraint equations (KC) are established where the overdetermined system of equations are solved using least square method. In addition, the cables tension distribution equation is derived for the fully constrained CDPM in order to guarantee a positive tension values for all the cables without discontinuity.

Section 3.2 is dedicated to model, symbolically, the reconfigurable CDPM and describing the driving constraints equations and hence solve for the forward and inverse kinematics. Section 3.3 presents the cable tension distribution equation in details and the suggested method to solve it. In addition, the results for three different trajectories are plotted and discussed.

3.2. Suggested simulation model

This section discusses the modeling analysis of CDPM by symbolically establishing the coordinate system and the kinematic constraints due to the translational joints as well as the driving constraints. The suggested model is six degrees of freedom mechanism driven by eight cables. The model is designed such that the upper attachment point on the rail is attached to the lower point on the mobile platform (crossed cable design) as will be discussed later. This crossed cables configuration allows increase of the mechanism stiffness [98], increase the workspace of the mechanism [99] and maximize force or torque that cables can exert on the end effector, along a certain directions [100]; hence, it is a trade-off between better features and interference between cables. Our proposed approach is then used to detect and avoid cables collision while keeping the end effector trajectory unchanged and allowing a better performance due to the crossed cables configuration.

3.2.1. Coordinate system and kinematics constraints

In our study, a fixed global frame (X-Y-Z) is set at the bottom left corner with the Z axis pointing vertically upward and the X-Y axes are set according to the right-hand rule as shown in Figure *8*. The mechanism consists of eight attachment points (Ai) that can move vertically up and down on four fixed rails and at the same time control the lengths of eight cables (in real implementation, the motors can be fixed on the ground and only the attachment points can be relocated by means of a pulley). The eight cables are attached (B_i) to the mobile end effector (in the shape of a rectangular prism) to manipulate its pose

(position and orientation) by extending and shortening the cables (ρ_i). The generalized coordinates ($\vec{\boldsymbol{q}}$) of the mechanism consist of the following:

$$\vec{\boldsymbol{q}} = \lceil (\vec{\boldsymbol{q}}_{er})^{\mathrm{T}}, (\vec{\boldsymbol{q}}_{ac})^{\mathrm{T}} \rceil^{\mathbf{T}} \tag{3-1}$$

$$\text{where } \left\{ \begin{matrix} \vec{\boldsymbol{q}}_{er} = [x_p, y_p, z_p, \theta_p, \beta_p, \gamma_p] \\ \vec{\boldsymbol{q}}_{ac} = [x_i, y_i, z_i] \end{matrix} \right\}, \text{ for } i = 1 \text{ to n} \tag{3-2}$$

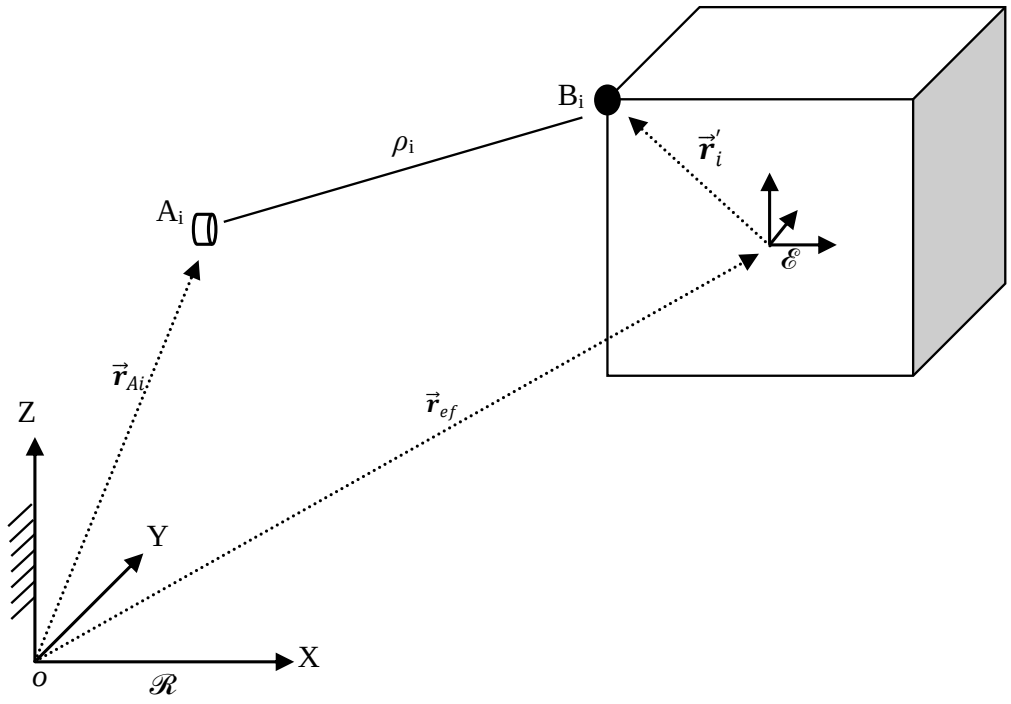

Figure 8 Kinematic diagram

where $\vec{\boldsymbol{q}}_{ac}$ and $\vec{\boldsymbol{q}}_{er}$ are the generalized coordinates of the attachment points on the rail and end effector respectively. Also, n is the number of cables. The kinematic constraints are defined as the constraints formed by the joints connecting rigid bodies [48]. In this model, the kinematics constraints can be described as the restrictions of the eight attachment points

to move only in the vertical direction (i.e., they cannot move in the x or y direction as they are restricted by the rails). This can be formulated mathematically as follows:

$$\begin{bmatrix} x_i \\ y_i \end{bmatrix} = \begin{bmatrix} k_i^1 \\ k_i^2 \end{bmatrix} \; for \; i = 1 \text{ to n}, \tag{3-3}$$

where x_i and y_i are the Cartesian coordinates of point A_i defined in the global coordinate system, and k is a constant based on the position of each attachment point with respect to the fixed global frame.

3.2.2. Driving constraints

The driving constraints, as described by Shabana [101], are the specified motion trajectories, which may depend on the system's generalized coordinates [48] and time. In our mechanism, the driving constraints consist of two groups. In the first group, driving constraints formulations are due to the vertical motion of the eight attachment points on the rails (refer to Figure 10), while in the second group, they are due to the extension and retraction of the eight cables attached to the end effector. The first driving constraint group can be mathematically represented as follows:

$$z_i = c_i(t, \vec{\boldsymbol{q}}), \quad \text{for } i = 1 \text{ to n}, \tag{3-4}$$

where z_i is the z coordinate of each attachment point A_i represented in the global coordinate system, and $c_i(t,\vec{\boldsymbol{q}})$ is the imposed function that drives the attachment point vertically and may be time and/or generalized coordinates ($\vec{\boldsymbol{q}}$) dependent. The formula of the second group of driving constraints is defined as change in the length of the eight cables (ρ_i). This constraint is shown in Figure 9, where the length of the cable will always be the hypotenuse

of a right angle triangle formed by the vertices A_1, B_1 and B_{1z}. This constraint can be represented mathematically as follows:

$$(B_x)_i^2 + (B_y)_i^2 + (A_i - (B_z)_i)^2 = \rho_i^2, \quad \text{for } i = 1 \text{ to n.} \tag{3-5}$$

The coordinates of point B_i can be represented as follows:

$$\vec{\boldsymbol{r}}_{B_i} = \vec{\boldsymbol{r}}_{ef} + \boldsymbol{R}\vec{\boldsymbol{r}}'_i, \text{for } i = 1 \text{ to n,} \tag{3-6}$$

where $\vec{\boldsymbol{r}}_{ef}$ is the position vector of the center of mass of the end effector, and $\boldsymbol{R}$ is the rotation matrix following XYZ convention. $\vec{\boldsymbol{r}}'_i$ is the local coordinate of the 8 vertices of the rectangular prism represented in the local coordinate frame attached to the mobile end effector $\mathscr{E}$.

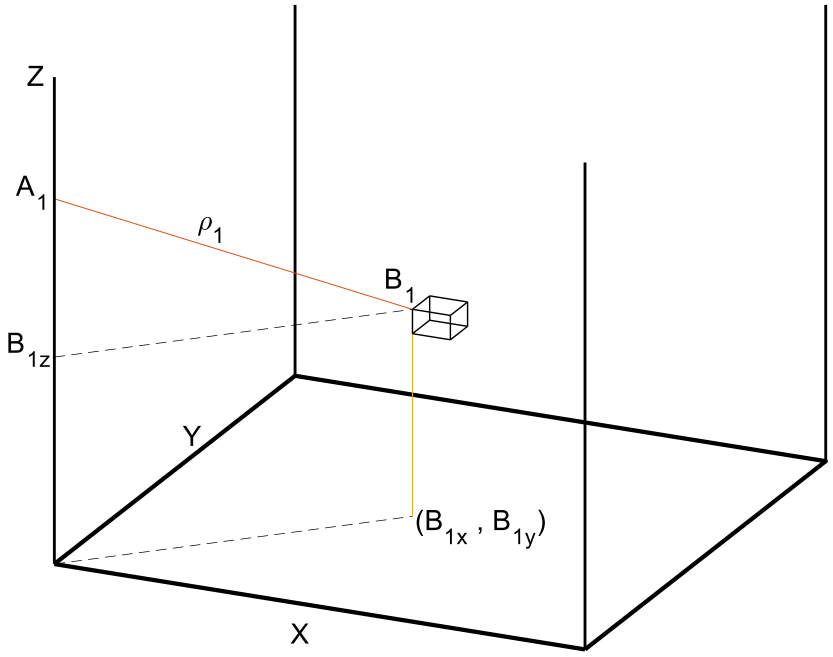

Figure 9 Geometry of second group of driving constraints

The total kinematic constraint (KC) equations are constructed as follows:

$$\varphi = \begin{bmatrix} x_i - k_i^1 \\ y_i - k_i^2 \\ z_i - c_i(t, \vec{q}) \\ (\mathrm{B}_x)_i^2 + (\mathrm{B}_y)_i^2 + (\mathrm{A}_i - (\mathrm{B}_z)_i)^2 - (\rho_i)^2 \end{bmatrix}, \quad \text{for } i = 1 \text{ to n.} \qquad 3\text{-}7$$

3.2.3. Crossed cable configuration

The crossed configuration of the mobile platform attachment points is shown in Figure 10, where the original configuration has been changed so that the upper attachment points on the rail are connected to the lower anchor points on the mobile platform and vice versa. The crossed cable configuration allows a better orientation workspace and stiffness map [15]. Figure 10 shows a schematic for the mobile platform, where $\mathscr{E}$ is a local frame attached to the mobile platform at its center of mass. The mobile platform dimensions are 0.5×0.5×0.5 m^3. The locations of the anchor points on the mobile platform are shown in Table *2* with respect to the local frame $\mathscr{E}$ in meters. In order to evaluate the presented approach, three different trajectories of the mobile platform are chosen such that the Z-height of the end effector is constant as well as its orientation (i.e. the mobile platform will perform a rectilinear and/or curvilinear translation for the three different trajectories). In order for the reader to be able to replicate the results, the three trajectories will be provided in appendix A in form of Cartesian coordinates of the center of mass of the end effector. The suggested trajectories will be confirmed to lie within the constant-orientation feasible closure workspace by computing and plotting the tension values within the eight cables. Hence, section 3.3 is dedicated to establishing the necessary formulas to solve for the cables tension distribution equation of the eight cables.

Table 2 Local positions of the eight anchor points (meters)

	B_1	B_2	B_3	B_4	B_5	B_6	B_7	B_8
x	-0.15	-0.25	-0.15	-0.25	0.15	0.25	0.15	0.25
y	-0.25	-0.15	0.25	0.15	0.25	0.15	-0.25	-0.15
z	-0.25	0.25	-0.25	0.25	-0.25	0.25	-0.25	0.25

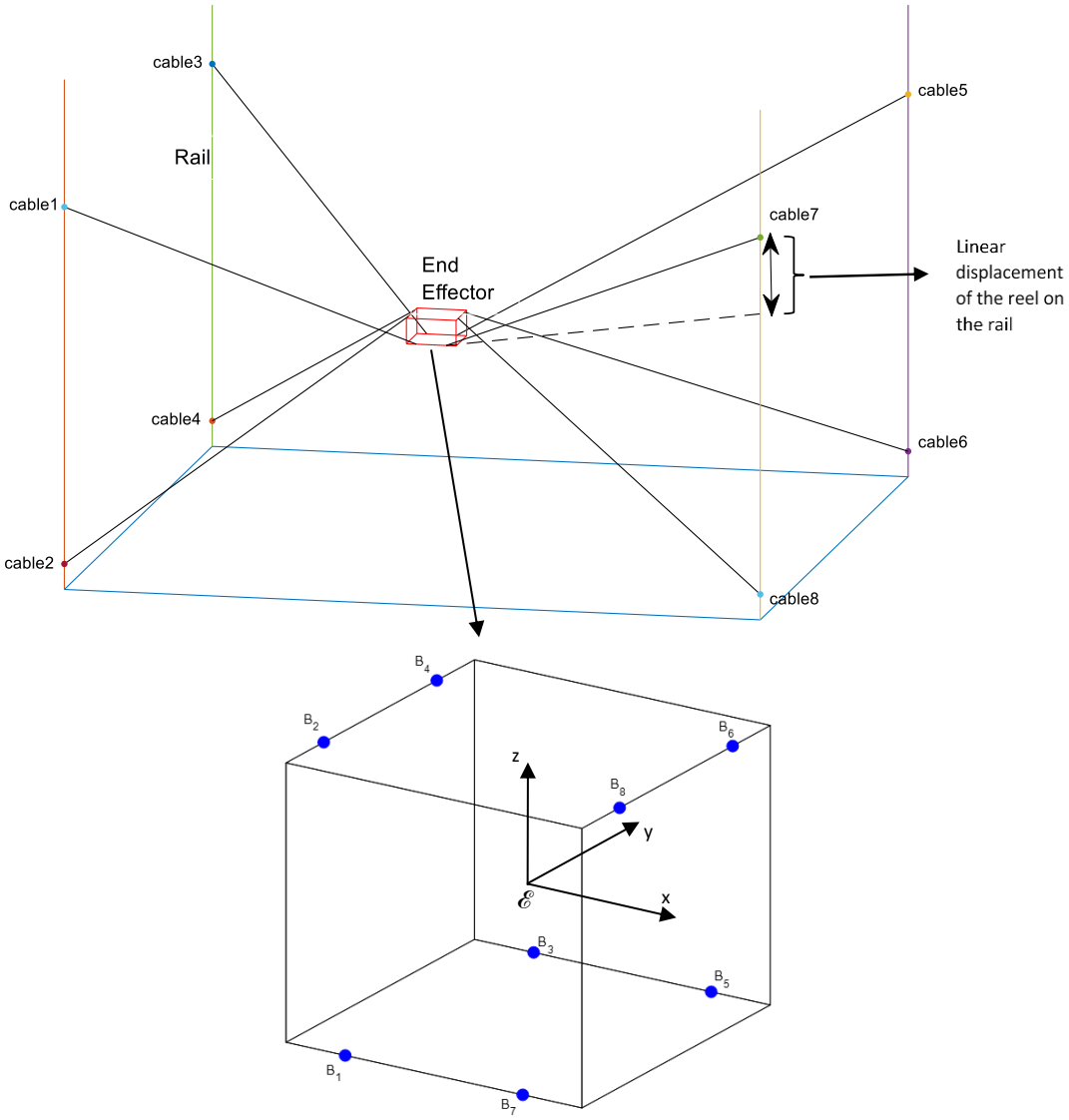

Figure 10 Arrangement of attachment points on the rails and mobile platform

3.2.4. Forward and inverse kinematics

Contrary to the inverse kinematics, the forward kinematics of CDPM is determining the position and orientation of the movable end-effector given the lengths of the actuated cables. Forward kinematics is a very important step in closed loop position control of parallel mechanisms. In our study, unlike conventional CDPM, the eight attachment points on the rails move vertically. Moreover, in conventional CDPM, the forward kinematics is defined as, (1) input: given the cables length, and (2) output: solve for the pose (position and orientation) of the end effector. However, in the reconfigurable CDPM presented in this research study, the forward kinematics is defined as, (1) input: given the cables length and the attachment point's location at the spool (motorized reel), and (2) output: solve for the pose of the end effector. In order to evaluate Algorithm 1, a first simulation is done by moving both attachment points $\vec{\boldsymbol{q}}_{ac}$ and cables length ρ_i as an input and $\vec{\boldsymbol{q}}_{er}$ as an output. The main issue with the kinematics problem in this model is that the system of equations is a set of nonlinear overdetermined equations. Least square method with lower and upper bounds on the variables [102,103] was used to solve the above set of equations. The forward kinematics problem is then solved given that the eight attachment points (actuators) on the rails move vertically up and down while the eight cables are being shortened or extended to manipulate and control the end effector. Indeed, the conventional cable driven mechanisms have the actuators fixed on the rails while controlling the cable lengths. The following section describes the equations and algorithm used to solve the forward and inverse kinematics. As mentioned earlier, the reconfigurable eight-cable driven mechanism model results in a nonlinear overdetermined set of equations where the number of unknowns is less than the number of equations [104]. The well-known

Levenberg Marquardt least squares method [105] is then used to solve the forward kinematics problem represented as KC (refer to Equation 3-7) according to the following algorithm:

Algorithm 1 FKP

***Procedure*:** OptimizeCableLengths
Initialization: $\vec{q}_{er}$, $\vec{q}_{ac}$, $\vec{q}$, time, counter = 1, tol=tolerance
for counter = 1, 2,…length (time) **do**
    set upper limit, lower limit
        while (min(||KC||)^2>tol)
            solve KC
        end while
    update $\vec{q}_{ac}$ and **record** $\vec{q}$
end for

In order for the reader to be able to replicate the results, parametric equations that describes the linear displacement ($c_i(t,\vec{q})$) of the eight attachment points (actuators) on the rails as well as the elongation and shortening of the eight cables (ρ_i) are shown below in Table 3 with the results shown in Figure 11. All the functions are given in terms of time (t) where time is ranged between 0 and 20 seconds in all the simulation results presented in this research study.

Table 3 Parametric equations of the actuators displacement and the change in cables length (meters)

i	Attachment points displacement ($c_i(t,\vec{q})$)	Cables length (ρ_i)
1	7.5+0.5×sin(t)	$((3\times(3.25)^2))^{0.5}$-0.5×sin(t)
2	0.5+0.5×sin(t)	$((3\times(3.25)^2))^{0.5}$-0.5×sin(t)
3	7.5+0.5×sin(t)	$((3\times(3.25)^2))^{0.5}$-0.5×sin(t)
4	0.5+0.5×sin(t)	$((3\times(3.25)^2))^{0.5}$-0.5×sin(t)
5	7.5-0.5×sin(t)	$((3\times(3.25)^2))^{0.5}$+0.5×sin(t)
6	0.5-0.5×sin(t)	$((3\times(3.25)^2))^{0.5}$+0.5×sin(t)
7	7.5-0.5×sin(t)	$((3\times(3.25)^2))^{0.5}$+0.5×sin(t)
8	0.5-0.5×sin(t)	$((3\times(3.25)^2))^{0.5}$+0.5×sin(t)

Figure 11 shows the Cartesian coordinates of the center of mass of the end effector given the position of the eight attachment points on the rails and the eight cable lengths.

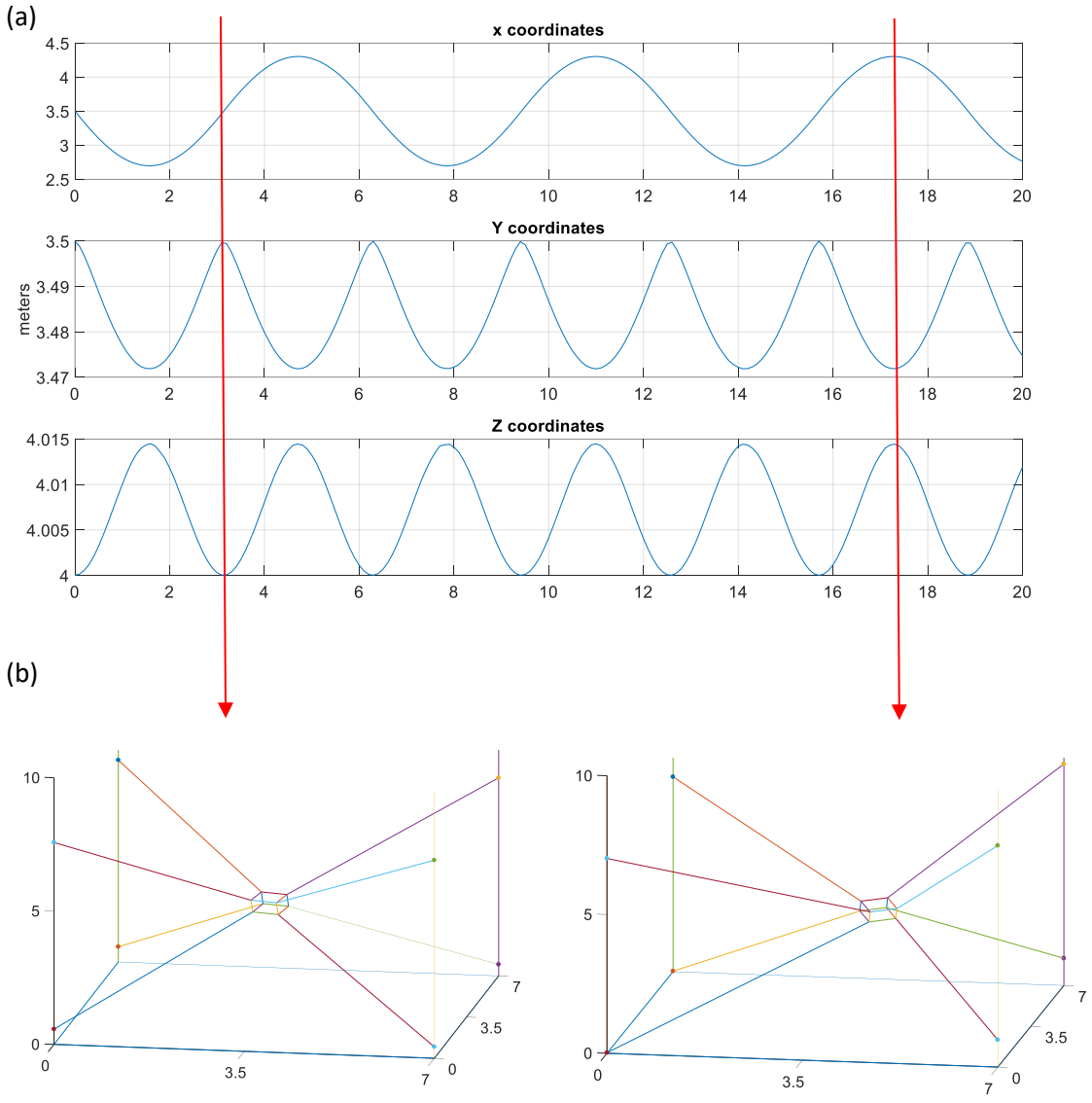

Figure 11 (a). X, Y and Z coordinates of the mobile platform center of mass; (b) two pose of the end effector used in the simulation

The inverse kinematic issue is solved; the pose (position and orientation) of the end effector is known in this case as well as the position of the attachment points on the rails, and the unknowns are the eight cables length. Regarding Figure 8, the vector loop-closure equation for cable *i* is obtained in equation (3-8) as following:

$$\rho_i = \left\| \vec{\boldsymbol{r}}_{ef} + \boldsymbol{R}\vec{\boldsymbol{r}}'_i - \vec{\boldsymbol{r}}_{Ai} \right\|, \quad \text{for } i = 1 \text{ to n} \tag{3-8}$$

Linear programming optimization tool in MATLAB was used to solve Equation 3-8 for each pose of the end effector. The proposed algorithm can be used also to determine the required positions of the attachment points on the rails given the eight cable lengths. Figure 12 shows the required cable lengths given the full configuration of the end effector (position and orientation) and the position of the attachment points.

(a)

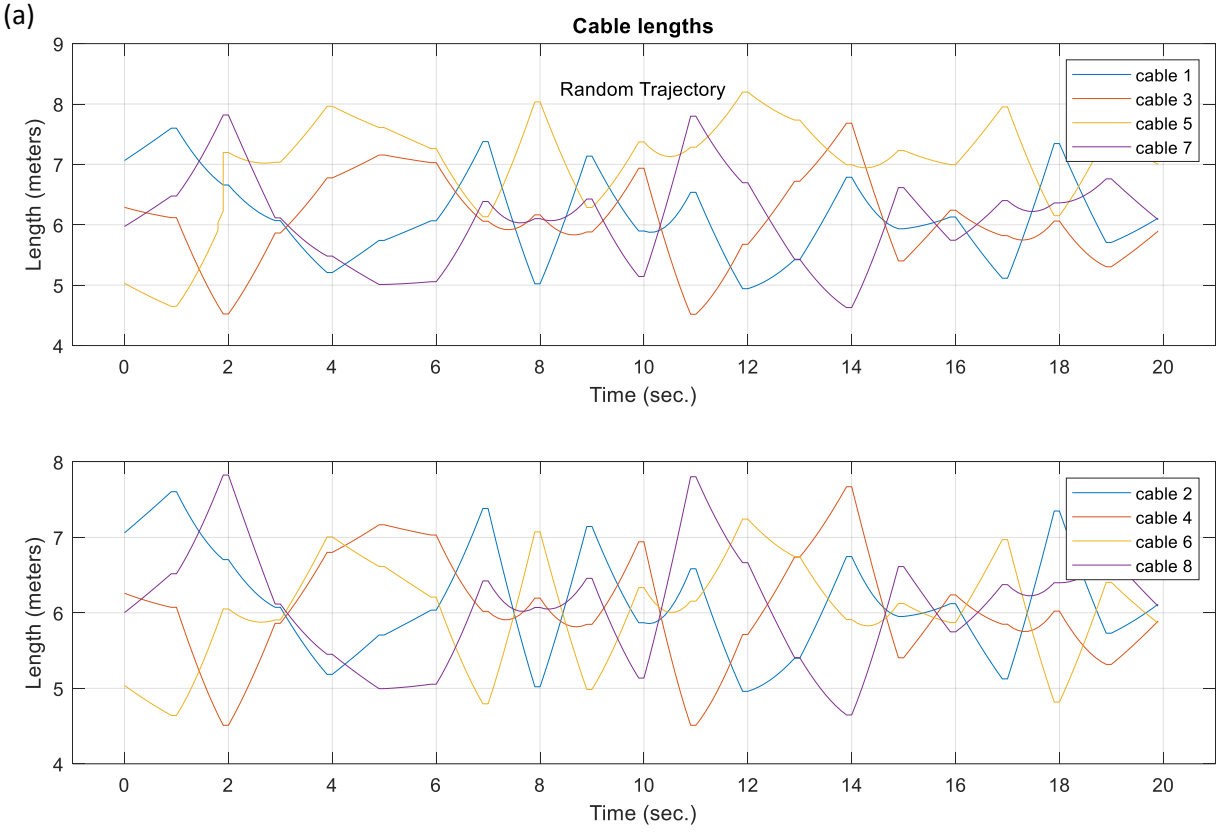

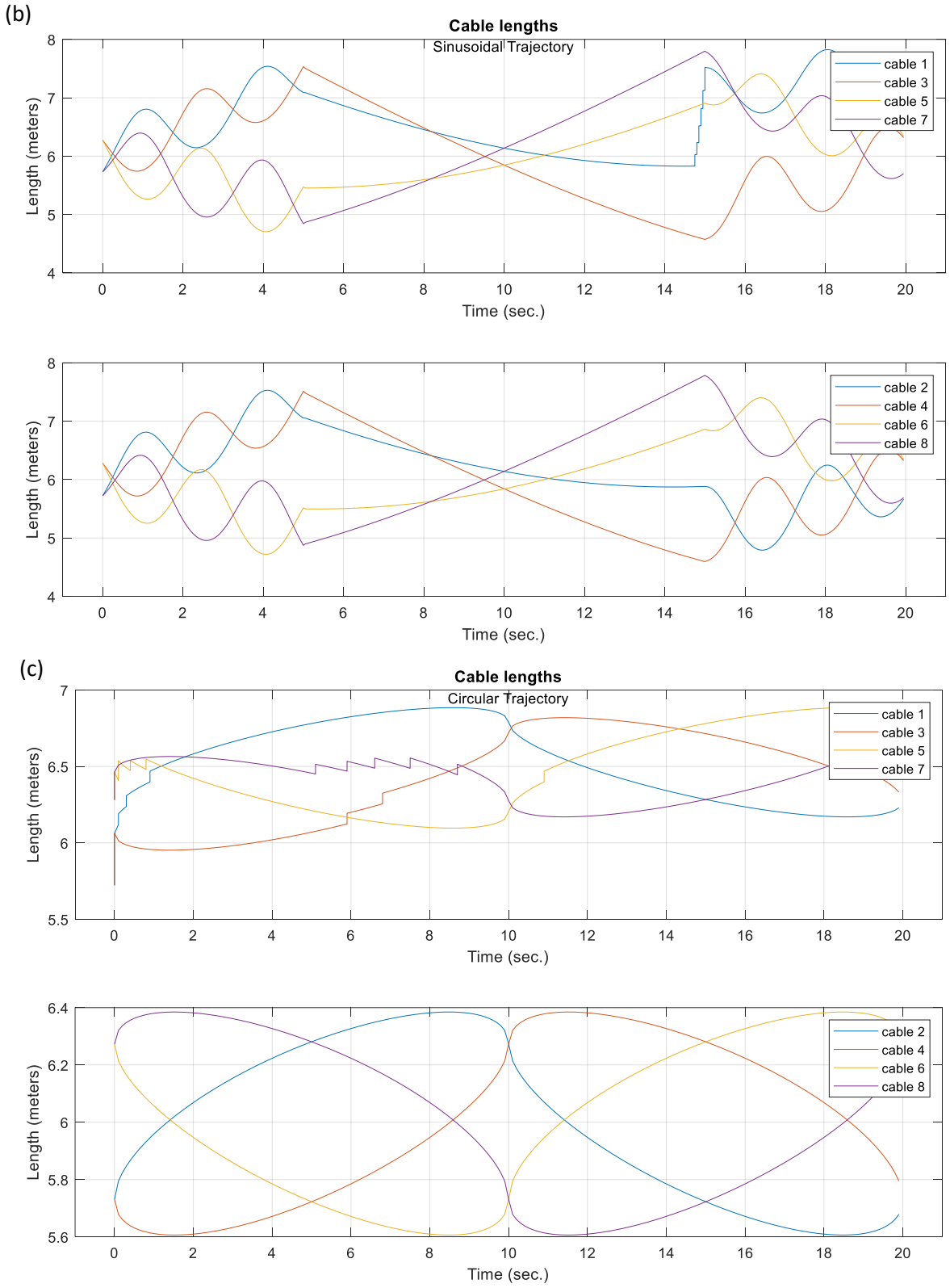

Figure 12 Cables length: a) Random trajectory, (b) Circular trajectory and (c) Sinusoidal trajectory

3.3. Cables tension distribution

Since CDPM is a mechanism in which cables control the end effector instead of rigid links, and due to the fact that cables can maintain tension forces only (i.e. cables cannot push but rather pull), it is a crucial matter that cables are to remain in tension all the time [106]. The cables tension distribution issue is very important in CDPM, since it is used for analysis of the mechanism workspace [107,108], stability [109] and stiffness [110,111]. In this section, the kinematic equations required to solve for tension in the eight cables of the CDPM are established to ensure positive tension among all the cables [112]. Figure 8 shows the schematic for the mobile platform and attachment point A_i, where $\mathscr{R}$ is the fixed global frame, and $\mathscr{E}$ is a local frame attached to the mobile platform.

In case of wrench closure workspace, the cables' tension distribution issue may be expressed as finding all the tensions $\vec{t_i}$ such that:

$$\widetilde{\boldsymbol{w}}\vec{t_i} + \vec{w_j} = \vec{\mathbf{0}}_6 \text{ , with } \vec{t_i} > 0, \text{ for } i = 1 \text{ to n.} \qquad 3\text{-}9$$

where,

$$\widetilde{\boldsymbol{w}} = \begin{bmatrix} \vec{u}_1 & \vec{u}_2 & \cdots & \vec{u}_8 \\ \vec{r}_1\vec{u}_1 & \vec{r}_2\vec{u}_2 & \cdots & \vec{r}_8\vec{u}_8 \end{bmatrix}_{6\times n} \text{ : Structure matrix,}$$

$$\vec{t_i} = \begin{bmatrix} t_1 \\ \vdots \\ t_8 \end{bmatrix}_{n\times 1} \text{ : Cables tension,}$$

$$\overrightarrow{\boldsymbol{w}_J} = \begin{bmatrix} f_x \\ f_y \\ f_z \\ m_x \\ m_y \\ m_z \end{bmatrix}_{6\times1}$$: External wrench acting on the end effector,

$$\vec{\mathbf{0}}_6 = \begin{bmatrix} 0 \\ \vdots \\ 0 \end{bmatrix}_{6\times1}$$: Zero vector.

where f_x, f_y, f_z, m_x, m_y and m_z are the components of the external force and moment acting in the X, Y and Z directions respectively. The two variables ($\vec{\boldsymbol{r}}_i$ and $\vec{\boldsymbol{u}}_i$) in the structure matrix $\widetilde{\boldsymbol{w}}$ are explicit functions in the mobile platform position and orientation as well as the attachments points position. These two variables can be computed as follows:

$$\vec{\boldsymbol{u}}_i = \frac{\vec{\boldsymbol{r}}_{ef} + \boldsymbol{R}\vec{\boldsymbol{r}}'_i - \vec{\boldsymbol{r}}_{A_i}}{\left\|\vec{\boldsymbol{r}}_{ef} + \boldsymbol{R}\vec{\boldsymbol{r}}'_i - \vec{\boldsymbol{r}}_{A_i}\right\|} \qquad 3\text{-}10$$

$$\vec{\boldsymbol{r}}_i = \boldsymbol{R}\vec{\boldsymbol{r}}'_i \qquad 3\text{-}11$$

In this study, the wrench feasible condition is applied and an extra condition is added to bind the tension values in the eight cables as follows:

$$t_{min.} < \vec{\boldsymbol{t}}_i < t_{max.,} \qquad 3\text{-}12$$

where $t_{min.}$ is the minimum allowable tension value to ensure that all the cables are taut, and $t_{max.}$ is the maximum allowable tension value depending on the actuators torque.

The constant-orientation feasible closure workspace was solved for all three trajectories given that the only external wrench acting on the end effector is its weight, 25 N, and the

maximum and minimum allowable tension values for all the cables are 20 and 120 N respectively. The initial attachment points' (A_i) locations on the rails for the eight cables are shown in Table 4 with respect to the global frame $\mathscr{R}$.

Table 4 Initial positions of the eight attachment points (meters)

	A_1	A_2	A_3	A_4	A_5	A_6	A_7	A_8
X	0	0	0	0	7	7	7	7
Y	0	0	7	7	7	7	0	0
Z	7.5	0.5	7.5	0.5	7.5	0.5	7.5	0.5

Cable tension distribution values are computed using linear programming optimization [30,92,113] to minimize an objective function subjected to equality constraints with lower and upper bounds. Linear programming is chosen since equation 3-9 represents linear constraints where the objective function is set to zero which means that we are not trying to minimize any quantity but rather we are just interested to find a feasible solution for equation 3-9. The results are presented in Figure 13 to guarantee a feasible wrench workspace for three different trajectories. The tension of the eight cables can be observed as positive values (over the zero limit), where the tension values lies between approximate minimum and maximum values, Tmin = 20 and Tmax = 90 N.

(a)

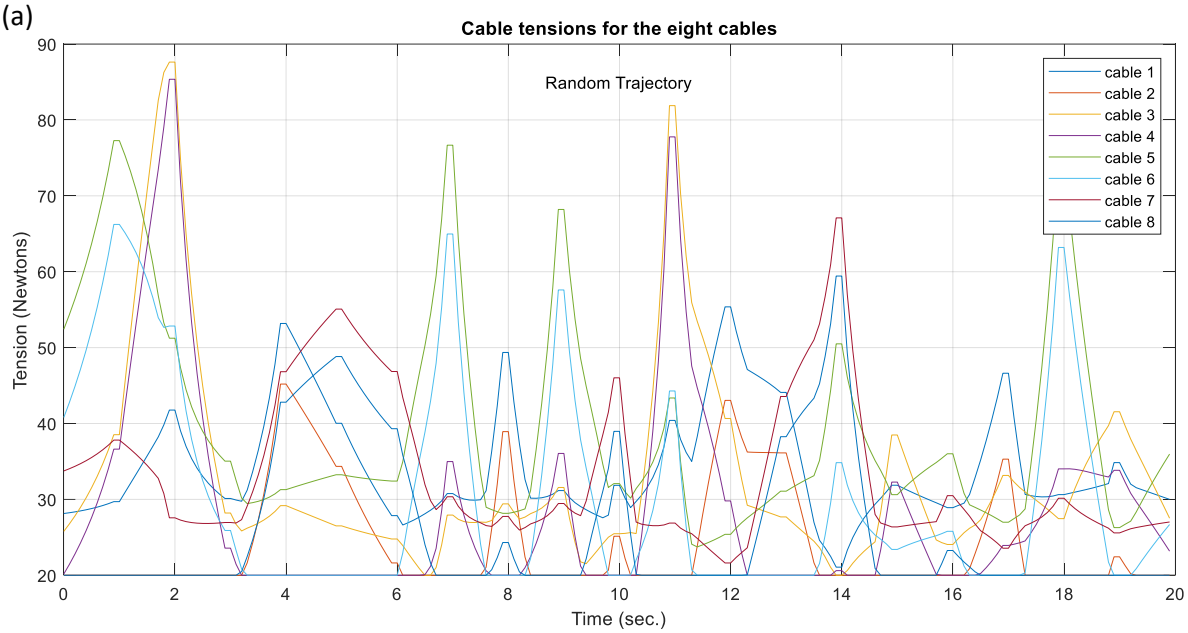
Cable tensions for the eight cables
Random Trajectory
cable 1
cable 2
cable 3
cable 4
cable 5
cable 6
cable 7
cable 8
Tension (Newtons)
Time (sec.)

(b)

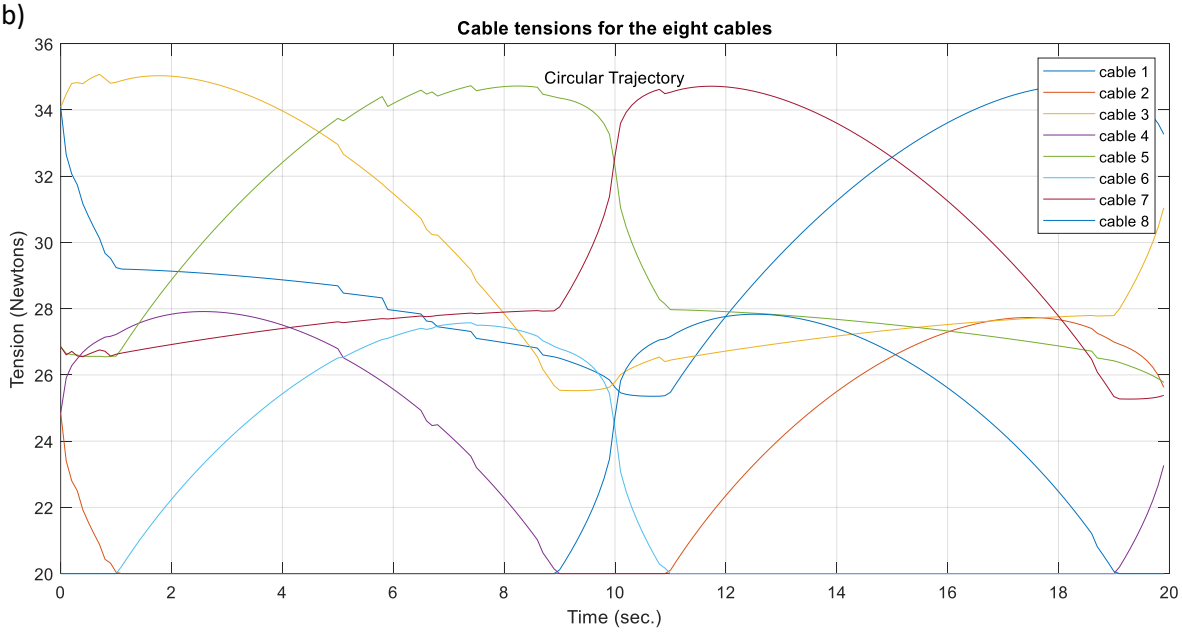
Cable tensions for the eight cables
Circular Trajectory
cable 1
cable 2
cable 3
cable 4
cable 5
cable 6
cable 7
cable 8
Tension (Newtons)
Time (sec.)

(c)

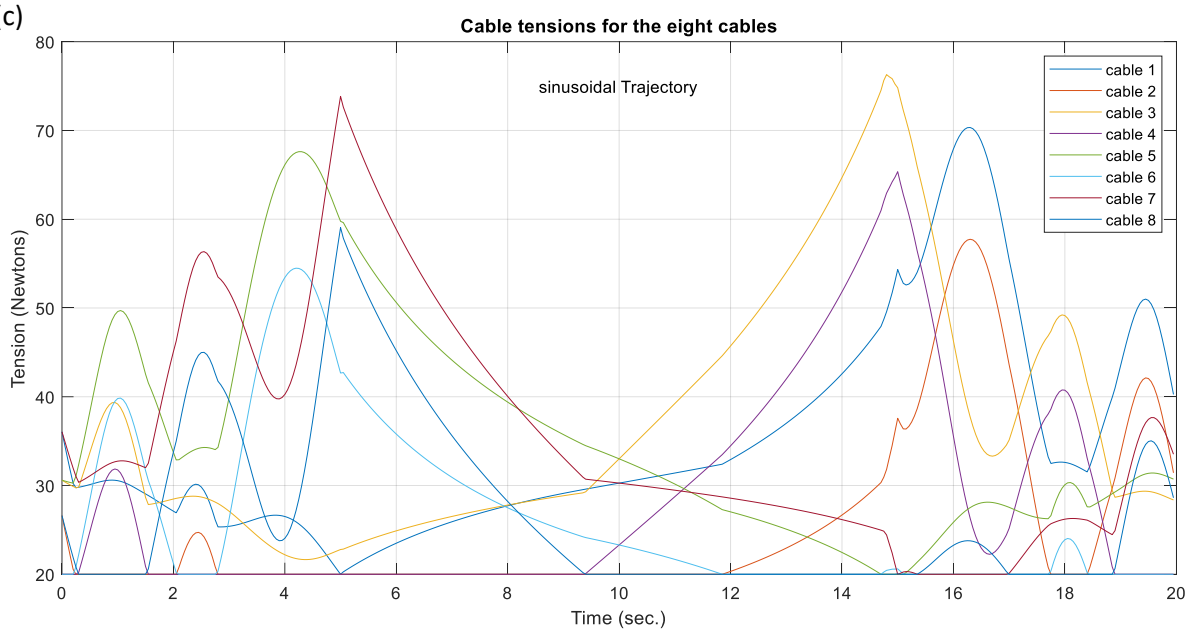

Figure 13 Computed cable tension for the eight cables (Newtons): (a) Random trajectory, (b) Circular trajectory and (c) Sinusoidal trajectory

3.4. Conclusion

A general fully constrained model of six DOF CDPM driven by eight cables is developed by establishing the mathematical representation of the kinematics and driving constraints equation. The forward kinematics issue is solved using least square method given that the attachment points are moving vertically as presented in the results in Figure 11. In addition, the inverse kinematics is obtained by solving the the vector loop-closure equation using linear programming to obtain the required cables length for a given pose of the end effector. The suggested model has been developed generally and can be used in modeling any architect of CDPM.

In addition, the cables tension distribution equation is developed and solved to guarantee a positive tension values for all the cables at each sampling time. Linear programming optimization tool is used again to find a feasible solution since the equation is represented as linear objective function with lower and upper bounds. The results are presented in Figure 13 where it shows continues smooth tension values for all the cables during the entire sampling time where the values lies between the lower and upper limits. Solving for the forward and inverse kinematics as well as the cables tension distribution is then used in the second main contribution of this research study, which is discussed in chapter 4.

CHAPTER 4

4. Avoiding interference between cables with online reconfiguration

4.1. Introduction

This chapter presents the geometrical method to compute the shortest distance between two lines in 3D as well as the suggested algorithm to detect and avoid cables collision. After solving the forward and inverse kinematics of the suggested reconfigurable CDPM presented in chapter 3, the second main contribution of this study is deliberated in this chapter which is the application of reconfigurable CDPM theory to detect and avoid interference between cables in real-time while keeping the end effector trajectory unchanged.

In conventional CDPM, cables are attached to the fixed rails on specific unchangeable positions, however in this study, the attachment points on the rails are relocated in case there is a near collision between two cables in order to increase the shortest distance between them in real-time. An algorithm has been created using MATLAB to achieve the objective of cables detection and avoidance and three different trajectories has been simulated and results are presented to proof the robustness of the suggested approach.

Section 4.2 is dedicated to explain the geometrical method used to compute the shortest distance between two lines in space knowing their start and end points coordinates. Section 4.3 presents in details the description of the proposed algorithm and simulation results are shown and discussed to demonstrate the effectiveness of the suggested approach.

4.2. Cable-cable collision detection

In our study, after solving the forward and inverse kinematics given that the attachment points on the rails move vertically, the reconfiguration idea is then used to avoid collision between cables while maintaining the end effector trajectory unchanged by relocating the attachment points on the fixed frame. In addition, the reconfigurable idea will be used to detect and avoid collision between cables and human, which will be discussed later in chapter 5. The online reconfiguration will definitely change the workspace (wrench closure workspace and feasible) of the mechanism; hence, chapter 6 shows the difference between initial and final workspace due to the relocation of the attachment points. A cable-cable collision can be treated as two-line interference in 3D, where a collision is detected when these two lines get close to each other to a certain threshold value. In this research study, the cables will be assumed to be massless and straight lines (without sagging), and collision between cables can be geometrically computed as discussed in [114]. A collision could occur in the range of the dimension of the cables but also outside their dimensions. A collision outside the dimensions of the cables occurring in a virtual extension of the cable by a line is not considered.

Lines 1 and 2 in Figure 14 can be expressed in 3D in terms of the coordinates of start and end points Q_1, P_1, Q_2 and P_2. One can say that there are two points on line 1 and 2 such that the line connecting these two points is the shortest distance between line 1 and 2. Let's express line 1 and 2 as follows:

$$\begin{Bmatrix} \vec{\boldsymbol{L}}_1 = \vec{\boldsymbol{r}}_{P1} + w\vec{\boldsymbol{d}}_1 \\ \vec{\boldsymbol{L}}_2 = \vec{\boldsymbol{r}}_{P2} + s\vec{\boldsymbol{d}}_2 \end{Bmatrix}, \qquad \text{where} \begin{Bmatrix} \vec{\boldsymbol{d}}_1 = \vec{\boldsymbol{r}}_{Q1} - \vec{\boldsymbol{r}}_{P1} \\ \vec{\boldsymbol{d}}_2 = \vec{\boldsymbol{r}}_{Q2} - \vec{\boldsymbol{r}}_{P2} \end{Bmatrix} \tag{4-1}$$

where $\vec{\boldsymbol{r}}_{\mathrm{P1}}$, $\vec{\boldsymbol{r}}_{\mathrm{P2}}$, $\vec{\boldsymbol{r}}_{\mathrm{Q1}}$ and $\vec{\boldsymbol{r}}_{\mathrm{Q2}}$ are the position vectors of P_1, P_2, Q_1 and Q_2 respectively.

w and s are two unique values if and only if lines 1 and 2 are not parallel. By finding w and s, we can define vector $\vec{\mathbf{v}}(w,s)$, whose length is the intended shortest distance between lines 1 and 2. In order to find the two values, w and s, corresponding to the shortest length between lines 1 and 2, it should be realized that $\vec{\mathbf{v}}(w,s)$ in this particular case is perpendicular to the two lines.

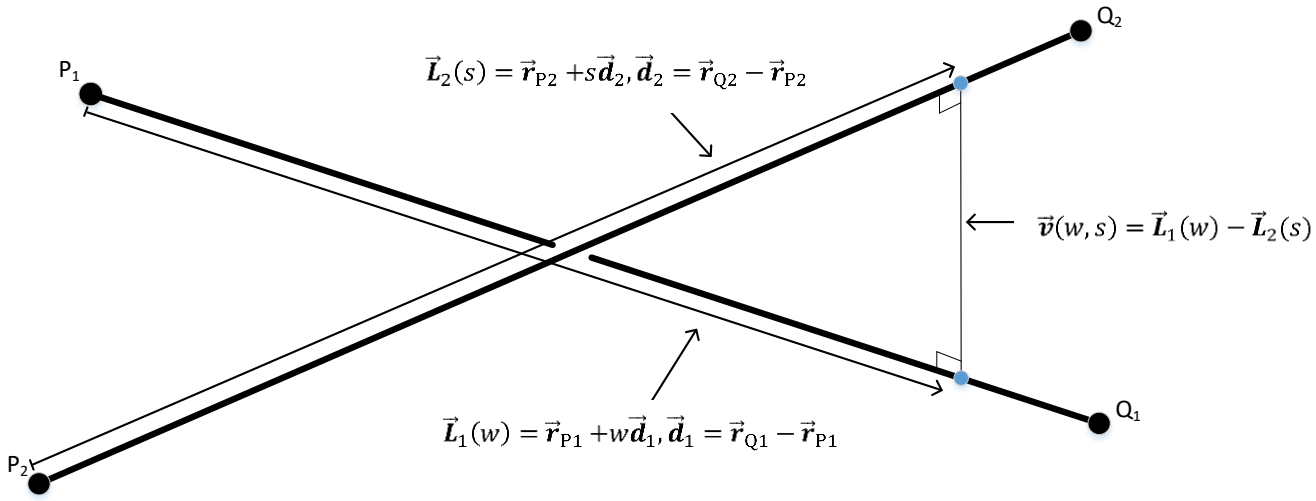

Figure 14 Vector $\vec{\boldsymbol{v}}(w,s)$ connecting the two closest points of two lines $\vec{\boldsymbol{L}}_1$ *and* $\vec{\boldsymbol{L}}_2$ as defined in [114]

The perpendicularity conditions can be expressed mathematically as follows:

$$\begin{Bmatrix} \vec{\boldsymbol{d}}_1 \cdot \vec{\boldsymbol{v}}(w,s) = 0 \\ \vec{\boldsymbol{d}}_2 \cdot \vec{\boldsymbol{v}}(w,s) = 0 \end{Bmatrix} \qquad 4\text{-}2$$

Therefore,

$$\begin{Bmatrix} \vec{\boldsymbol{d}}_1 \cdot \left(\vec{\boldsymbol{L}}_1(w) - \vec{\boldsymbol{L}}_2(s)\right) = \vec{\boldsymbol{d}}_1 \cdot \left((\vec{\boldsymbol{r}}_{P1} - \vec{\boldsymbol{r}}_{P2}) + w\vec{\boldsymbol{d}}_1 - s\vec{\boldsymbol{d}}_2\right) = 0 \\ \vec{\boldsymbol{d}}_2 \cdot \left(\vec{\boldsymbol{L}}_1(w) - \vec{\boldsymbol{L}}_2(s)\right) = \vec{\boldsymbol{d}}_2 \cdot \left((\vec{\boldsymbol{r}}_{P1} - \vec{\boldsymbol{r}}_{P2}) + w\vec{\boldsymbol{d}}_1 - s\vec{\boldsymbol{d}}_2\right) = 0 \end{Bmatrix} \qquad 4\text{-}3$$

Rearranging the above equations, *s* and *w* may be determined as follows:

$$\begin{Bmatrix} s = (bf - ce)/d \\ w = (af - bc)/d \end{Bmatrix}, \quad \text{4-4}$$

where, $a = \vec{\boldsymbol{d}}_1.\vec{\boldsymbol{d}}_1, b = \vec{\boldsymbol{d}}_1.\vec{\boldsymbol{d}}_2, c = \vec{\boldsymbol{d}}_1.\vec{r}, e = \vec{\boldsymbol{d}}_2.\vec{\boldsymbol{d}}_2, f = \vec{\boldsymbol{d}}_2.\vec{r},\ \vec{r} = \vec{\boldsymbol{r}}_{\mathrm{P1}} - \vec{\boldsymbol{r}}_{\mathrm{P2}}$ and $d = ae - b^2$.

After obtaining *s* and *w*, $\vec{\boldsymbol{L}}_1(w)$ and $\vec{\boldsymbol{L}}_2(s)$ can then be computed as well as the coordinates of the two points connecting the shortest distance ($\vec{\boldsymbol{v}}(w, s)$). The shortest distance between any two cables can then be determined, which is the length of the vector $\vec{\boldsymbol{v}}(w, s)$; hence, it is compared with a threshold value such that the shortest distance value is increased by relocating vertically up and down the corresponding attachment point until the shortest distance between cables exceeds the threshold value, which means that the collision has been avoided, as will be discussed later.

4.3. Cables interference detection and avoidance

One of the key contribution of this study is the use of online reconfiguration by changing the location of the attachment points of the cables on the fixed rails to avoid a near collision between two cables. A Matlab code was generated to use the idea of reconfiguration in detecting and eliminating cable-cable interference in real time, as shown the algorithm presented in Figure 15.

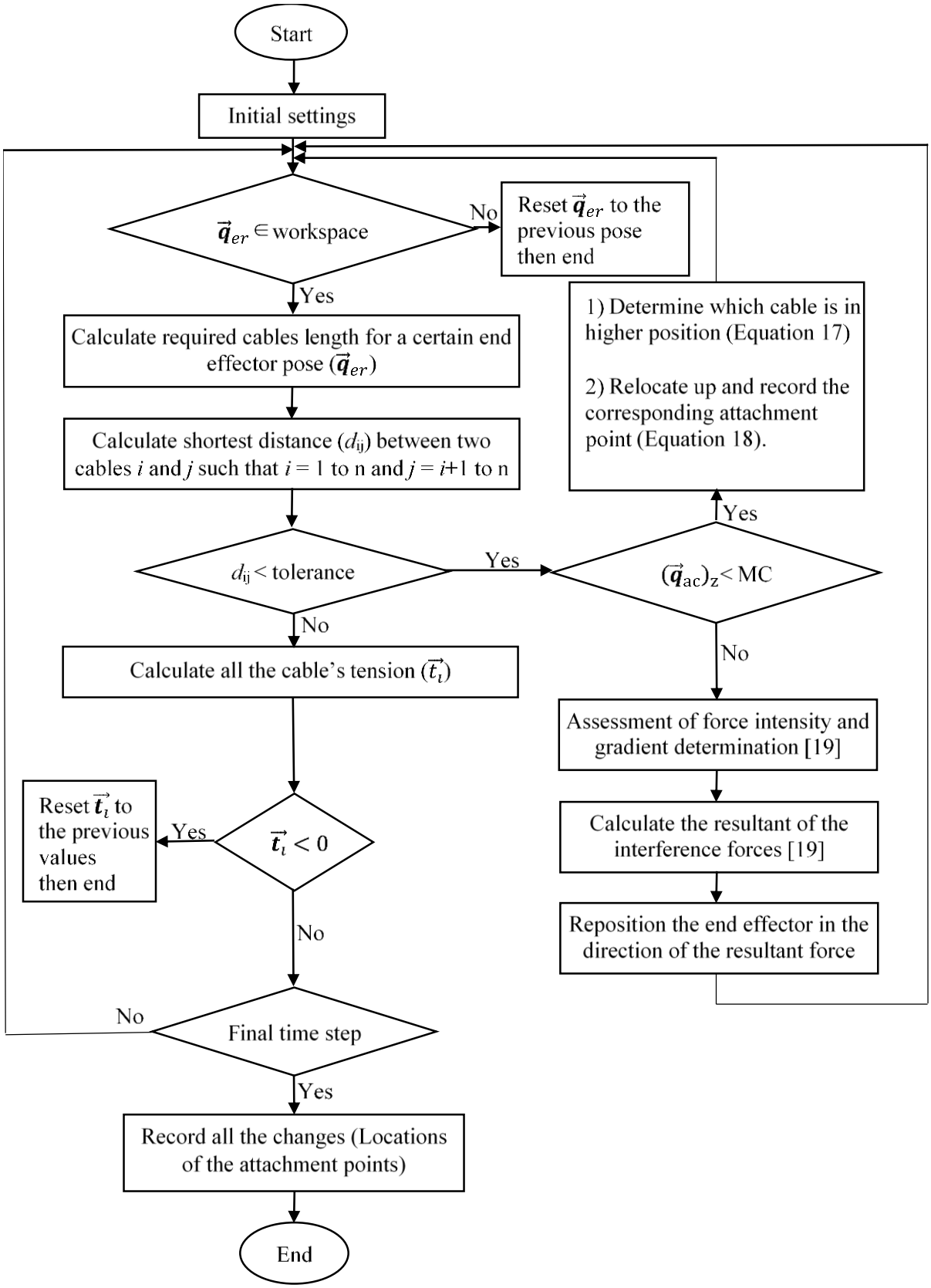

Figure 15 Real time algorithm for detecting and eliminating cable interference

At each sampling time, the proposed algorithm computes the shortest physical distance (d_{ij}) between all the cables such that i = 1 to n and j = i+1 to n and compares it with a threshold value (tolerance) that is defined by the user. The shortest distance computation depends on the position of the attachment points of the cables on the fixed rails, the pose of the mobile platform and the location of the anchor points on the end effector. In case of a near collision between any two cables, the algorithm computes $\vec{\boldsymbol{L}}_1(w)$ and $\vec{\boldsymbol{L}}_2(s)$ (as shown in Figure 14) and recognizes the coordinates of the two points connecting the shortest distance ($\vec{\mathbf{v}}(w,s)$) and accordingly determines which cable is currently in a higher position as follows:

$$\left\{\begin{array}{c}\text{if } ((\vec{\boldsymbol{q}}_{\text{ac}})_{\text{z}})_i \geq ((\vec{\boldsymbol{q}}_{\text{ac}})_{\text{z}})_j \rightarrow \text{then } ((\vec{\boldsymbol{q}}_{\text{ac}})_{\text{z}})_i \text{ is relocated} \\ \text{Otherwise} \rightarrow ((\vec{\boldsymbol{q}}_{\text{ac}})_{\text{z}})_j \text{ is relocated}\end{array}\right\} \text{ for } i = 1 \text{ to n.} \qquad 4\text{-}5$$

Hence, it moves up the corresponding attachment point on the rail by a step Δq that is defined by the user. Therefore, the new location of the corresponding attachment point is updated and recorded as follows:

$$(((\vec{\boldsymbol{q}}_{\text{ac}})_{\text{z}})_{\textbf{new}})_{\boldsymbol{i}} = (((\vec{\boldsymbol{q}}_{\text{ac}})_{\text{z}})_{\textbf{initial}})_{\boldsymbol{i}} + \Delta q \text{ for } i = 1 \text{ to n.} \qquad 4\text{-}6$$

In this research study, the step Δq is set to be equal to 0.1 meters, which is approximately 1.5% of the vertical distance between two attachment points on the same rail; however, it can be changed by the user according to the dimension of the mechanism.

It is important to mention here that the location of the reel is moved using a servo linear actuator. The computed location is a set point to the servo controller included in the linear actuator. The servo controller will move the location at its current dynamic like a Heaviside input (step response). This dynamic of the linear actuator is a second order system with

damping fixed at 0.7 (compromise between overshoot and settling time). Another solution could be to use a fifth order polynomial trajectory (or a trapezoidal function). However, this will not improve the settling time since the limit is defined by the actuator dynamic. In addition, the robustness of the proposed approach is validated by adding a mechanical limit (MC), as shown in Figure 15, wherein each cable has a maximum vertical location on the rail. MC is defined by the user and consider the size of the linear actuator, and it describes a position on the rail (in meters) that an attachment point cannot exceed. In a case of near collision between two cables where the intended attachment point has already reached its MC, approach suggested by Meziane et al. is adopted [47] since it will be impossible to continue the initial trajectory of the end effector while avoiding cable interference. In the aforementioned method, a repulsive force is generated by a controller, which is computed from the gradient of the shortest distance between the two cables. This repulsive force will act on the end effector in a direction such that the distance between the two cables will be increased.

In order to verify the proposed approach, a simulation was conducted using the above algorithm for three different trajectories. In the first trajectory, the end effector performs curvilinear translation (given in Appendix A). The following figures shows the computed shortest distance between pairs of interfered cables, the recorded position of the corresponding attachment point and the computed tension values for the corresponding cable. Figure 16 shows the computed distance between cables 1 and 2 as well as the location of the displaced attachment point of cable 1 and its computed tension values for a circular trajectory of the end effector. With the minimum allowable distance (tolerance) between any two cables equal to 0.132 m during the entire sampling time and due to the

chosen path of the end effector, an interference between pairs of cables is detected within the trajectory of the mobile platform at different times.

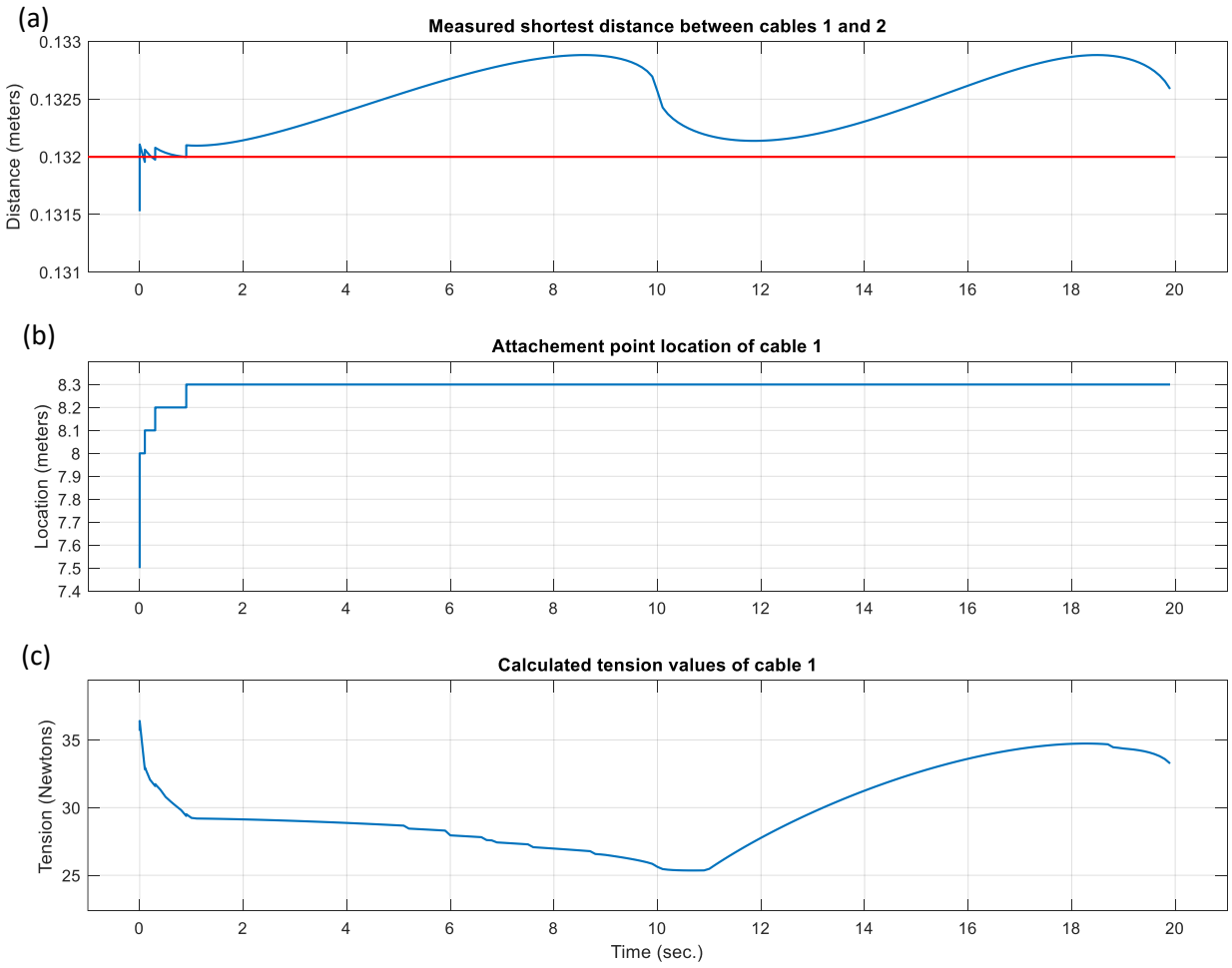

Figure 16 Circular trajectory: (a) measured distance between cables 1 and 2; (b) attachment point location of cable 1; (c) computed tension of cable 1

As shown in Figure 16, at t=0 s, the algorithm detects the shortest distance between cables 1 and 2 below the threshold value (0.132 m – horizontal line in red). Also, it determines that cable 1 is in a higher position; hence, the attachment point of cable 1 which was initially at location 7.5 m, measured from the ground, starts to increase with an increment of 0.1 m. Of course, the lower cable attachment point could relocate down to increase the

shortest distance between the two cables; however, the lower cable attachment point will always be restricted by its distance from the ground. Cable 1 attachment point keeps increasing while the distance is being measured until the distance between the two cables reaches more than 0.132 m and the attachment point location reaches 8.3 m at t=0.9 s. After that, the measured shortest distance between the two cables is above the threshold value. Figure 17 shows the computed distance between cables 3 and 4 as well as the location of the displaced attachment point of cable 3 and its computed tension values.

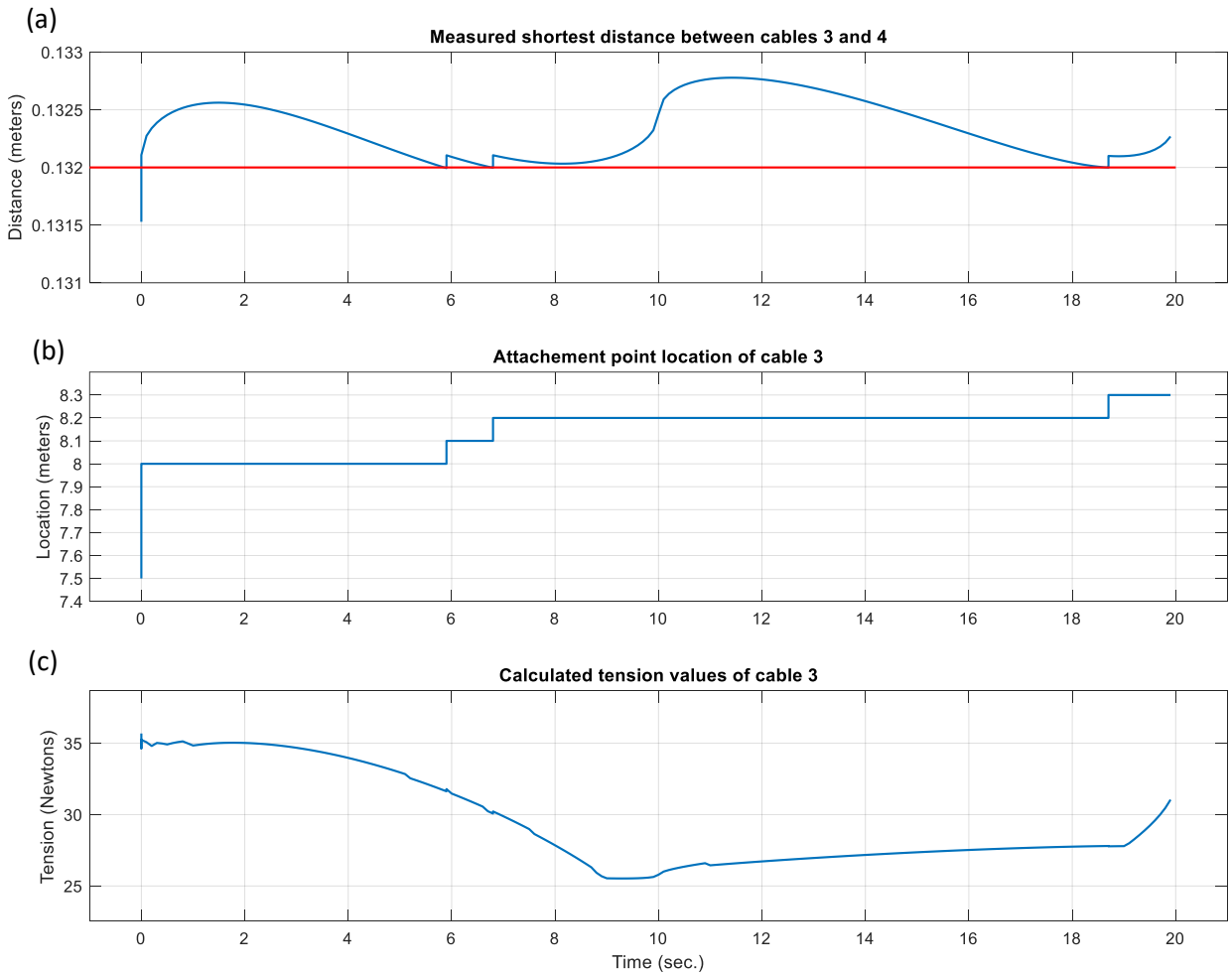

Figure 17 Circular trajectory: (a) measured distance between cables 3 and 4; (b) attachment point location of cable 3; (c) computed tension of cable 3

As shown in Figure 17, the algorithm detected a near collision (distance between cables is less than 0.132 meters) between cables 3 and 4 at t=0, 5.9, 6.8 and 18.7 seconds. Moreover, the algorithm identified that attachment point of cable 3 should be located up since the relocation of cable 3 will increase the distance between the two cables. At t=0, cable 3 attachment point location was initially at 7.5 meters measured from the ground and started to relocate up while the distance between cables 3 and 4 are being computed by the algorithm until it reached 8 meters. After that, the distance can be observed over the allowable minimum threshold value until t=5.9 seconds, therefore the attachment point of cable 3 kept relocated up until it reaches 8.1 and then 8.2 meters at 6.8 seconds. The computed distance between the two cables is then observed to be over the allowable limit until t=18.7 seconds, so the attachment point location is relocated again from 8.2 meters to 8.3 meters. In addition, it can be observed from Figure 17(c) that the tension values of the corresponding cable (3), which is relocated to avoid interference with cable 4, has no significant or sudden change which indicates a smooth transition in the tension values. Figure 18 shows the computed distance between cables 5 and 6 as well as the location of the displaced attachment point of cable 5 and its computed tension values.

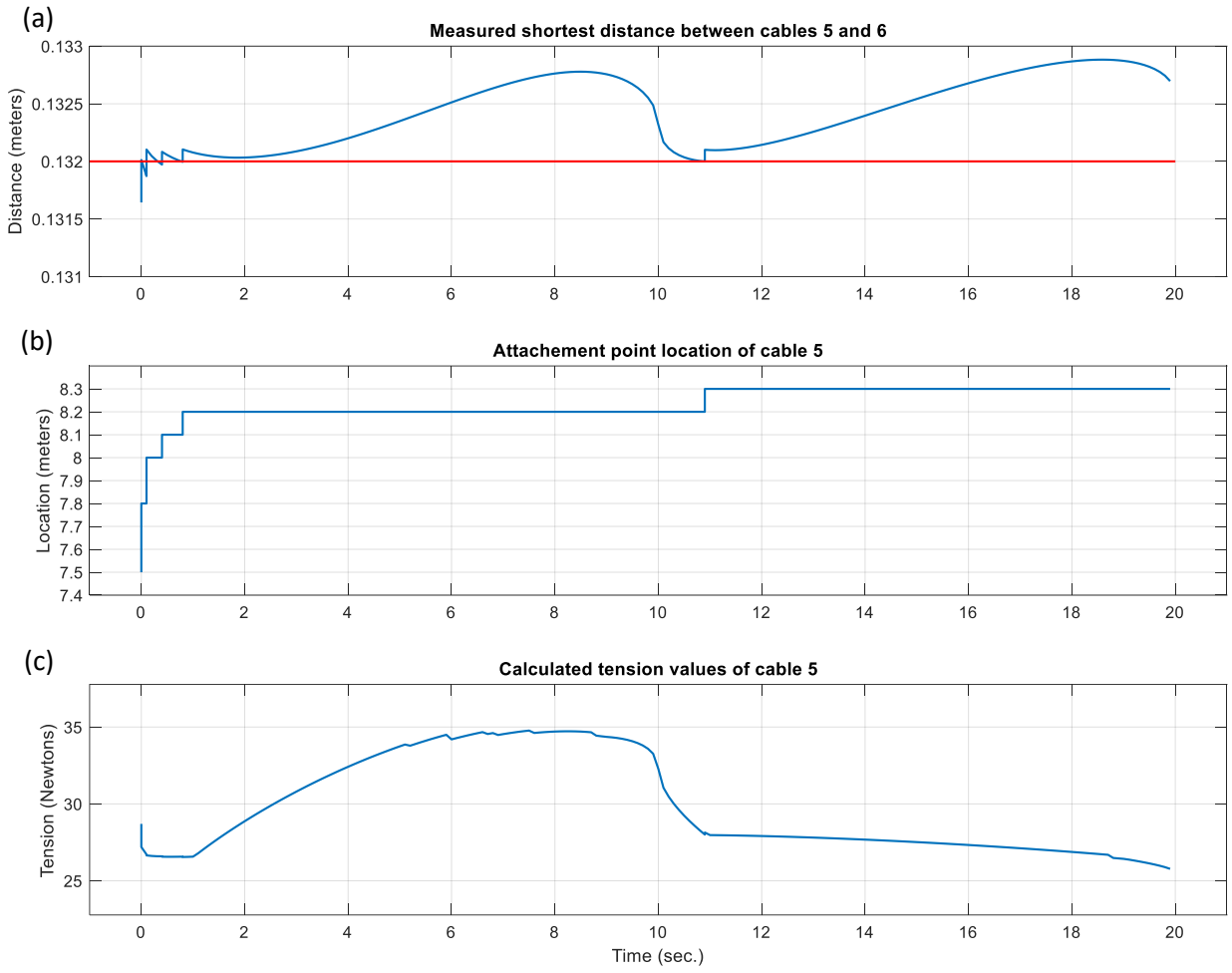

Figure 18 Circular trajectory: (a) measured distance between cables 5 and 6; (b) attachment point location of cable 5; (c) computed tension of cable 5

As shown in Figure 18, the algorithm detected a near collision (distance between cables is less than 0.132 meters) between cables 5 and 6 at t=0, 0.1, 0.4, 0.8 and 10.9 seconds. Also, the algorithm identified that attachment point of cable 5 should be located up since the relocation of cable 5 will increase the distance between the two cables. At t=0, cable 5 attachment point location was initially at 7.5 meters measured from the ground and started to relocate up while the distance between cables 5 and 6 are being computed by the algorithm until it reached 7.8 meters. After that, between 0 and 0.1 seconds, the distance

can be observed to fall again below the allowable minimum threshold value, therefore the attachment point of cable 5 kept relocated up until it reaches 8 meters and then 8.1 meters at 0.4 seconds and finally, 8.2 at 0.8 seconds. The computed distance between the two cables is then observed to be over the allowable limit until t=10.9 seconds, so the attachment point location is relocated again from 8.2 meters to 8.3 meters. In addition, it can be observed from Figure 18(c) that the tension values of the corresponding cable (5), which is relocated to avoid interference with cable 6, has no significant or sudden change in values especially at the relocation times, where the values lies between 25 and 35 Newtons. Figure 19 shows the computed distance between cables 7 and 8 as well as the location of the displaced attachment point of cable 7 and its computed tension values.

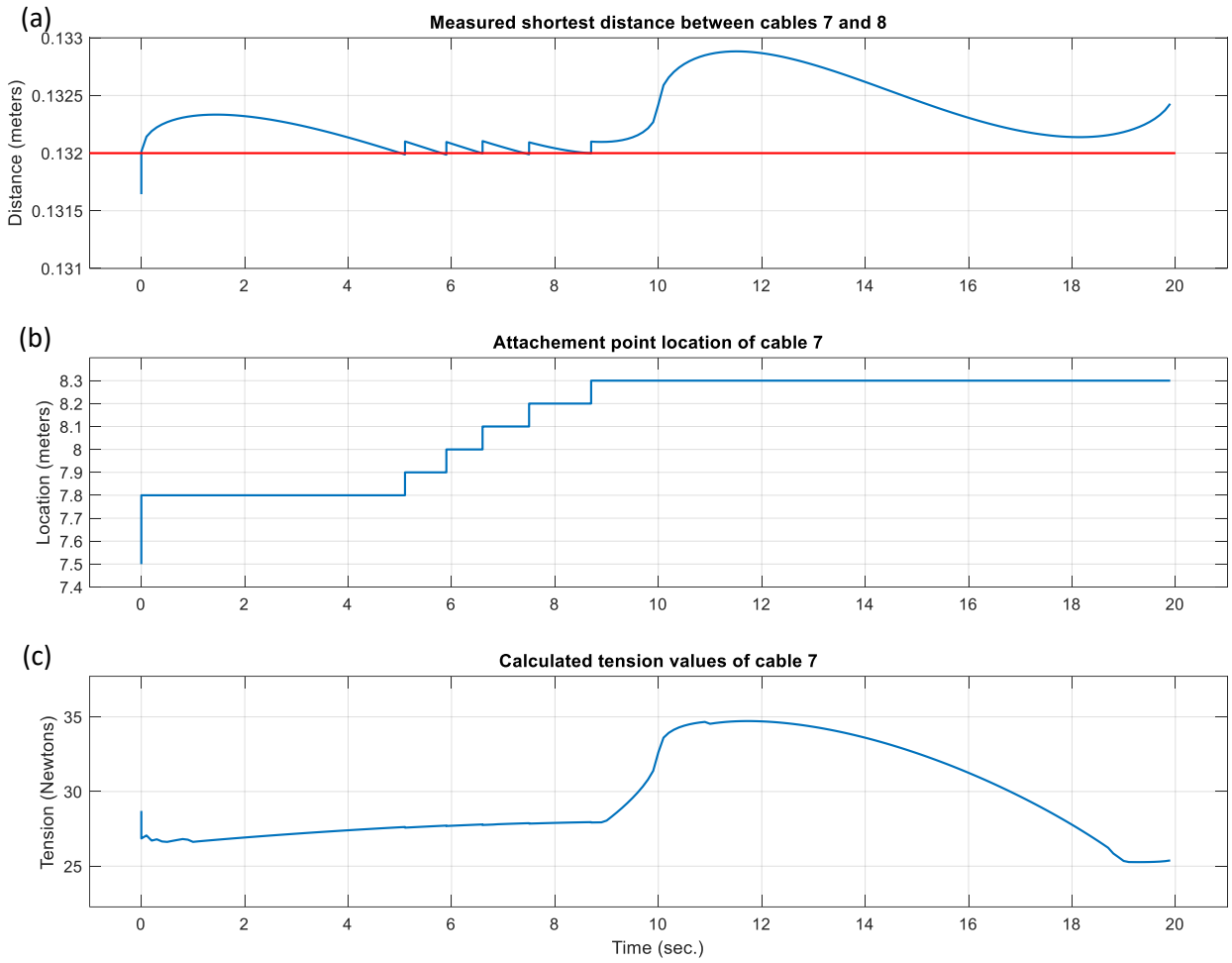

Figure 19 Circular trajectory: (a) measured distance between cables 7 and 8; (b) attachment point location of cable 7; (c) computed tension of cable 7

As shown in Figure 19, the algorithm detected a near collision (distance between cables is less than 0.132 meters) between cables 7 and 8 at t=0, 5.1, 5.9, 6.6, 7.5 and 8.7 seconds. Moreover, the algorithm identified that attachment point of cable 7 should be located up since the relocation of cable 7 will increase the distance between the two cables. At t=0, cable 7 attachment point location was initially at 7.5 meters measured from the ground and started to relocate up while the distance between cables 7 and 8 are being computed by the algorithm until it reached 7.8 meters. After that, the distance can be observed over the allowable minimum threshold value until t=5.1 seconds, therefore the attachment point of

cable 7 kept relocating up until it reaches 7.9 meters at t=5.9 seconds, 8 at t=6.6, 8.1 at t=7.5 and then 8.7 meters at 8.7 seconds. The computed distance between the two cables is then observed to be over the allowable limit until the end. In addition, it can be observed from Figure 19(c) that the tension values of the corresponding cable (7), which is relocated to avoid interference with cable 8, has no significant or sudden change which indicates a smooth transition in the tension values.

In the second trajectory, the end effector performs sinusoidal motion with constant orientation (given in Appendix A). The following figure shows the computed shortest distance between pairs of interfered cables, the recorded position of the corresponding attachment point and the computed tension values for the corresponding cable. Figure 20 shows the computed distance between cables 1 and 2 as well as the location of the displaced attachment point of cable 1 and its computed tension values for a sinusoidal trajectory of the end effector. With the minimum allowable distance (tolerance) between any two cables equal to 0.118 meters during the entire sampling time and due to the chosen path of the end effector, an interference between pair of cables is detected within the trajectory of the mobile platform at different times. For this trajectory, the distance between cables 1 and 2 is detected by the algorithm to fall below the threshold values while the distance between all the other cables were observed to be above the allowable distance and therefore, it was not shown below.

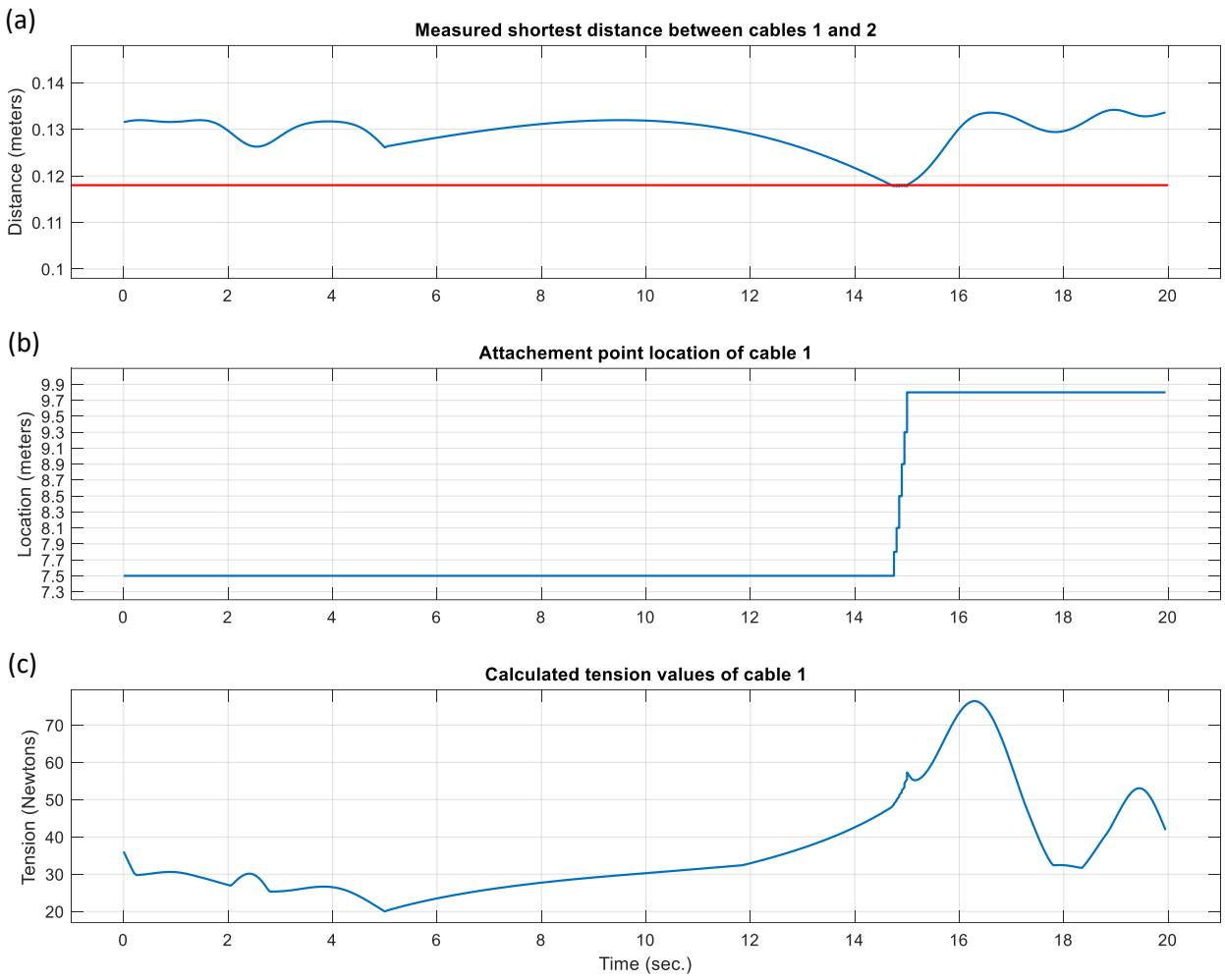

Figure 20 Sinusoidal trajectory: (a) measured distance between cables 1 and 2; (b) attachment point location of cable 1; (c) computed tension of cable 1

As shown in Figure 20, the algorithm detected a near collision (distance between cables is less than 0.118 meters) between cables 1 and 2 at time duration between 14.75 and 15 seconds. Moreover, the algorithm identified that attachment point of cable 1 should be located up since the relocation of cable 1 will increase the distance between the two cables. Cable 1 attachment point location was initially at 7.5 meters measured from the ground and started to relocate up while the algorithm is computing the distance between cables 1 and 2 until it reached 9.8 meters. After that, the distance can be observed over the allowable

minimum threshold value until the end. In addition, it can be observed from Figure 20(c) that the tension values of the corresponding cable (1), which is relocated to avoid interference with cable 2, has no significant or sudden change which indicates a smooth transition in the tension values especially at the relocation times, where the values lies between the lower and upper limits that was defined before.

In the third trajectory, the end effector performs random motion with constant orientation (given in Appendix A). The random trajectory in Cartesian coordinates was generated by MATLAB; however, as mentioned earlier, the trajectory data are available in appendix A in order to allow the reader to be able to replicate the results. The following figure shows the computed shortest distance between pairs of interfered cables, the recorded position of the corresponding attachment point and the computed tension values for the corresponding cable. Figure 21 shows the computed distance between cables 5 and 6 as well as the location of the displaced attachment point of cable 5 and its computed tension values for a random trajectory of the end effector. With the minimum allowable distance (tolerance) between any two cables equal to 0.119 meters during the entire sampling time and due to the chosen path of the end effector, an interference between pair of cables is detected within the trajectory of the mobile platform at different times. For this trajectory, the distance between cables 5 and 6 is detected by the algorithm to fall below the threshold values while the distance between all the other cables were observed to be above the allowable distance and therefore, it was not shown below.

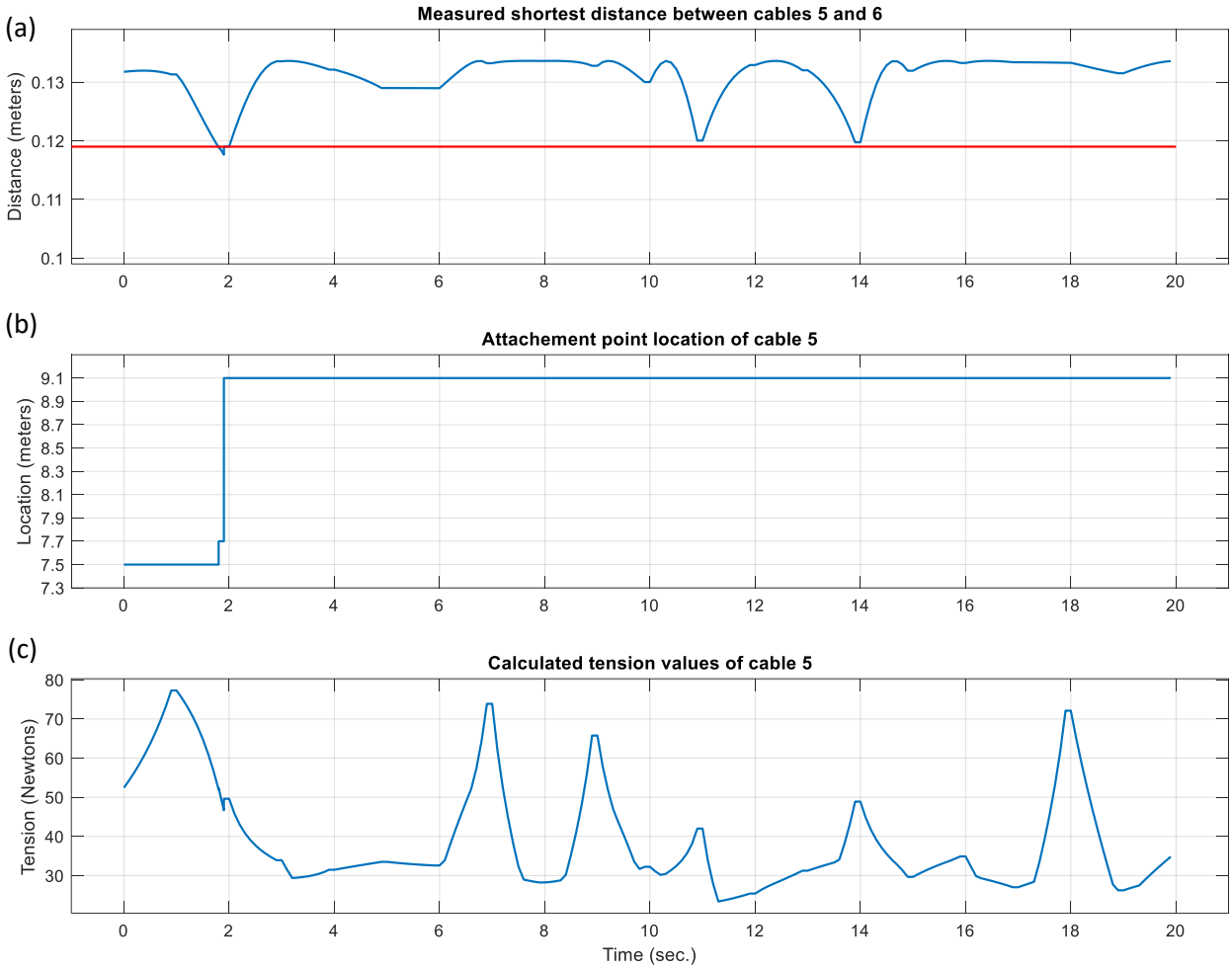

Figure 21 Random trajectory: (a) measured distance between cables 5 and 6; (b) attachment point location of cable 5; (c) computed tension of cable 5

As shown Figure 21, the algorithm detected a near collision (distance between cables is less than 0.119 meters) between cables 5 and 6 at time duration between 1.8 and 1.9 seconds. Moreover, the algorithm identified that attachment point of cable 5 should be located up since the relocation of cable 1 will increase the distance between the two cables. Cable 5 attachment point location was initially at 7.5 meters measured from the ground and started to relocate up while the algorithm is computing the distance between cables 1 and 2 until it reached 7.7 meters at 1.8 seconds. After that, the distance can be observed to fall again below the allowable distance at 1.9 seconds; therefore, the attachment point is

relocated up again until it reaches 9.1 meters. After that, the distance can be observed over the allowable minimum threshold value until the end. In addition, it can be observed from Figure 21(c) that the tension values of the corresponding cable (5), which is relocated to avoid interference with cable 6, has no significant or sudden change which indicates a smooth transition in the tension values especially at the relocation times, where the values lies between the lower and upper limits that was defined before.

4.4. Conclusion

In this chapter, the new idea of reconfiguration is applied for the application of interference detection and avoidance between cables while keeping the end effector trajectory unchanged. The computation approach to measure the shortest distance between two cables in space has been derived using simple and direct method. In addition, the suggested algorithm has been presented and explained by outlining the idea on how to chose the corresponding attachment point to be relocated in case of a near collision.

Three different trajectories have been simulated using the suggested approach and results are presented. The effectiveness of the new theory of reconfiguration has been proofed in figuresFigure 16 -Figure *21* which shows the computed distance between two cables about to collide and how the algorithm detect which cable attachment point is to be relocated as well as its corresponding tension values. Chapter 5 is presents the use of the reconfigurable idea to avoid collision between cables and human.

CHAPTER 5

5. Avoiding interference between cables and human with online reconfiguration

5.1. Introduction

This chapter outlines and discusses the application of the real-time reconfiguration to avoid collision between cables and a virtual human sharing the same workspace with moving parts of the mechanism. This chapter is an extension of chapter 4 where the reconfiguration idea is applied to avoid cables interference while maintain the end effector trajectory unchanged.

In real implementation, a human position and coordinates can be detected by means of wearable sensors or by high definition camera that cover the whole workspace. In this research study, human limbs represented as coordinates of its skeleton is inserted inside the CDPM workspace. An algorithm has been created using MATLAB to compute the shortest distance between all the cables and a virtual human each sampling time and in case of a near collision between any cable and human, the corresponding attachment point is relocated in a direction such that the distance between cable and human is increased. Three different trajectories have been simulated and results are presented to proof the robustness of the suggested approach.

Section 5.2 is dedicated to explain the creation of virtual human inside the workspace. Section 5.3 presents in details the description of the proposed algorithm and simulation results are shown and discussed to demonstrate the effectiveness of the suggested approach.

5.2. Human model

With the aim of verifying the robustness of the proposed approach to avoid collision between cables and an operator sharing the same workspace of the mechanism in a dynamic environment, a simulation was conducted where a human skeleton is inserted within a colliding distance with cables as shown in Figure 22. A near collision is detected if the shortest distance between any cable and a human limb, which is represented as coordinates of a skeleton, reaches a specific threshold value. In real implementation, human posture and position recognitions can be determined by mainly two methods. First, wearable devices sensors attached on the human limbs [115] such as Xsens sensors [116] and second, via camera that cover the entire installation space and can provides information like distance, position and orientation of existing dynamic objects [117,118] such as standard motion capture [119]. In this research project, the human limbs are considered straight objects in 3D [120,121] walking within a dynamic environment where the end effector is moving to perform a specific task. The suggested approach of interference detection and avoidance will be tested by performing a simulation of three different trajectories while the virtual operator is sharing the same workspace.

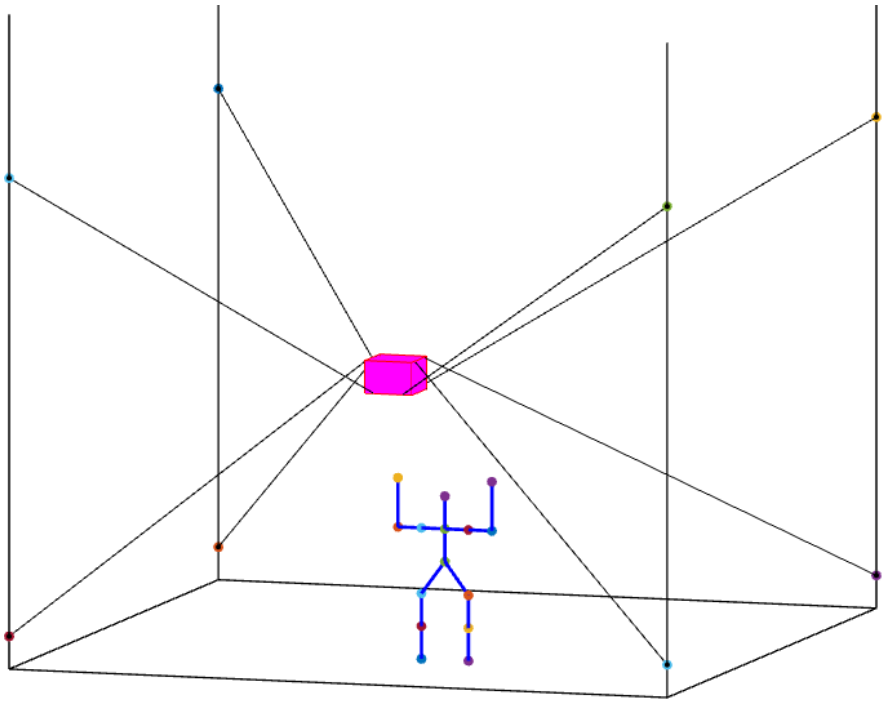

Figure 22 Virtual human representation

5.3. Cables-human interference detection and avoidance

On of the key contribution of this study is the usage of online reconfiguration by changing the location of the attachment points of the cables on the fixed rails to avoid a near collision between a cable and human limb. A Matlab code was generated to use the idea of reconfiguration in detecting and eliminating cable-human interference in real time, as shown in the flow chart of the algorithm presented in Figure 23.

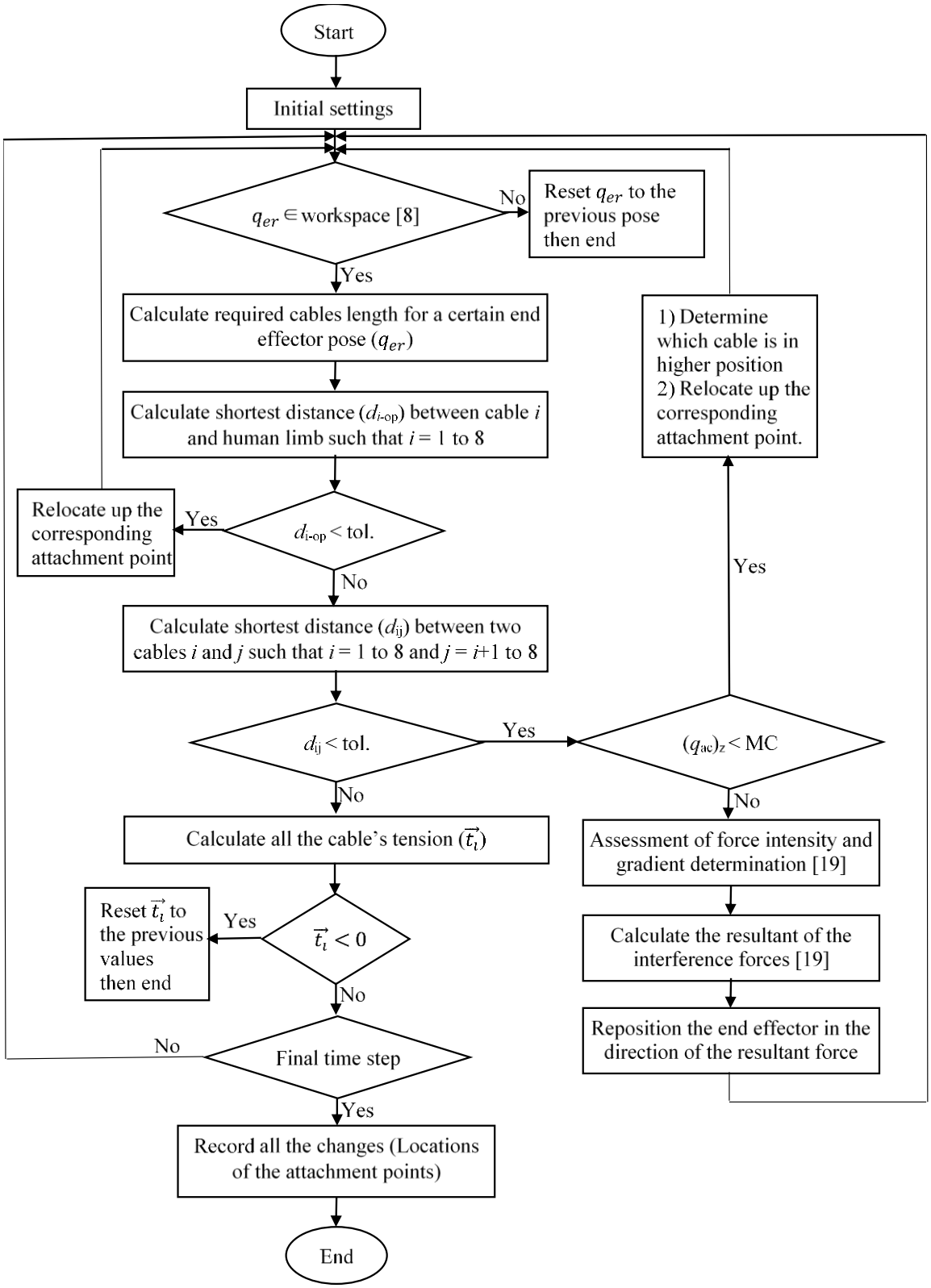

Figure 23 Real time algorithm for detecting and eliminating cable-human interference

At each sampling time, the proposed algorithm computes the shortest physical distance ($d_{i\text{-}op}$) between all the cables and a human limb such that i = 1 to n and compares it with a threshold value (tolerance) that is defined by the user. The shortest distance computation depends on the position of the attachment points of the cables on the fixed rails, the pose of the mobile platform, the location of the anchor points on the end effector and of course the position of human limb. In case of a near collision between any cable and human, the algorithm computes $\vec{\boldsymbol{L}}_1(w)$ and $\vec{\boldsymbol{L}}_2(s)$ such that $\vec{\boldsymbol{L}}_1(w)$ represents cable i and $\vec{\boldsymbol{L}}_2(s)$ is the human limb (as shown in Figure 14) and hence compute shortest distance ($\vec{\mathbf{v}}(w,s)$). Accordingly, it moves up the corresponding attachment point on the rail of cable i by a step Δq that is defined by the user. Therefore, the new location of the corresponding attachment point is updated and recorded.

In order to verify the proposed approach, a simulation was conducted using the above algorithm for three different trajectories with three different allowable distance between human and cables where a virtual human is inserted within a colliding distance with cables and the results are shown below. Figure 24 shows the measured distance between cable 8 and human arm, attachment point's location of cable 8 and the computed tension of cable 8 where the end effector performs constant orientation circular trajectory. The minimum allowable distance between any cable and a human limb is set to be 0.35, 0.45 and 0.5 meters for the circular trajectory, sinusoidal trajectory and random trajectory respectively.

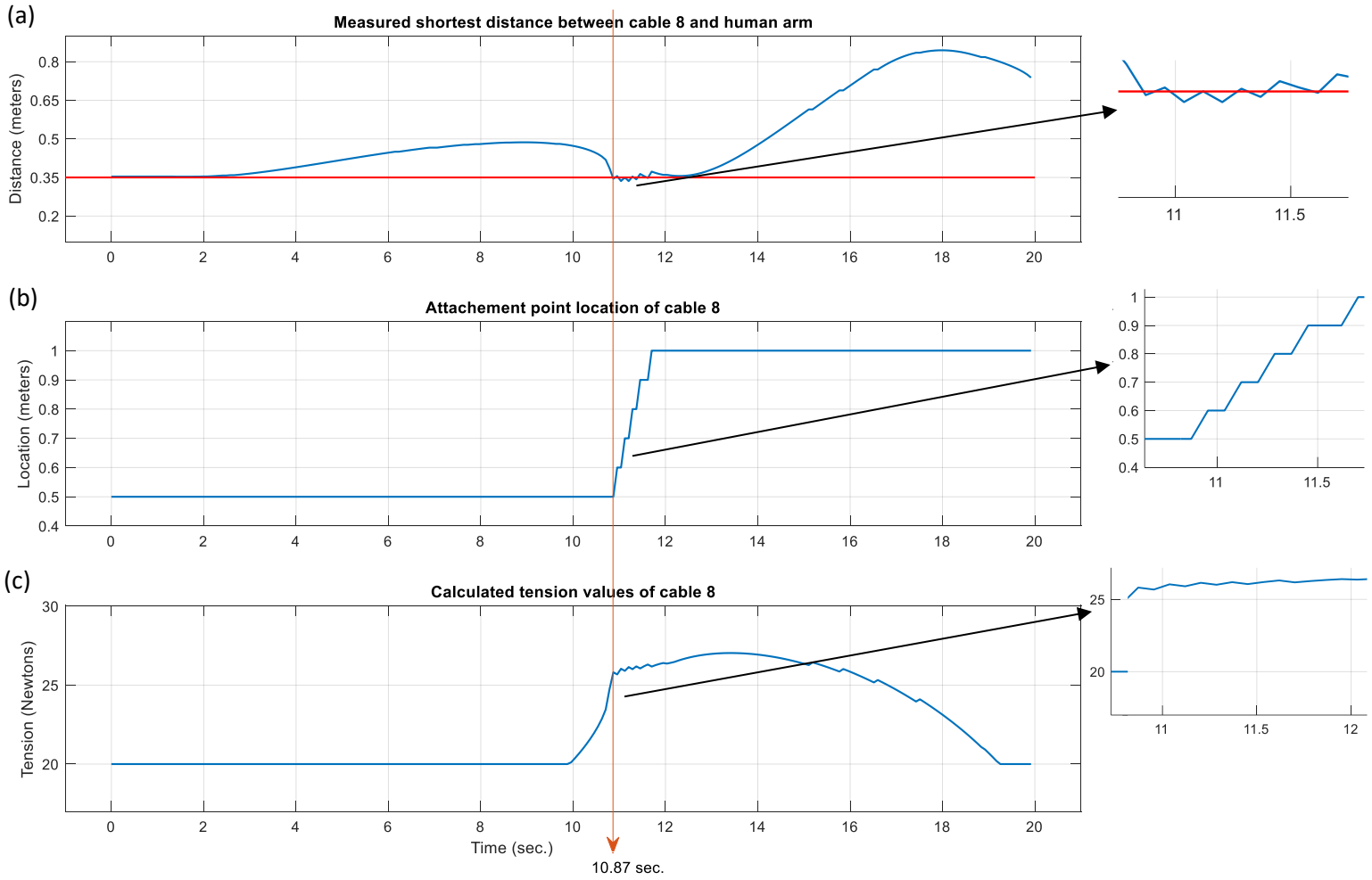

Figure 24 Circular trajectory: (a) measured distance between cable 8 and human arm; (b) attachment point's location of cable 8; (c) computed tension of cable 8

As shown in Figure 24(a), the algorithm detected the first shortest distance (below 0.35 meters) between human limb and cable 8 at 10.87 seconds. Accordingly, the end effector was restricted to pause its motion and the attachment point of the corresponding cable, which is cable 8 in this case, is relocated up (Figure 24(b)). The new shortest distance is computed and the trajectory of the end effector is kept unchanged. Due to the motion of the human arm and the end effector simultaneously, the shortest distance is noticed to keep

falling below the threshold value and thus the algorithm kept pausing the end effector motion and relocate the attachment point until 11.7 seconds. After that, the measured distance is seen to be increasing until the end of the simulation time. Also, the computed tension in cable 8 is shown in Figure 24(c), where at the duration of the near collision (between 10.87 and 11.7 seconds), the values of the tension were ranging between 25 and 26 Newtons. These tension values indicates a smooth transition of the attachment point in terms of dynamics. For the second simulation, the end effector performs a sinusoidal constant orientation trajectory where the minimum allowable distance between human and cables is set to be 0.45 meters. The computed distance between cable 8 and human arm, attachment point's location of cable 8 and the computed tension of cable 8 are shown in Figure 25 below.

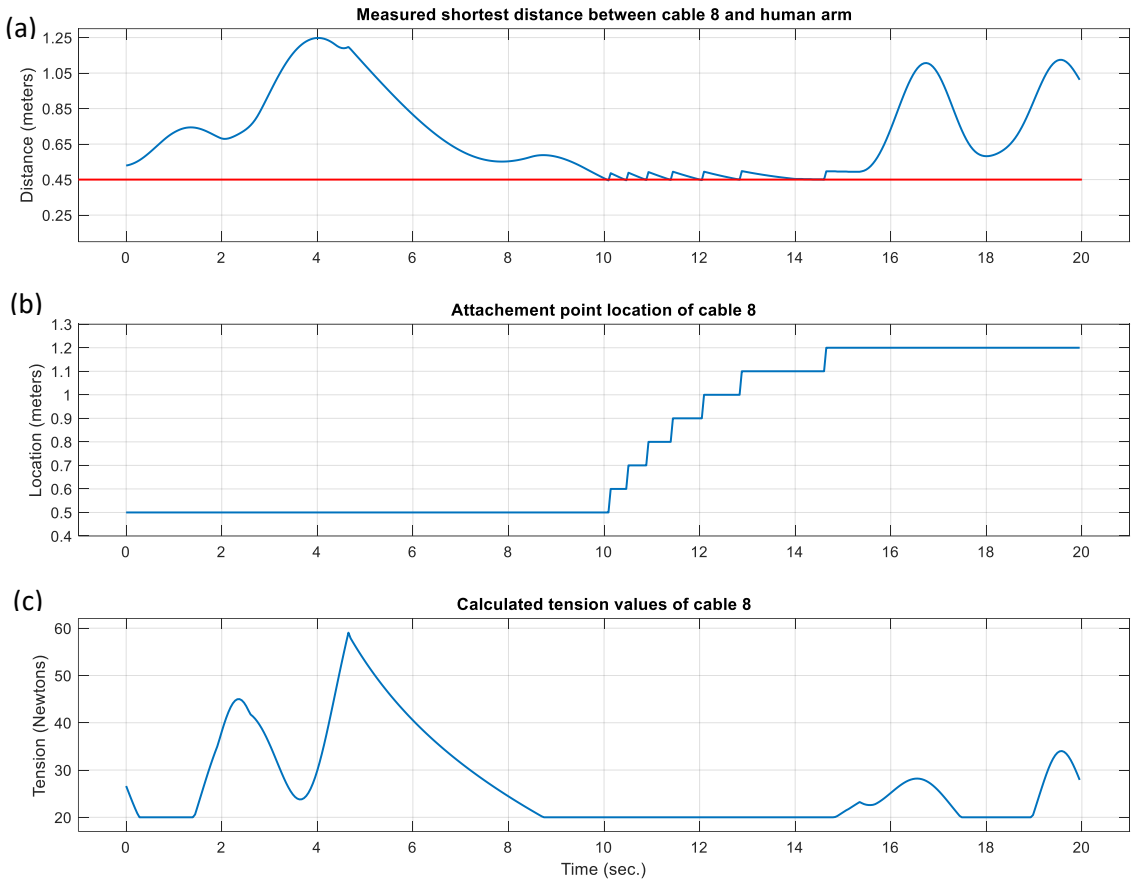

Figure 25 Sinusoidal trajectory: (a) measured distance between cable 8 and human arm; (b) attachment point's location of cable 8; (c) computed tension of cable 8

As shown in Figure 25(a), the algorithm detected the first shortest distance (below 0.45 meters) between human limb and cable 8 at 10.05 seconds. Accordingly, the end effector was restricted to pause its motion and the attachment point of the corresponding cable, which is cable 8 in this case, is relocated up (Figure 25(b)). Due to the motion of the human arm and the end effector simultaneously, the shortest distance is noticed to keep falling below the threshold value and thus the algorithm kept pausing the end effector motion and relocate the attachment point until 14.6 seconds. After that, the measured distance is observed to be over the allowable limit until the end of the simulation time. Also, the

computed tension in cable 8 is shown in Figure 25(c), where at the duration of the near collision (between 10.05 and 14.6 seconds), the values of the tension were constant at 20 Newtons.

For the third simulation, the end effector performs a random constant orientation trajectory where the minimum allowable distance between human and cables is set to be 0.5 meters. The random trajectory in Cartesian coordinates were generated by MATLAB tools. The computed distance between cable 8 and human arm, attachment point's location of cable 8 and the computed tension of cable 8 are shown in Figure 26 below.

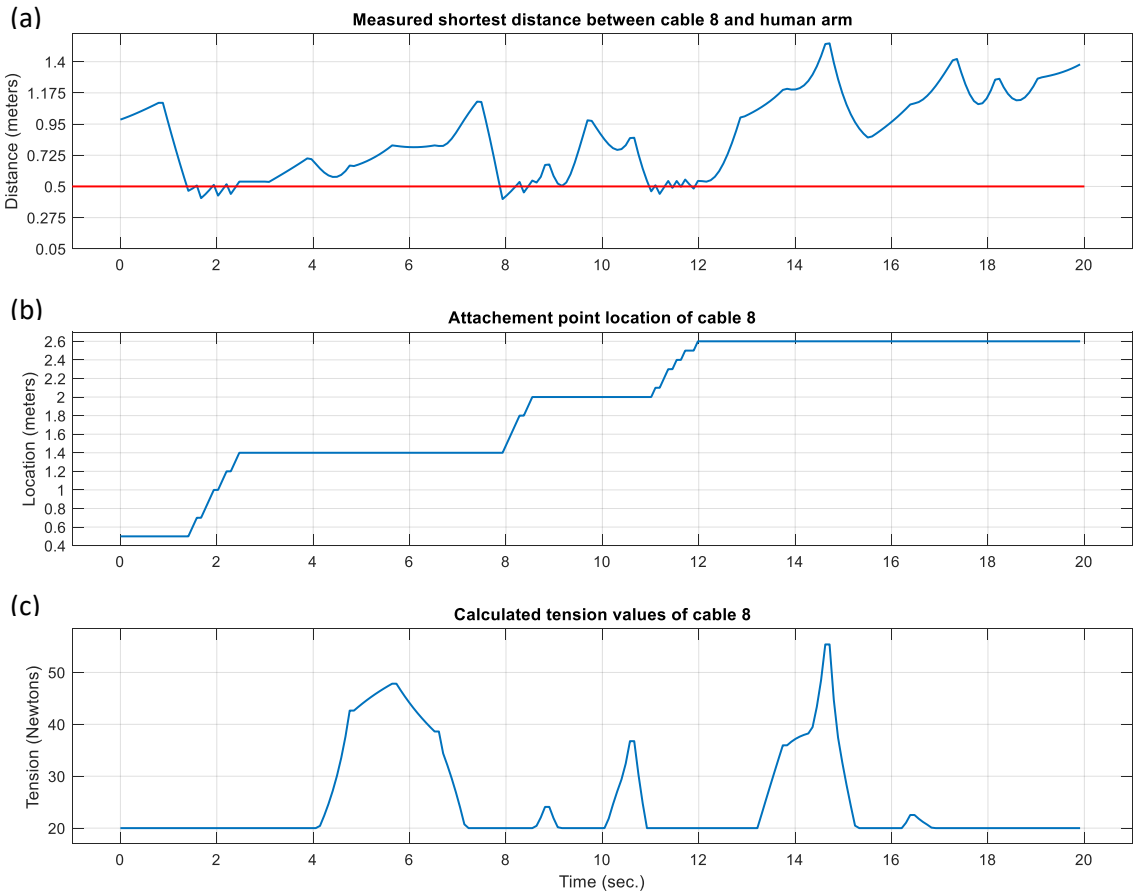

Figure 26 Random trajectory: (a) measured distance between cable 8 and human arm; (b) attachment point's location of cable 8; (c) computed tension of cable 8

As shown in Figure 26, the algorithm detected the first near collision (distance less than 0.5 meters) between cable 8 and human arm at t=1.4 until t=2.4 seconds. At t=0, cable 8 attachment point location was initially at 0.5 meters measured from the ground and started to relocate up while the distance between cable 8 and human arm is being computed by the algorithm until the attachment point location of cable 8 reached 1.4 meters. After that, between 7.9 and 8.5 seconds, the distance can be observed to fall again below the allowable minimum threshold value, therefore the attachment point of cable 8 kept relocated up until it reaches 2 meters and then between 11 and 11.98 seconds it finally reaches 2.6 meters. The computed distance between the cable 8 and the human arm is then observed to be over the allowable limit until the end time. In addition, it can be observed from Figure 26(c) that the tension values of the corresponding cable (8), which is relocated to avoid interference with human arm, has no significant or sudden change in values especially at the relocation times, where the values is observed to be 20 Newtons.

5.4. Conclusion

In this chapter, the new idea of reconfiguration is applied again for the application of interference detection and avoidance between cables and human sharing the same workspace of the mechanism while keeping the end effector trajectory unchanged. The computation approach to measure the shortest distance between cables and human limbs is similar to the approach discussed in chapter 4.

Three different trajectories have been simulated using the suggested approach and results are presented. The effectiveness of the new theory of reconfiguration has been proofed in figures Figure 24 - Figure 26 which shows the computed distance between cables and human

limbs about to collide and how the algorithm relocate the attachment point. Due to the real-time reconfiguration of the CDPM, workspace mapping will accordingly change. Hence chapter 6 is dedicated to present different types of workspaces for general CDPM and the different methods used for mapping the workspace. In addition, the formulation and method of computation of the workspace of the suggested reconfigurable CDPM is presented and the results of real-time change in workspace due to the reconfiguration is discussed.

CHAPTER 6

6. Real-time workspace analysis

6.1. Introduction

This chapter outlines and discusses the change of the CDPM workspace due to real-time reconfiguration of the attachment points on the rails, which was presented in chapter 4 and 5. Workspace analysis is a critical topic when designing CDPM since it describes the ability of the mobile platform to translate and/or rotate under certain constraints. In fact, workspace is one of the main reasons CDPMs have attracted much attention in the recent years over conventional parallel manipulators.

CDPM workspace has many classifications. However, the most general definition could be expressed as all the set of poses where the end effector can reach while maintaining a positive tension among all the cables. In this research study, the constant-orientation wrench feasible workspace is mapped due to relocation of the attachment points where a comparison between initial and final workspace is presented and discussed.

Section 6.2 outlines different types of workspace of CDPM and different methods to compute it. Section 6.3 is dedicated to describe the procedure for mapping the workspace and hence simulation results are presented and discussed in 6.4.

6.2. Workspace of CDPM

Workspace analysis is a very critical step in designing any mechanism in order to assesse its ability to translate and/or rotate and then be able to execute the requested task. Workspace in CDPM as a general rule is defined as all the positions and orientation that the end effector can reach where any set of external wrench acting on the end effector can be sustained by positive tension in all the cables [122,123]. Adding certain conditions and limitation on the latter definition lead to many classifications of CDPM workspace [124]. Duan et al. [125] categorised the workspace of CDPM into five main divisions, which are static equilibrium workspace, wrench closure workspace, wrench feasible workspace, dynamic workspace, and collision-free workspace. The static equilibrium workspace is defined as all the poses (position and orientation) that the end effector can reach where all the cables are in tension and only gravity is considered without any external wrenches [126]. This definition may be expressed mathematically as:

$$\widehat{\boldsymbol{w}}\vec{\boldsymbol{t}} + \vec{\boldsymbol{w}}_{\boldsymbol{J}} = \vec{\mathbf{0}}_6 \text{ , with } \vec{\boldsymbol{t}} > 0 \qquad 6\text{-}1$$

where, $\widehat{\boldsymbol{w}}, \vec{\boldsymbol{t}}, \vec{\boldsymbol{w}}_{\boldsymbol{J}}$ and $\vec{\mathbf{0}}_6$ are the structure matrix, cables tension vector, external wrench and zero vector respectively as been discussed earlier in section 3.3. The extra condition in case of static equilibrium workspace is that $\vec{\boldsymbol{w}}_{\boldsymbol{J}}$ vector contains only the weight of the end effector due to gravity acting in its perspective direction and zero elsewhere (i.e. no external forces or moments acting on the end effector).

The wrench closure workspace of CDPM is defined as all the poses that the end effector can reach where any set of external wrench acting on the end effector can be sustained by

at least one set of positive tension vector in all the cables [127]. The mathematical representation of wrench closure workspace is the same as equation 6-1, where $\vec{w}_J$ in this case is a vector contains external forces and/or moments acting on the end effector beside the weight of the end effector itself.

The wrench feasible workspace of CDPM is defined as all the poses that the end effector can reach where any set of external wrenches acting on the end effector can be sustained by at least one set of positive tension vector in all the cables. However, the tension vector in all the cables is limited between lower and upper values [128] where each cable can have its own boundary values (i.e. it is not necessary to specify one limit for all the cables). The mathematical representation of wrench feasible workspace is represented as follow:

$$\widetilde{w}\vec{t} + \vec{w}_J = \vec{0}_6 \text{ , with } t_{min.} < \vec{t} < t_{max.} \quad 6\text{-}2$$

where $t_{min.}$ and $t_{max.}$ are the minimum and maximum values for the cables tension respectively.

The dynamic workspace of CDPM is defined as all the poses that the end effector can reach where any set of external wrench acting on the end effector can be sustained by at least one set of positive tension vector in all the cables with lower and upper values and in addition with at least one kinematic state (position, velocity, and acceleration) [129–131]. This definition may be expressed mathematically as follow [132]:

$$\widetilde{w}\vec{t} + \vec{w}_J + \widetilde{M}\ddot{\vec{q}}_{er} + \vec{C}(\dot{\vec{q}}_{er}, \vec{q}_{er}) = \vec{0}_6 \text{ , with } t_{min.} < \vec{t} < t_{max.} \quad 6\text{-}3$$

where $\widetilde{M}$, $\ddot{\vec{q}}_{er}, \dot{\vec{q}}_{er}, \vec{q}_{er}$ and $\vec{C}$ are the inertia matrix, end effector generalized coordinates acceleration vector, end effector generalized coordinates velocity vector, end effector

generalized coordinates vector and the centrifugal and Coriolis force vector respectively. It is important to note that $\vec{w}_J$ includes both external wrench vector and the gravitational force vector.

Finally, the collision-free workspace of CDPM is defined as all the poses that the end effector can reach where there is no interference between cables and itself, cables and end effector, cables and the environment or end effector and the environment [87,125,133]. In this research project, new condition to the latter definition is added which is avoid collision between cables and an operator sharing the same workspace while the mechanism is moving.

In order to map any of the previously mentioned workspaces, its perspective cables tension distribution equation that is represented in equations (6-1 till 6-3) has to be solved first. Many methods has been presented to solve for cables tension distribution equation such as linear programming [134,135], quadratic programming [136,137], non-linear programming [138,139], closed-form solution [8,140,141] and gradient-based optimization [110,142,143]. Some other methods have been reported to solve for cables tension distribution equation, however, the most famous ones are listed in this thesis. Bo et al. [144] solved the cables tension distribution equation for six degrees of freedom cable-driven parallel manipulator driven by eight cables using a rapid optimization method based on linear programming. Despite reporting that using linear programming method to solve for the cables tension distribution equation in CDPM suffer from discontinuity that may lead to vibration issue [70,145,146] and is not capable for real-time computation [35], the authors demonstrated the opposite [144]. They concluded that the proposed method for optimizing the tension distribution of CDPM with redundant cables is rapid and showed

computational efficiency where it can be executed in real time and the results of the cables tension distribution values are continuous in all of the simulation trials even if the tension distribution may be discontinuous in theory [147]. Bryson et al. [148] solved the wrench closure workspace for three DOF mechanism driven by four cables to actuate a robot leg to perform a walking-gait motion. Experimental and theoretical results were presented in order to proof the suggested approach. Again, the cable tensions distribution problem were computed using linear programming to minimize an objective function represented in the summation of all the cable tensions subjected to equality constraints. The authors confirmed that theoretical results from linear optimization is consistent with experimental results. Song et al. [149] solved wrench feasible workspace by computing cable tensions distribution using linear programming algorithm for a fully constrained six DOF mechanism driven by eight cables. The authors concluded that the proposed tension distribution method is continuous and real-time capable by comparing the results with two other methods which are minimum norm method [19,150,151] and safety tension method [36]. The required mean time for the suggested algorithm to reach a feasible solution was 0.002 seconds compared to 0.0052 seconds for the minimum norm and 0.0071 seconds for the safe tension. The computation process was implemented in MATLAB with Intel Core i5-3470, 3.2 GHz, and 16G RAM.

6.3. Online workspace mapping

In this study, the constant-orientation feasible workspace is mapped by satisfying equation 6-2 by testing a 3D grid of points lying within the physical limits of the mechanism as shown in Figure 27.

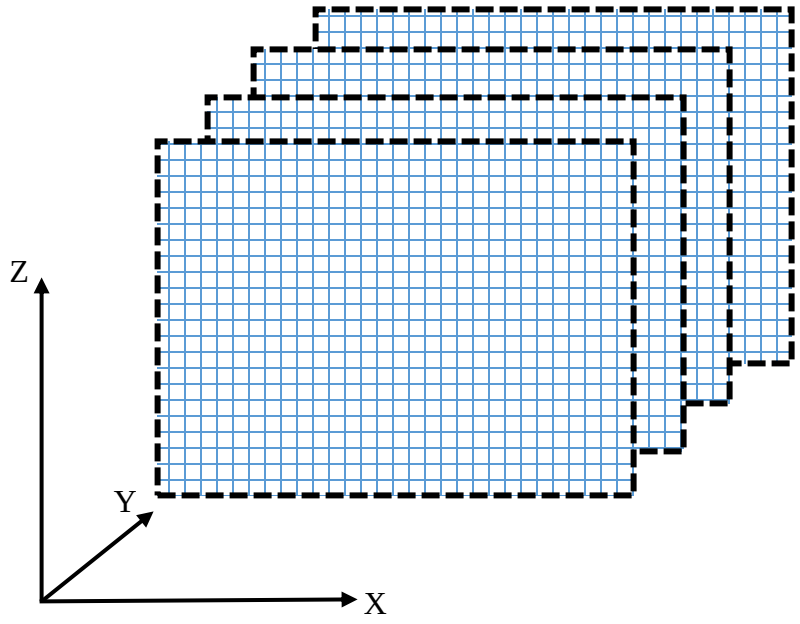

Figure 27 3D grid of points

To map the reconfigurable mechanism workspace, the computational algorithm is proposed based on linear programming and the procedures are presented as follows (referring to Figure 28):

1) Set the first point in the grid as the pose of the end effector.
2) Compute the coordinates of the anchor points on the end effector (B_i).
3) Compute the vector $\vec{\boldsymbol{u}}_i$.
4) Compute the vector $\vec{\boldsymbol{r}}_i$.
5) Construct the structure matrix using $\vec{\boldsymbol{u}}_i$ and $\vec{\boldsymbol{r}}_i$.
6) Using linear programming, if the tension distribution satisfies equation 6-2, the pose is included in the wrench feasible workspace. Otherwise, proceed to next pose.

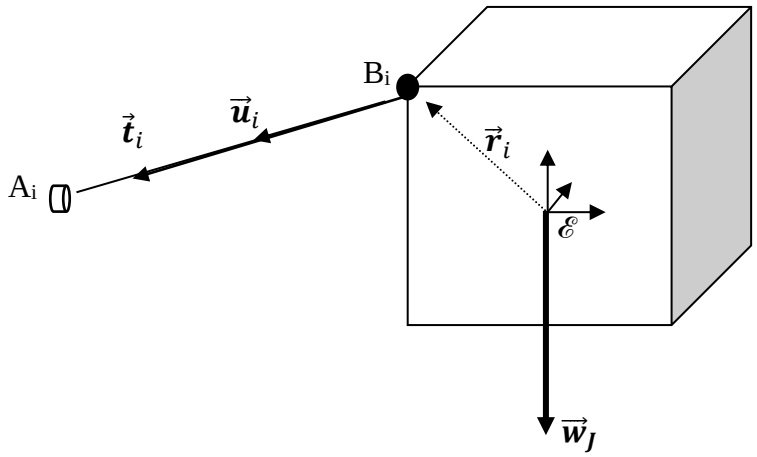

Figure 28 Free body diagram of the end effector

Linear programming was chosen to find a feasible solution (if one exist) since it has been reported previously that its computational speed is fast and is capable to cover the entire workspace unlike other methods such as quadratic programming and closed-form [35]. In addition it satisfies the continuity condition when solving cables tension distribution [149]. The span between grid points was set to 0.1 meters and a point is recorded if a feasible solution is found. With respect to Equation 6-2, the external wrench in this study is set to 25 N acting in the negative Z direction, which represents the weight of the mobile platform. In addition, the allowed upper and lower tensions induced within the eight cables were set to 120 N and 20 N respectively. It is also possible to set specific upper and/or lower values for each cable separately. The constant-orientation feasible workspace was mapped for every change occurring in any of the attachment points on the rails. However, the initial and final workspaces are shown in this study for the sake of comparison.

6.4. Simulation results

In this section, simulation results are presented to verify the aforementioned procedure to map the constant-orientation wrench feasible workspace for the reconfigurable spatial CDPM. For each example, the initial and final workspace will be presented in one figure where each figure is consist of 8 subfigures which are the 3D view of the workspace, the front view (X-Z), side view (Y-Z) and top view (X-Y) for both initial and final workspace. The initial and final workspace mapping are presented for the three different trajectories performed in chapter 3. Of course, the workspace mapping depends mainly on the architecture of the mechanism and external wrench (i.e. dimensions, location of the attachment points on the rails, location of anchor points on the end effector and forces/moments acting on the end effector) and does not depends on the trajectory of the end effector. However, the online reconfigurable method changes the architecture of the mechanism in real-time to avoid cable-cable and/or cable-human interference. Accordingly, the workspace mapping will definitely change and thus presenting the differences in this section.

6.4.1. Circular trajectory “avoid cable-cable interference”

Figure 29 presents the initial and workspace mapping due to the real-time reconfiguration of the mechanism while the end effector performs circular motion.

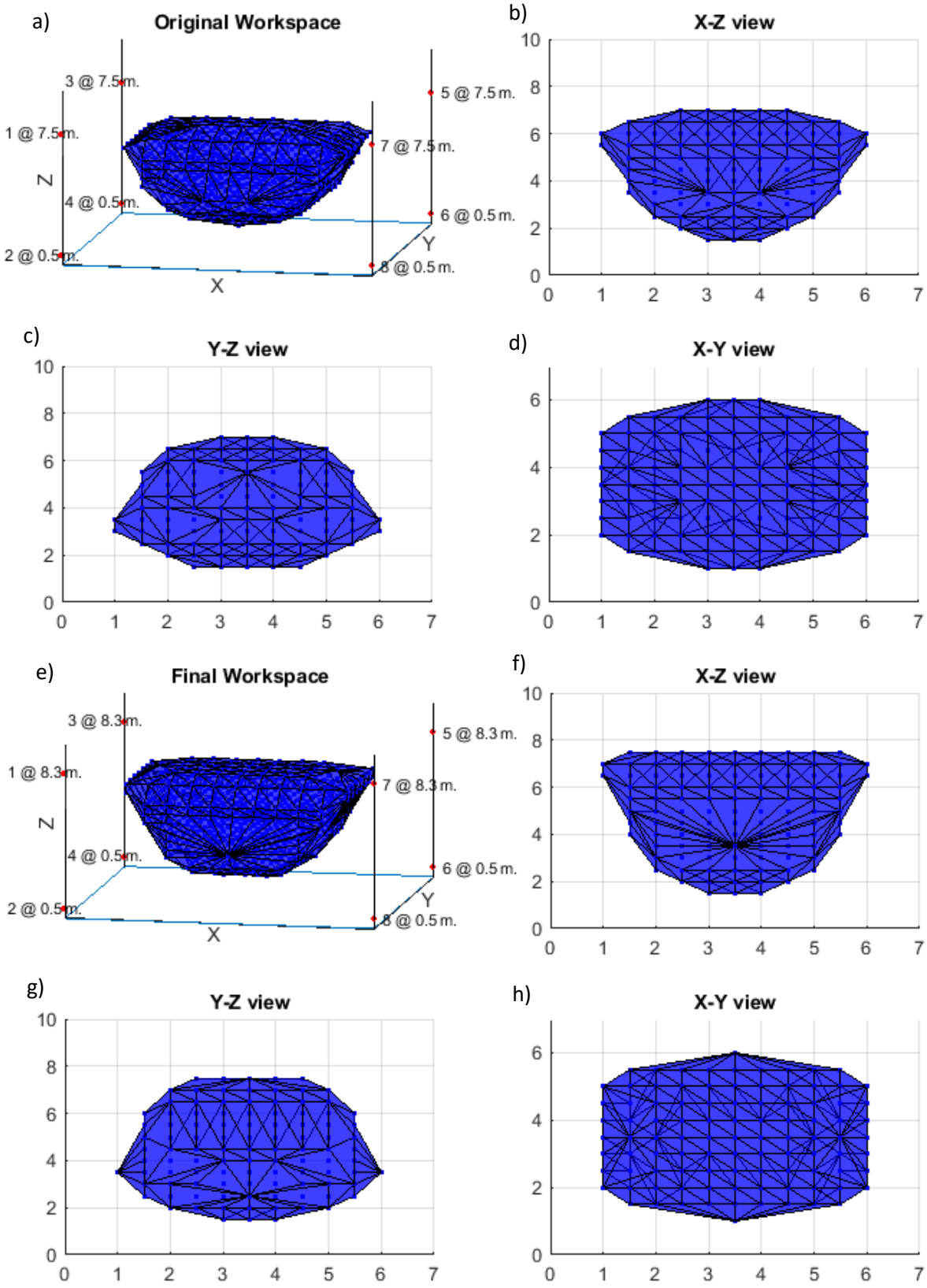

Figure 29 Circular trajectory(Cable-cable collision): (a) Initial workspace 3D, (b) Front view, (c) Side view, (d) Top view, (e) Final workspace 3D, (f) Front view, (g) Side view, (h) Top view

In this simulation results presented in Figure 29, the change occurred in the workspace followed a relocation of the attachment points on the rails to avoid collision between cables while the end effector trajectory kept unchanged. The initial location of the upper attachment points (1, 3, 5 and 7) were at 7.5 meters and relocated by the end of the simulation to 8.3 meters for all of them. It can be observed from the 3D views (Figure 29 (a) and (e)) that the final workspace is slightly increased and expanded on the top part compared to the initial workspace. This observation can be seen clearly when comparing between the X-Z views (Figure 29 (b) and (f)), where the top part in the final workspace has increased and gain more volume on the left and right parts. This remark can be explained due to the relocation of the four upper attachment points. On the other hand, it can be observed that there was no noteworthy change between the initial and final workspace when comparing the X-Y views (Figure 29 (d) and (h)) or the Y-Z views (Figure 29 (c) and (g)).

6.4.2. Sinusoidal trajectory “avoid cable-cable interference”

Figure 30 presents the initial and workspace mapping due to the real-time reconfiguration of the mechanism while the end effector performs sinusoidal motion.

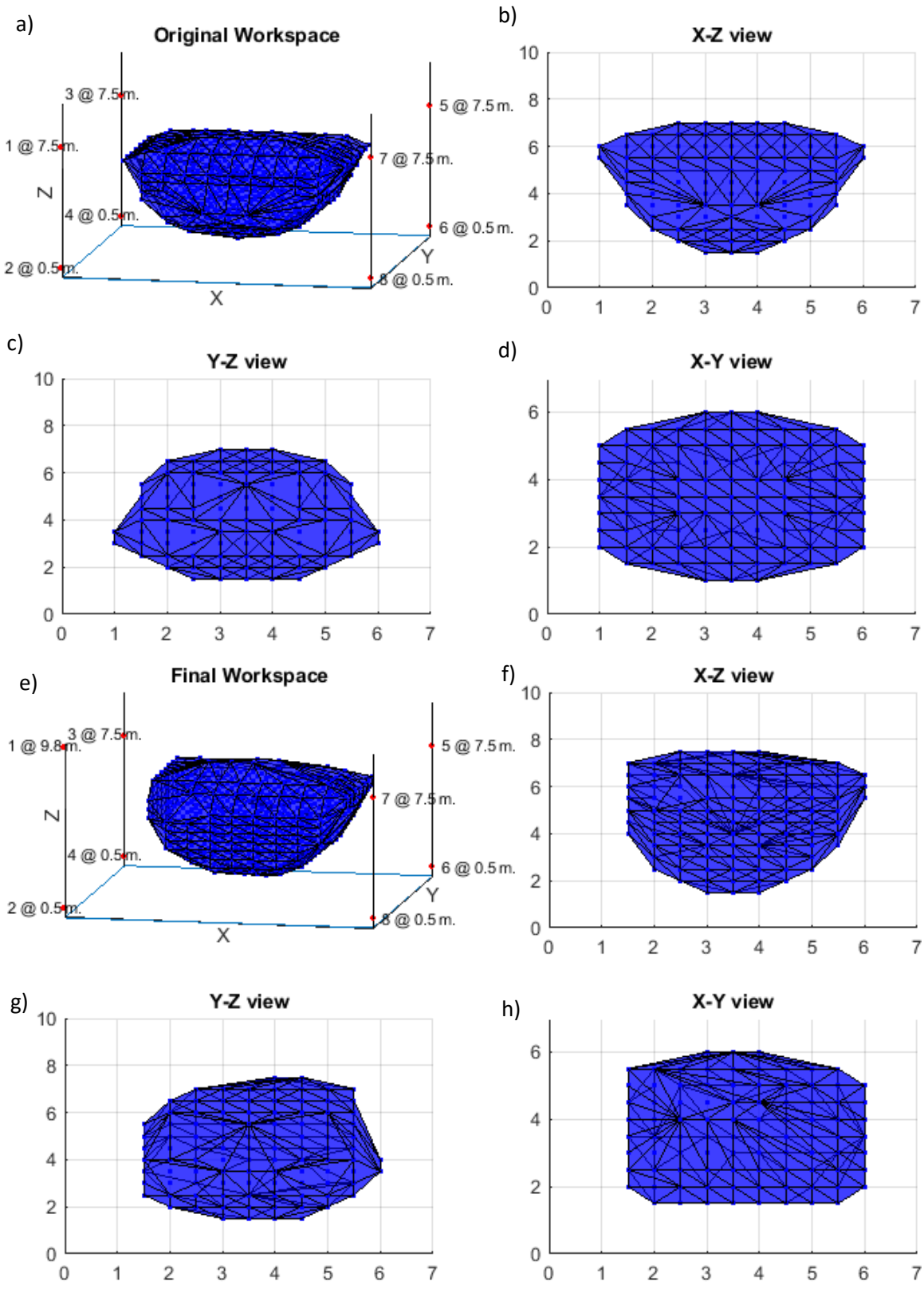

Figure 30 Sinusoidal trajectory(Cable-cable collision): (a) Initial workspace 3D, (b) Front view, (c) Side view, (d) Top view, (e) Final workspace 3D, (f) Front view, (g) Side view, (h) Top view

In this simulation results presented in Figure 30, the change occurred in the workspace followed a relocation of the attachment points on the rails to avoid collision between cables while the end effector trajectory kept unchanged. The initial location of the upper attachment point (1) was at 7.5 meters and relocated by the end of the simulation to 9.8 meters. It can be observed from the 3D views (Figure 30 (a) and (e)) that the final workspace is slightly changed compared to the initial workspace. This observation can be seen clearly when comparing between the X-Z views (Figure 30 (b) and (f)), where the left part in the final workspace has decreased and lost some volume, but on the right parts, it can be noticed almost the same. On the other hand, it can be observed that there was a noticeable reduction change between the initial and final workspace when comparing the X-Y views (Figure 30 (d) and (h)) and the Y-Z views (Figure 30 (c) and (g)).

6.4.3. Random trajectory “avoid cable-cable interference”

Figure 31 presents the initial and workspace mapping due to the real-time reconfiguration of the mechanism while the end effector performs random motion.

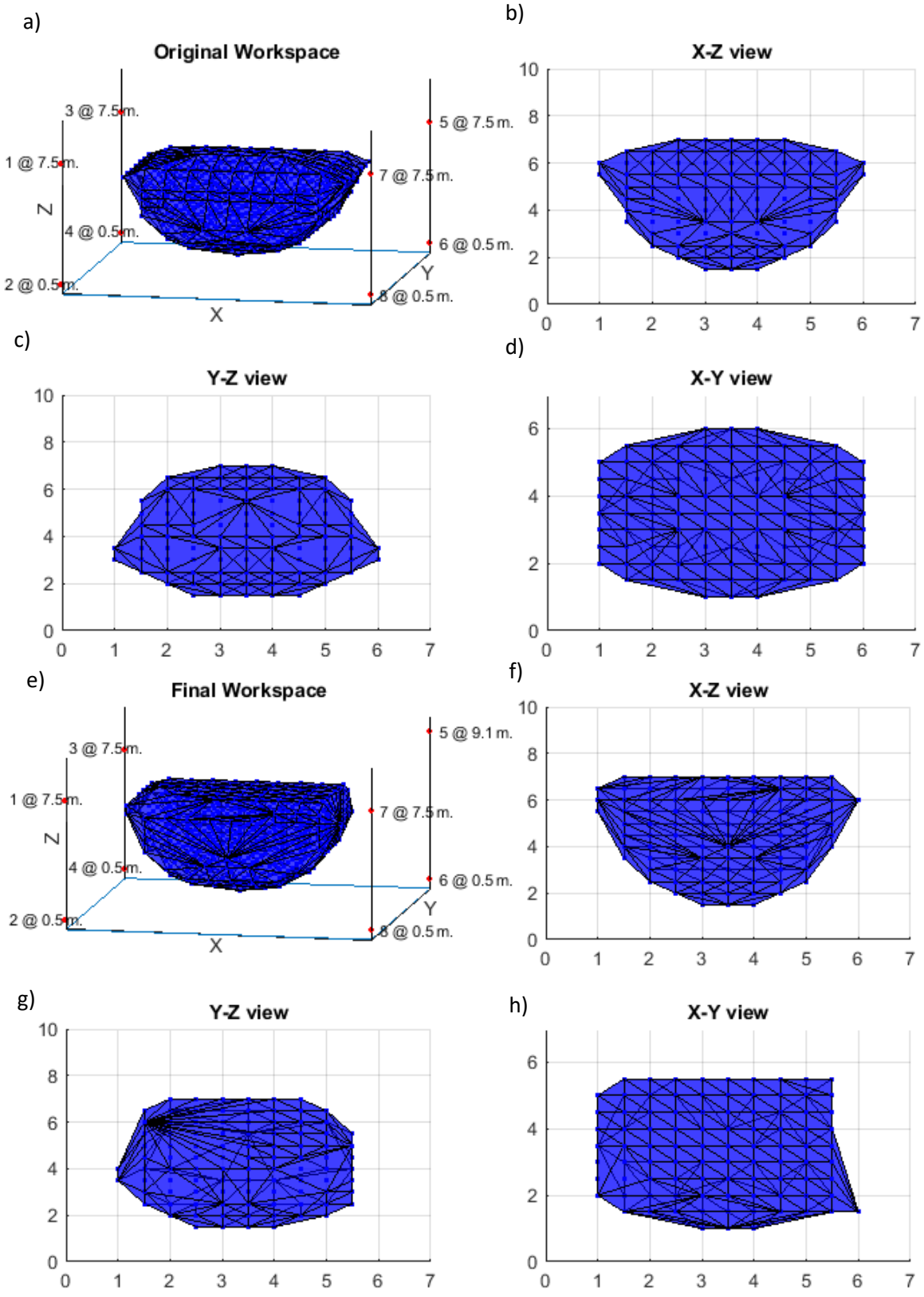

Figure 31 Random trajectory(Cable-cable collision): (a) Initial workspace 3D, (b) Front view, (c) Side view, (d) Top view, (e) Final workspace 3D, (f) Front view, (g) Side view, (h) Top view

In this simulation results presented in Figure 31, the change occurred in the workspace followed a relocation of the attachment points on the rails to avoid collision between cables while the end effector trajectory kept unchanged. The initial location of the upper attachment point (5) was at 7.5 meters and relocated by the end of the simulation to 9.1 meters. It can be observed from the 3D views (Figure 31 (a) and (e)) that the final workspace is slightly changed compared to the initial workspace in the top part of the view. This observation can be seen clearly when comparing between the X-Z views (Figure 31 (b) and (f)), where the top part in the final workspace has become more flat and gained some volume, but on the right and left parts, it can be noticed almost the same. On the other hand, it can be observed that there was a noticeable reduction change between the initial and final workspace when comparing the X-Y views (Figure 31 (d) and (h)) and the Y-Z views (Figure 31 (c) and (g)) where the right side of both views has been contracted.

6.4.4. Circular trajectory "avoid cable-human collision"

Figure 32 presents the initial and workspace mapping due to the real-time reconfiguration of the mechanism while the end effector performs circular motion.

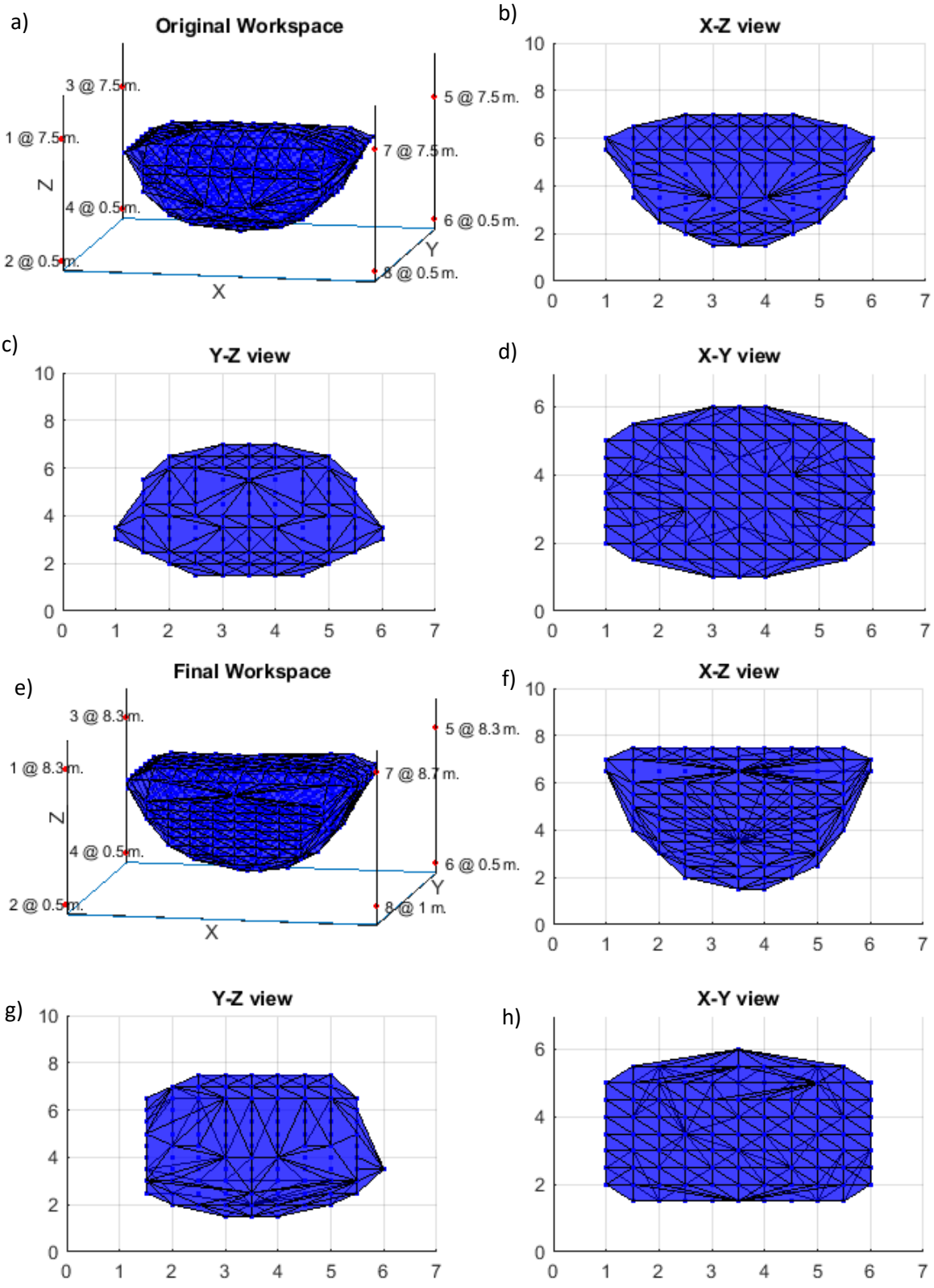

Figure 32 Circular trajectory(Cable-human collision): (a) Initial workspace 3D, (b) Front view, (c) Side view, (d) Top view, (e) Final workspace 3D, (f) Front view, (g) Side view, (h) Top view

In this simulation results presented in Figure 32, the change occurred in the workspace followed a relocation of the attachment points on the rails to avoid cable-cable and cable-human collision while the end effector trajectory kept unchanged in its circular motion. The initial location of the upper attachment points (1, 3, 5 and 7) were at 7.5 meters and relocated by the end of the simulation to 8.3 meters for all of them and cable (8) was initially at 0.5 meters and relocated to 1 meter. It can be observed from the 3D views (Figure 32 (a) and (e)) that the final workspace is slightly increased and expanded on the top part compared to the initial workspace. This observation can be seen clearly when comparing between the X-Z views (Figure 32 (b) and (f)), where the top part in the final workspace has increased and gain more volume on the left and right parts. This remark can be explained due to the relocation of the four upper attachment points. On the other hand, it can be observed that there was no noteworthy change between the initial and final workspace when comparing the X-Y views (Figure 32 (d) and (h)) or the Y-Z views (Figure 32 (c) and (g)). In addition, by comparing the final workspace views in Figure 29 and Figure 32, there is no significant change due to the change of position of cable (8) which was relocated to avoid cable-human collision.

6.4.5. Sinusoidal trajectory "avoid cable-human collision"

Figure 33 presents the initial and workspace mapping due to the real-time reconfiguration of the mechanism while the end effector performs sinusoidal motion.

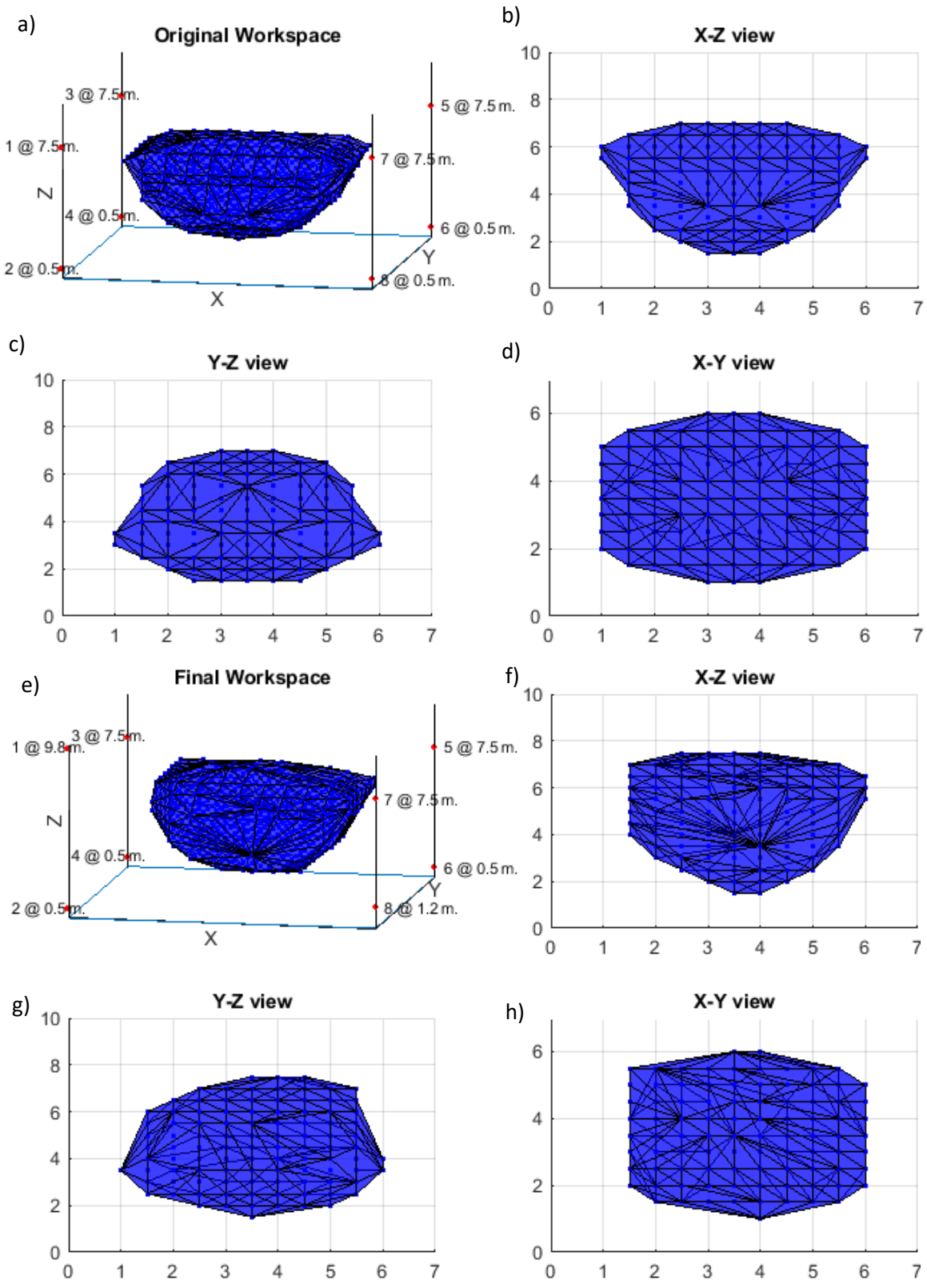

Figure 33 Sinusoidal trajectory(Cable-human collision): (a) Initial workspace 3D, (b) Front view, (c) Side view, (d) Top view, (e) Final workspace 3D, (f) Front view, (g) Side view, (h) Top view

In this simulation results presented in Figure 33, the change occurred in the workspace followed a relocation of the attachment points on the rails to avoid cable-cable and cable-human collision while the end effector trajectory kept unchanged in its sinusoidal motion. The initial location of the upper attachment point (1) was at 7.5 meters and relocated by the end of the simulation to 9.8 meters and cable (8) was initially at 0.5 meters and relocated to 1.2 meters. It can be observed from the 3D views (Figure 33 (a) and (e)) that the final workspace is slightly changed compared to the initial workspace. This observation can be seen clearly when comparing between the X-Z views (Figure 33 (b) and (f)), where the left part in the final workspace has decreased and lost some volume, but on the right parts, it can be noticed almost the same. On the other hand, it can be observed that there was a noticeable reduction change between the initial and final workspace when comparing the X-Y views (Figure 33 (d) and (h)) and the Y-Z views (Figure 33 (c) and (g)). In addition, by comparing the final workspace views in Figure 30 and Figure 33, there is no significant change due to the change of position of cable (8) which was relocated to avoid cable-human collision.

6.4.6. Random trajectory “avoid cable-human collision”

Figure 34 presents the initial and workspace mapping due to the real-time reconfiguration of the mechanism while the end effector performs random motion.

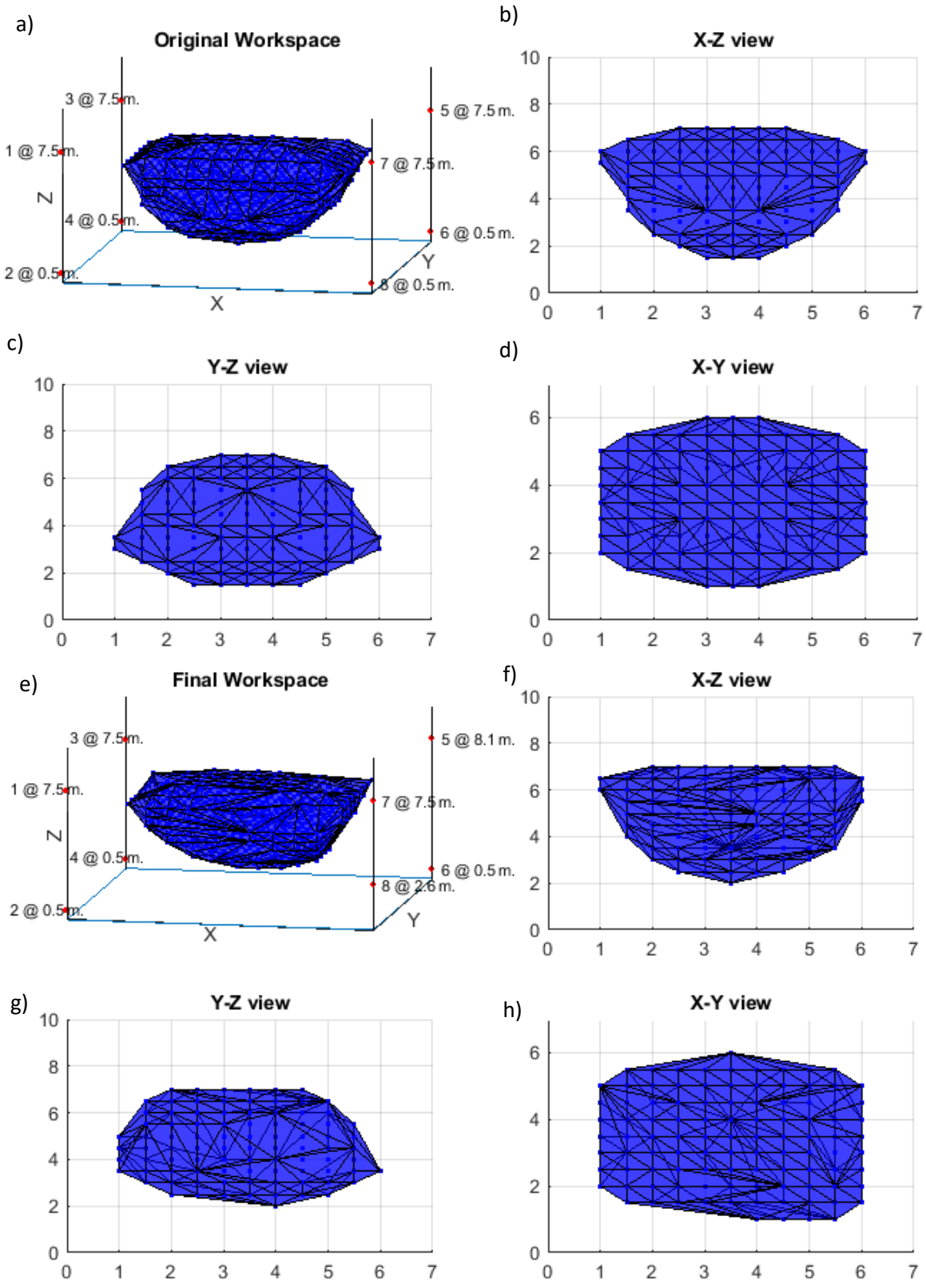

Figure 34 Random trajectory(Cable-human collision): (a) Initial workspace 3D, (b) Front view, (c) Side view, (d) Top view, (e) Final workspace 3D, (f) Front view, (g) Side view, (h) Top view

In this simulation results presented in Figure 34, the change occurred in the workspace followed a relocation of the attachment points on the rails to avoid cable-cable and cable-human collision while the end effector trajectory kept unchanged in its random motion. The initial location of the upper attachment point (5) was at 7.5 meters and relocated by the end of the simulation to 8.1 meters and cable (8) was initially at 0.5 meters and relocated to 2.6 meters. It can be observed from the 3D views (Figure 34 (a) and (e)) that the final workspace is slightly changed compared to the initial workspace in the top part of the view. This observation can be seen clearly when comparing between the X-Z views (Figure 34 (b) and (f)), where the top part in the final workspace has become more flat and gained some volume, but on the right and left parts, it can be noticed almost the same. On the other hand, it can be observed that there was a noticeable increase between the initial and final workspace when comparing the X-Y views (Figure 34 (d) and (h)) where the right side of the view has been increased due to the change in position of cable 8 which was relocated to avoid collision with human arm.

6.5. Conclusion

In this chapter, the effect of the real-time reconfiguration theory on the constant-orientation wrench feasible workspace of the CDPM has been presented and results were shown by comparing the initial and final workspace figures. Classifications of different workspace and its perspective mathematical representation has been listed as well as its method of computation.

Three different trajectories have been simulated and due to the real-time reconfiguration of the CDPM to avoid cable-cable and cable-human collisions, workspace mapping was changed. Chapter 6 is the last chapter in this research study and hence chapter 7 is dedicated for concluding remarks on this research project and emphasize on the validity of the suggested approach. Recommendations and suggestions are also presented for future work.

CHAPTER 7

7. Conclusions and Recommendations

This research project is concentrated on three main topics. First, modeling of on-line reconfigurable six DOF fully constrained cable driven parallel mechanism driven by eight cables. Unlike conventional CDPMs, where the attachment points are firmly fixed on specific locations on the rails, this model presents an on-line reconfigurable mechanism where the attachment points may relocate in real-time application. Second, the reconfigurable idea is used in an application to detect and avoid cable-cable and cable-human interference while maintaining the initial trajectory of the end effector unchanged. Maintaining trajectory is a key issue for an optimal assembly process in flexible manufacturing systems. For example, in human robot interaction applications, the trajectory of the end effector is coming directly from the operator to perform a specific task, therefore, for a smooth maneuver; the trajectory of the end effector should not be changed to avoid cables interference and/or collision with the operator.

Third, the effect of relocation of the attachment points on the rails, in order to avoid collision between cables and/or between cables and human, on the constant-orientation wrench feasible workspace of the mechanism is presented and discussed. The following conclusions are presented based on the symbolic representation and simulation analysis of the suggested method in chapters 3, 4, 5 and 6 of this thesis. A summary of the contributions of this research project is presented in section **Error! Reference source not found.** in a chapter wise representation, to demonstrate the robustness of the suggested method

compared to previous approaches described in the literature review. Recommendations for future work are provided at the end of this chapter.

7.1. Conclusions

Chapter 1 presents general introduction about different types of mechanisms and an outline about cable driven mechanisms such as, its concept, advantages and applications. In addition, the problem statement and originality as well as the scope of the thesis are presented in this chapter.

Chapter 2 is dedicated to the literature review about CDPM where related terminologies and basic concepts that are used specifically in the study of CDPM kinematics and dynamics are presented. In addition, a literature review of recent and up to date research studies relevant to cable interference detection and avoidance in CDPM is presented as well as suggested methods to solve for cables tension distribution equation.

Chapter 3 is devoted to explain in details and construct the symbolic representation of the suggested simulation model along with the cables tension distribution equation where the coordinates system and the generalized coordinates of the moving parts are defined. The kinematic and driving constraints are symbolically derived and the total kinematic constraint equations (KC) are established resulting in a set of overdetermined system of equations. Least square method with lower and upper bounds on the variables was used to solve the previously mentioned set of equations. The forward kinematics problem is then solved given that the eight attachment points (actuators) on the rails move vertically up and down while the eight cables are being shortened or extended to manipulate and control the

end effector. Several figures were obtained and presented to show the computed Cartesian coordinates of the end effector's center of mass as well as its orientation given the movable position of the attachment points and the fluctuating cables length. In addition, the vector loop-closure equation is constructed and hence using linear programming, the inverse kinematics is solved by determining the required cables lengths for a given pose of the end effector. Linear programming with equality constraints and no objective function was used which means that we are trying to determine a feasible solution without minimizing any physical quantity. In order to assure a positive tension values in the cables, the cables tension distribution equation was obtained and solved using linear programming again to compute the cables tension for a given trajectory of the end effector. The simulation of three different trajectories for the end effector were performed where the required cables tensions and lengths were computed and plotted. Chapter 3 is considered the first contribution in this thesis where, unlike conventional CDPMs, the forward and inverse kinematics were solved given that the eight attachment points on the rails are relocating in real-time.

Chapter 4 presented the geometric computation of the shortest distance between two lines in space. Hence, the reconfigurable theory that was discussed in chapter 3 is used to detect and avoid interference between two cables by relocating the attachment points on the rails. An algorithm has been developed using MATLAB to compute the shortest physical distance between all the cables for a given trajectory of the end effector and compares it with a threshold value (tolerance) that is defined by the user. In case of a near collision between any two cables, the algorithm computes the shortest distance and accordingly, it detects which cable should be relocated and moves up the corresponding attachment point

on the rail of the corresponding cable by a given step in order to increase the distance between the two cables while maintaining the end effector trajectory unchanged. The robustness of the suggested method has been shown by simulating three different trajectories and plotting three main measures, which are the shortest distance between two cables about to collide, the location of the attachment points of the cable to be relocated and the computed tension values of the corresponding cable. The developed algorithm has been proven to effectively detect and avoid cable-cable interference where the second contribution of the current thesis was presented in this chapter.

Chapter 5 is an extension of chapter 4, where the idea of online reconfiguration is used again to detect and avoid collision between cables and human sharing the same workspace with the moving parts of the mechanism. Human limbs are considered straight objects in space where a human skeleton is inserted with a colliding distance with the cables in three different simulation where the end effector is performing different types of motion. An algorithm is developed in MATLAB to detect and avoid collision between all cables and human limbs at each sampling time while maintaining the end effector trajectory unchanged. Several figures for the three different trajectories have been plotted to show the shortest distance between a cable and human limb about to collide and how effectively the algorithm paused the motion of the end effector and relocate the attachment point of the corresponding cable to avoid collision.

Chapter 6 presented the change of the CDPM constant-orientation wrench feasible workspace due to the real-time reconfiguration of the attachment points on the rails, which was presented in chapter 4 and 5. In this chapter, a concise literature about different types of CDPM workspace is presents as well as different methods to solve for the cables

distribution tensions equation, which is the key foundation to map the workspace. The workspace mapping was based on testing a grid of 3D points lying within the geometry of the mechanism where linear programming was used to solve for the cables tension distribution equation and the point (end effector pose) is recorded if a feasible solution is found. For each of the simulated trajectories, the initial and final workspaces due to the change of the attachment points location on the fixed rails were mapped in one figure to show the differences between them. For a better visualization in 3D, front view, side view and top view of the workspace were plotted.

7.2. Recommendations for future work

The promising results achieved in this research project concerning the online reconfiguration and the newly suggested method to detect and avoid cable-cable and cable-human collisions could be a start for more interesting investigations. The following scientific contributions are recommended as next steps that can be considered in order to move forward:

1) Compare between vertical and horizontal relocation of attachment points in order to facilitate the attachment points repositioning process by means of overcome the weight of the end effector. The workspace mapping is recommended to be compared in both cases.
2) Construct experimental prototype and compare between theoretical and experimental results.

3) Develop nonlinear modeling for the suggested approach in this research project by considering elasticity and sagging effects in the cables and compare results between both models.
4) Compute Real time attachment points location on the fixed rails to increase the workspace. This is not an easy task since it should contain an optimization and synthesis methods to find locations for the attachment points so that the end effector could reach positions outside the idiomatic workspace.
5) Develop a faster method for mapping the workspace (or the boundary of workspace) in order to be used for real-time computations.
6) Design a workspace index in order to compare between the volume of workspaces change.
7) Use the model for control purposes.

References

[1] M.W. Spong, S. Hutchinson, M. Vidyasagar, Robot modeling and control, IEEE Control Syst. 26 (2006) 113–115. https://doi.org/10.1109/MCS.2006.252815.

[2] R. Ben-Horin, M. Shoham, S. Djerassi, Kinematics, dynamics and construction of a planarly actuated parallel robot, Robot. Comput. Integr. Manuf. (1998). https://doi.org/10.1016/S0736-5845(97)00035-5.

[3] J.P. Merlet, Jacobian, manipulability, condition number, and accuracy of parallel robots, J. Mech. Des. Trans. ASME. (2006). https://doi.org/10.1115/1.2121740.

[4] Serial manipulator, (n.d.). https://en.wikipedia.org/wiki/Serial_manipulator#/media/File:Robot_arm_model_1.png.

[5] Parallel manipulator, (n.d.). https://en.wikipedia.org/wiki/Parallel_manipulator#/media/File:Hexapod0a.png.

[6] N.G. Dagalakis, J.S. Albus, B.L. Wang, J. Unger, J.D. Lee, Stiffness Study of a Parallel Link Robot Crane for Shipbuilding Applications, J. Offshore Mech. Arct. Eng. (1989). https://doi.org/10.1115/1.3257146.

[7] A. Pott, Cable-Driven Parallel Robots, 2013. https://doi.org/10.1007/978-3-642-31988-4.

[8] A. Pott, Cable-driven parallel robots: Theory and application, in: Springer Tracts Adv. Robot., 2018. https://doi.org/10.1007/978-3-319-76138-1.

[9] J. Albus, R. Bostelman, N. Dagalakis, NIST SPIDER, a robot crane, J. Res. Natl.

Inst. Stand. Technol. 97 (1992) 373–385. https://doi.org/10.6028/jres.097.016.

[10] P. Gallina, G. Rosati, A. Rossi, 3-d.o.f. wire driven planar haptic interface, J. Intell. Robot. Syst. Theory Appl. (2001). https://doi.org/10.1023/A:1012095609866.

[11] M.J.-D. Otis, T.-L. Nguyen Dang, T. Laliberte, D. Ouellet, D. Laurendeau, C.M. Gosselin, Cable Tension Control and Analysis of Reel Transparency for 6-DOF haptic foot platform on a cable-driven locomotion interface, World Acad. Sci. Eng. Technol. 40 (2009) 520–532. https://doi.org/10.1016/j.ijpharm.2005.11.029.

[12] K. Usher, G. Winstanley, P. Corke, D. Stauffacher, R. Carnie, Air vehicle simulator: An application for a cable array robot, Proc. - IEEE Int. Conf. Robot. Autom. 2005 (2005) 2241–2246. https://doi.org/10.1109/ROBOT.2005.1570446.

[13] C.W.S.K. Hitoshi Kino, High-speed manipulation by using parallel wire-driven robots, Robotica. 18 (2000) 13–21.

[14] M. Hiller, S. Fang, S. Mielczarek, R. Verhoeven, D. Franitza, Design, analysis and realization of tendon-based parallel manipulators, Mech. Mach. Theory. 40 (2005) 429–445. https://doi.org/10.1016/j.mechmachtheory.2004.08.002.

[15] M. Gouttefarde, C.M. Gosselin, Analysis of the wrench-closure workspace of planar parallel cable-driven mechanisms, IEEE Trans. Robot. 22 (2006) 434–445. https://doi.org/10.1109/TRO.2006.870638.

[16] N. Zhang, W. Shang, S. Cong, Dynamic trajectory planning for a spatial 3-DoF cable-suspended parallel robot, Mech. Mach. Theory. 122 (2018) 177–196.

https://doi.org/10.1016/j.mechmachtheory.2017.12.023.

[17] A. Pott, An Algorithm for Real-Time Forward Kinematics of Cable-Driven Parallel Robots, in: J. Lenarcic, M.M. Stanisic (Eds.), Adv. Robot Kinemat. Motion Man Mach., Springer Netherlands, Dordrecht, 2010: pp. 529–538.

[18] M. Gouttefarde, J. Lamaury, C. Reichert, T. Bruckmann, A Versatile Tension Distribution Algorithm for n-DOF Parallel Robots Driven by n + 2 Cables, IEEE Trans. Robot. (2015). https://doi.org/10.1109/TRO.2015.2495005.

[19] G. Barrette, C.M. Gosselin, Determination of the Dynamic Workspace of Cable-Driven Planar Parallel Mechanisms, J. Mech. Des. 127 (2005) 242. https://doi.org/10.1115/1.1830045.

[20] X. Diao, O. Ma, Vibration analysis of cable-driven parallel manipulators, Multibody Syst. Dyn. (2009). https://doi.org/10.1007/s11044-008-9144-0.

[21] B. Zhang, W. Shang, S. Cong, Optimal RRT* Planning and Synchronous Control of Cable-Driven Parallel Robots, 2018 3rd Int. Conf. Adv. Robot. Mechatronics. (2019) 95–100. https://doi.org/10.1109/icarm.2018.8610680.

[22] M.J.-D. Otis, T.-L. Nguyen-Dang, D. Laurendeau, C. Gosselin, Interference estimated time of arrival on a 6-DOF cable-driven haptic foot platform, in: 2009 IEEE Int. Conf. Robot. Autom., 2009. https://doi.org/10.1109/ROBOT.2009.5152182.

[23] D.Q. Nguyen, M. Gouttefarde, On the improvement of cable collision detection algorithms, in: Mech. Mach. Sci., 2015. https://doi.org/10.1007/978-3-319-09489-

2_3.

[24] R.G. Roberts, T. Graham, T. Lippitt, On the inverse kinematics, statics, and fault tolerance of cable-suspended robots, J. Robot. Syst. (1998). https://doi.org/10.1002/(SICI)1097-4563(199810)15:10<581::AID-ROB4>3.0.CO;2-P.

[25] M.J.D. Otis, S. Comtois, D. Laurendeau, C. Gosselin, Human safety algorithms for a parallel cable-driven haptic interface, in: Adv. Intell. Soft Comput., 2010. https://doi.org/10.1007/978-3-642-16259-6_15.

[26] B. Zi, B.Y. Duan, J.L. Du, H. Bao, Dynamic modeling and active control of a cable-suspended parallel robot, Mechatronics. (2008). https://doi.org/10.1016/j.mechatronics.2007.09.004.

[27] A. Ghasemi, M. Eghtesad, M. Farid, Neural network solution for forward kinematics problem of cable robots, J. Intell. Robot. Syst. Theory Appl. (2010). https://doi.org/10.1007/s10846-010-9421-z.

[28] A. El-Badawy, K. Youssef, On modeling and simulation of 6 degrees of freedom Stewart platform mechanism using multibody dynamics approach, in: Proc. ECCOMAS Themat. Conf. Multibody Dyn. 2013, 2013.

[29] M.L. Husty, An algorithm for solving the direct kinematics of general Stewart-Gough platforms, Mech. Mach. Theory. (1996). https://doi.org/10.1016/0094-114X(95)00091-C.

[30] G. Liwen, X. Huayang, L. Zhihua, Kinematic analysis of cable-driven parallel

mechanisms based on minimum potential energy principle, Adv. Mech. Eng. (2015). https://doi.org/10.1177/1687814015622339.

[31] M.J.D. Otis, M. Mokhtari, C. Du Tremblay, D. Laurendeau, F.M. De Rainville, C.M. Gosselin, Hybrid control with multi-contact interactions for 6DOF haptic foot platform on a cable-driven locomotion interface, in: Symp. Haptics Interfaces Virtual Environ. Teleoperator Syst. 2008 - Proceedings, Haptics, 2008. https://doi.org/10.1109/HAPTICS.2008.4479937.

[32] S. Lahouar, E. Ottaviano, S. Zeghoul, L. Romdhane, M. Ceccarelli, Collision free path-planning for cable-driven parallel robots, Rob. Auton. Syst. (2009). https://doi.org/10.1016/j.robot.2009.07.006.

[33] E. Moreira, A.M. Pinto, J.P. Sousa, J. Lima, P. Costa, A cable-driven robot for architectural constructions: a visual-guided approach for motion control and path-planning, Auton. Robots. 41 (2016) 1487–1499. https://doi.org/10.1007/s10514-016-9609-6.

[34] M. Gouttefarde, C.M. Gosselin, On the properties and the determination of the wrench-closure workspace of planar parallel cable-driven mechanisms, in: Proc. ASME Des. Eng. Tech. Conf., 2004. https://doi.org/10.1115/detc2004-57127.

[35] A. Pott, An improved force distribution algorithm for over-constrained cable-driven parallel robots, in: Mech. Mach. Sci., 2014. https://doi.org/10.1007/978-94-007-7214-4_16.

[36] P.H. Borgstrom, B.L. Jordan, G.S. Sukhatme, M.A. Batalin, W.J. Kaiser, Rapid computation of optimally safe tension distributions for parallel cable-driven robots,

IEEE Trans. Robot. (2009). https://doi.org/10.1109/TRO.2009.2032957.

[37] C.B. Pham, G. Yang, S.H. Yeo, Dynamic analysis of cable-driven parallel mechanisms, in: IEEE/ASME Int. Conf. Adv. Intell. Mechatronics, AIM, 2005. https://doi.org/10.1109/aim.2005.1511050.

[38] A.F. Cote, P. Cardou, C. Gosselin, A tension distribution algorithm for cable-driven parallel robots operating beyond their wrench-feasible workspace, in: Int. Conf. Control. Autom. Syst., 2016. https://doi.org/10.1109/ICCAS.2016.7832301.

[39] W.B. Lim, S.H. Yeo, G. Yang, S.K. Mustafa, Z. Zhang, Tension optimization for cable-driven parallel manipulators using gradient projection, in: IEEE/ASME Int. Conf. Adv. Intell. Mechatronics, AIM, 2011. https://doi.org/10.1109/AIM.2011.6027019.

[40] C. Gosselin, M. Grenier, On the determination of the force distribution in overconstrained cable-driven parallel mechanisms, Meccanica. (2011). https://doi.org/10.1007/s11012-010-9369-x.

[41] J. Piao, E.S. Kim, H. Choi, C.B. Moon, E. Choi, J.O. Park, C.S. Kim, Indirect force control of a cable-driven parallel robot: Tension estimation using artificial neural network trained by force sensor measurements, Sensors (Switzerland). (2019). https://doi.org/10.3390/s19112520.

[42] J. Wainer, D.J. Feil-Seifer, D.A. Shell, M.J. Matarić, The role of physical embodiment in human-robot interaction, in: Proc. - IEEE Int. Work. Robot Hum. Interact. Commun., 2006. https://doi.org/10.1109/ROMAN.2006.314404.

[43] G. Reinhart, R. Spillner, Y. Shen, Approaches of applying human-robot-interaction-technologies to assist workers with musculoskeletal disorders in production, in: Lect. Notes Comput. Sci. (Including Subser. Lect. Notes Artif. Intell. Lect. Notes Bioinformatics), 2012. https://doi.org/10.1007/978-3-642-33515-0_8.

[44] C. Carignan, K. Cleary, Closed-loop force control for haptic simulation of virtual environments, Haptics-E. (2000). https://doi.org/10.1.1.63.2330.

[45] A. Campeau-Lecours, M.J.D. Otis, C. Gosselin, Modeling of physical human-robot interaction: Admittance controllers applied to intelligent assist devices with large payload, Int. J. Adv. Robot. Syst. (2016). https://doi.org/10.1177/1729881416658167.

[46] Y. Wischnitzer, N. Shvalb, M. Shoham, Wire-driven parallel robot: Permitting collisions between wires, Int. J. Rob. Res. (2008). https://doi.org/10.1177/0278364908095884.

[47] R. Meziane, P. Cardou, M.J.D. Otis, Cable interference control in physical interaction for cable-driven parallel mechanisms, Mech. Mach. Theory. (2019). https://doi.org/10.1016/j.mechmachtheory.2018.10.002.

[48] E. Haug, Computer Aided Kinematics and Dynamics of Mechanical Systems, Allyn and Bacon, 1989.

[49] G. Boschetti, G. Carbone, C. Passarini, Cable failure operation strategy for a rehabilitation Cable-Driven Robot, Robotics. (2019). https://doi.org/10.3390/robotics8010017.

[50] C. Reichert, T. Bruckmann, Unified contact force control approach for cable-driven parallel robots using an impedance/admittance control strategy, in: 2015 IFToMM World Congr. Proceedings, IFToMM 2015, 2015. https://doi.org/10.6567/IFToMM.14TH.WC.OS13.020.

[51] W. Bin Lim, G. Yang, S.H. Yeo, S.K. Mustafa, A generic force-closure analysis algorithm for cable-driven parallel manipulators, Mech. Mach. Theory. (2011). https://doi.org/10.1016/j.mechmachtheory.2011.04.006.

[52] J.P. Merlet, On the redundancy of cable-driven parallel robots, in: Mech. Mach. Sci., 2015. https://doi.org/10.1007/978-3-319-09411-3_4.

[53] D.Q. Nguyen, M. Gouttefarde, O. Company, F. Pierrot, On the simplifications of cable model in static analysis of large-dimension cable-driven parallel robots, in: IEEE Int. Conf. Intell. Robot. Syst., 2013. https://doi.org/10.1109/IROS.2013.6696461.

[54] T. Dallej, M. Gouttefarde, N. Andreff, P.E. Hervé, P. Martinet, Modeling and vision-based control of large-dimension cable-driven parallel robots using a multiple-camera setup, Mechatronics. (2019). https://doi.org/10.1016/j.mechatronics.2019.05.004.

[55] D. Li, P. Wang, L. Qian, M. Krco, A. Dunning, P. Jiang, Y. Yue, C. Jin, Y. Zhu, Z. Pan, R. Nan, FAST in Space: Considerations for a Multibeam, Multipurpose Survey Using China's 500-m Aperture Spherical Radio Telescope (FAST), IEEE Microw. Mag. (2018). https://doi.org/10.1109/MMM.2018.2802178.

[56] D. Li, Z. Pan, The Five-hundred-meter Aperture Spherical Radio Telescope

project, Radio Sci. (2016). https://doi.org/10.1002/2015RS005877.

[57] B. Zi, B. Wang, D. Wang, Design and analysis of a novel cable-actuated palletizing robot, Int. J. Adv. Robot. Syst. (2017). https://doi.org/10.1177/1729881417741084.

[58] M. Gouttefarde, J.F. Collard, N. Riehl, C. Baradat, Geometry Selection of a Redundantly Actuated Cable-Suspended Parallel Robot, IEEE Trans. Robot. (2015). https://doi.org/10.1109/TRO.2015.2400253.

[59] R. Nan, D. Li, C. Jin, Q. Wang, L. Zhu, W. Zhu, H. Zhang, Y. Yue, L. Qian, The five-hundred-meter Aperture Spherical radio Telescope (FAST) project, Int. J. Mod. Phys. D. (2011). https://doi.org/10.1142/S0218271811019335.

[60] M. Tanaka, Y. Seguchi, S. Shimada, Kinemato-statics of SKYCAM-type wire transport system, in: 1988.

[61] C.A. Balafoutis, R. V. Patel, C.A. Balafoutis, R. V. Patel, Manipulator Forward Dynamics, in: Dyn. Anal. Robot Manip., 1991. https://doi.org/10.1007/978-1-4615-3952-0_6.

[62] C.A. Balafoutis, R. V. Patel, C.A. Balafoutis, R. V. Patel, Manipulator Inverse Dynamics, in: Dyn. Anal. Robot Manip., 1991. https://doi.org/10.1007/978-1-4615-3952-0_5.

[63] Y.B. Bedoustani, H.D. Taghirad, M.M. Aref, Dynamics analysis of a redundant parallel manipulator driven by elastic cables, in: 2008 10th Int. Conf. Control. Autom. Robot. Vision, ICARCV 2008, 2008.

https://doi.org/10.1109/ICARCV.2008.4795575.

[64] M.A. Khosravi, H.D. Taghirad, Dynamic analysis and control of cable driven robots with elastic cables, in: Trans. Can. Soc. Mech. Eng., 2011. https://doi.org/10.1139/tcsme-2011-0033.

[65] Z. Yadeta, Lyapunov's Second Method for Estimating Region of Asymptotic Stability, Open Sci. Repos. Math. (2013). https://doi.org/10.7392/Mathematics.70081944.

[66] Y.P. Chan, J. Eden, D. Lau, D. Oetomo, A survey on inverse dynamics solvers for cable-driven parallel robots, in: Australas. Conf. Robot. Autom. ACRA, 2017.

[67] H.D. Taghirad, Y.B. Bedoustani, An analytic-iterative redundancy resolution scheme for cable-driven redundant parallel manipulators, IEEE Trans. Robot. (2011). https://doi.org/10.1109/TRO.2011.2163433.

[68] R.J. Caverly, J.R. Forbes, Flexible Cable-Driven parallel manipulator control: Maintaining positive cable tensions, IEEE Trans. Control Syst. Technol. (2018). https://doi.org/10.1109/TCST.2017.2728007.

[69] H. Li, X. Zhang, R. Yao, J. Sun, G. Pan, W. Zhu, Optimal force distribution based on slack rope model in the incompletely constrained cable-driven parallel mechanism of FAST telescope, in: Mech. Mach. Sci., 2013. https://doi.org/10.1007/978-3-642-31988-4_6.

[70] P.H. Borgstrom, N.P. Borgstrom, M.J. Stealey, B. Jordan, G.S. Sukhatme, M.A. Batalin, W.J. Kaiser, Design and implementation of NIMS3D, a 3-D cabled robot

for actuated sensing applications, IEEE Trans. Robot. (2009). https://doi.org/10.1109/TRO.2009.2012339.

[71] J.F. Collard, P. Cardou, Computing the lowest equilibrium pose of a cable-suspended rigid body, Optim. Eng. (2013). https://doi.org/10.1007/s11081-012-9191-5.

[72] R. Chellal, L. Cuvillon, E. Laroche, A kinematic vision-based position control of a 6-DoF cable-driven parallel robot, in: Mech. Mach. Sci., 2015. https://doi.org/10.1007/978-3-319-09489-2_15.

[73] S. Fang, D. Franitza, M. Torlo, F. Bekes, M. Hiller, Motion control of a tendon-based parallel manipulator using optimal tension distribution, IEEE/ASME Trans. Mechatronics. (2004). https://doi.org/10.1109/TMECH.2004.835336.

[74] M. Hassan, A. Khajepour, Optimization of actuator forces in cable-based parallel manipulators using convex analysis, IEEE Trans. Robot. (2008). https://doi.org/10.1109/TRO.2008.919289.

[75] P. Tempel, F. Schnelle, A. Pott, P. Eberhard, Design and Programming for Cable-Driven Parallel Robots in the German Pavilion at the EXPO 2015, Machines. (2015). https://doi.org/10.3390/machines3030223.

[76] R.L. Williams, P. Gallina, Planar cable-direct-driven robots: Design for wrench exertion, J. Intell. Robot. Syst. Theory Appl. (2002). https://doi.org/10.1023/A:1021158804664.

[77] R. Bordalba, J.M. Porta, L. Ros, Randomized kinodynamic planning for cable-

suspended parallel robots, in: Mech. Mach. Sci., 2018. https://doi.org/10.1007/978-3-319-61431-1_17.

[78] T. Makino, T. Harada, Cable collision avoidance of a pulley embedded cable-driven parallel robot by kinematic redundancy, in: Proc. 4th Int. Conf. Control. Mechatronics Autom. - ICCMA ’16, 2016. https://doi.org/10.1145/3029610.3029620.

[79] M.J.D. Otis, S. Perreault, T.L. Nguyen-Dang, P. Lambert, M. Gouttefarde, D. Laurendeau, C. Gosselin, Determination and management of cable interferences between two 6-DOF foot platforms in a cable-driven locomotion interface, IEEE Trans. Syst. Man, Cybern. Part ASystems Humans. (2009). https://doi.org/10.1109/TSMCA.2009.2013188.

[80] S. Perreault, P. Cardou, C.M. Gosselin, M.J.-D. Otis, Geometric Determination of the Interference-Free Constant-Orientation Workspace of Parallel Cable-Driven Mechanisms, J. Mech. Robot. (2010). https://doi.org/10.1115/1.4001780.

[81] M. Ismail, S. Lahouar, L. Romdhane, Collision-free and dynamically feasible trajectory of a hybrid cable–serial robot with two passive links, Rob. Auton. Syst. 80 (2016) 24–33. https://doi.org/10.1016/J.ROBOT.2016.03.001.

[82] E. Barnett, C. Gosselin, Time-optimal trajectory planning of cable-driven parallel mechanisms for fully specified paths with G1-discontinuities, J. Dyn. Syst. Meas. Control. Trans. ASME. (2015). https://doi.org/10.1115/1.4029769.

[83] X. Zhou, C.P. Tang, V. Krovi, Cooperating mobile cable robots: Screw theoretic analysis, in: Lect. Notes Electr. Eng., 2013. https://doi.org/10.1007/978-3-642-

33971-4_7.

[84] M. Anson, A. Alamdari, V. Krovi, Orientation Workspace and Stiffness Optimization of Cable-Driven Parallel Manipulators With Base Mobility, J. Mech. Robot. 9 (2017) 031011. https://doi.org/10.1115/1.4035988.

[85] H. Tourajizadeh, M.H. Korayem, Optimal regulation of a cable suspended robot equipped with cable interfering avoidance controller, Adv. Robot. (2016). https://doi.org/10.1080/01691864.2016.1198719.

[86] M. Arsenault, Computation of the interference-free wrench feasible workspace of a 3-DoF translational tensegrity robot, in: Mech. Mach. Sci., 2019. https://doi.org/10.1007/978-3-030-20751-9_16.

[87] M. Fabritius, C. Martin, A. Pott, Calculation of the cable-platform collision-free total orientation workspace of cable-driven parallel robots, in: Mech. Mach. Sci., 2019. https://doi.org/10.1007/978-3-030-20751-9_12.

[88] A. Martin, S. Caro, P. Cardou, Geometric determination of the cable-cylinder interference regions in the workspace of a cable-driven parallel robot, in: Mech. Mach. Sci., 2018. https://doi.org/10.1007/978-3-319-61431-1_11.

[89] B. Wang, B. Zi, S. Qian, D. Zhang, Collision free force closure workspace determination of reconfigurable planar cable driven parallel robot, in: Proc. 2016 Asia-Pacific Conf. Intell. Robot Syst. ACIRS 2016, 2016. https://doi.org/10.1109/ACIRS.2016.7556182.

[90] M. Lesellier, M. Gouttefarde, A bounding volume of the cable span for fast

collision avoidance verification, in: Mech. Mach. Sci., 2019. https://doi.org/10.1007/978-3-030-20751-9_15.

[91] L. Blanchet, J.P. Merlet, Interference detection for cable-driven parallel robots (CDPRs), in: IEEE/ASME Int. Conf. Adv. Intell. Mechatronics, AIM, 2014. https://doi.org/10.1109/AIM.2014.6878280.

[92] G. Boschetti, A. Trevisani, Cable robot performance evaluation by Wrench exertion capability, Robotics. 7 (2018). https://doi.org/10.3390/robotics7020015.

[93] L. Barbazza, F. Oscari, S. Minto, G. Rosati, Trajectory planning of a suspended cable driven parallel robot with reconfigurable end effector, Robot. Comput. Integr. Manuf. (2017). https://doi.org/10.1016/j.rcim.2017.02.001.

[94] M. Fabritius, C. Martin, A. Pott, Calculation of the collision-free printing workspace for fully-constrained cable-driven parallel robots, in: Proc. ASME Des. Eng. Tech. Conf., 2018. https://doi.org/10.1115/DETC2018-85961.

[95] A. Pott, Determination of the cable span and cable deflection of cable-driven parallel robots, in: Mech. Mach. Sci., 2018. https://doi.org/10.1007/978-3-319-61431-1_10.

[96] T. Rasheed, P. Long, D. Marquez-Gamez, S. Caro, Path planning of a mobile cable-driven parallel robot in a constrained environment, in: Mech. Mach. Sci., 2019. https://doi.org/10.1007/978-3-030-20751-9_22.

[97] J.H. Bak, S.W. Hwang, J. Yoon, J.H. Park, J.O. Park, Collision-free path planning of cable-driven parallel robots in cluttered environments, Intell. Serv. Robot.

(2019). https://doi.org/10.1007/s11370-019-00278-7.

[98] L. Gagliardini, S. Caro, M. Gouttefarde, Dimensioning of cable-driven parallel robot actuators, gearboxes and winches according to the twist feasible workspace, in: IEEE Int. Conf. Autom. Sci. Eng., 2015. https://doi.org/10.1109/CoASE.2015.7294046.

[99] D.S. Vu, E. Barnett, A.M. Zaccarin, C. Gosselin, On the design of a three-DOF cable-suspended parallel robot based on a parallelogram arrangement of the cables, in: Mech. Mach. Sci., 2018. https://doi.org/10.1007/978-3-319-61431-1_27.

[100] G. Boschetti, A. Trevisani, Cable robot performance evaluation by Wrench exertion capability, Robotics. (2018). https://doi.org/10.3390/robotics7020015.

[101] A.A. Shabana, Computational Dynamics, Third Edition, 2009. https://doi.org/10.1002/9780470686850.

[102] T.F. Coleman, Y. Li, An Interior Trust Region Approach for Nonlinear Minimization Subject to Bounds, SIAM J. Optim. (1996). https://doi.org/10.1137/0806023.

[103] N. Sagara, M. Fukushima, A hybrid method for the nonlinear least squares problem with simple bounds, J. Comput. Appl. Math. (1991). https://doi.org/10.1016/0377-0427(91)90023-D.

[104] M. DEDIEU, J. P; SHUB, Newton's Method for Overdetermined Systems of Equations, Math. Comput. 69 (1999) 1099–1115.

[105] J.J. Moré, The Levenberg-Marquardt algorithm: Implementation and theory,

(2006) 105–116. https://doi.org/10.1007/bfb0067700.

[106] M. Hassan, A. Khajepour, Analysis of bounded cable tensions in cable-actuated parallel manipulators, IEEE Trans. Robot. (2011). https://doi.org/10.1109/TRO.2011.2158693.

[107] C. GOSSELIN, Cable-driven parallel mechanisms: state of the art and perspectives, Mech. Eng. Rev. (2014). https://doi.org/10.1299/mer.2014dsm0004.

[108] S. Qian, B. Zi, W.W. Shang, Q.S. Xu, A review on cable-driven parallel robots, Chinese J. Mech. Eng. (English Ed. (2018). https://doi.org/10.1186/s10033-018-0267-9.

[109] M. Carricato, J.P. Merlet, Stability analysis of underconstrained cable-driven parallel robots, IEEE Trans. Robot. (2013). https://doi.org/10.1109/TRO.2012.2217795.

[110] Yang, Yang, Chen, Wang, Zhang, Fang, Zheng, Wang, Study on Stiffness-Oriented Cable Tension Distribution for a Symmetrical Cable-Driven Mechanism, Symmetry (Basel). (2019). https://doi.org/10.3390/sym11091158.

[111] S. Zhang, D. Cao, B. Hou, S. Li, H. Min, X. Zhang, Analysis on variable stiffness of a cable-driven parallel–series hybrid joint toward wheelchair-mounted robotic manipulator, Adv. Mech. Eng. (2019). https://doi.org/10.1177/1687814019846289.

[112] C.B. Pham, S.H. Yeo, G. Yang, Tension analysis of cable-driven parallel mechanisms, in: 2005 IEEE/RSJ Int. Conf. Intell. Robot. Syst. IROS, 2005. https://doi.org/10.1109/IROS.2005.1545368.

[113] G. Yang, C.B. Pham, S.H. Yeo, Workspace performance optimization of fully restrained cable-driven parallel manipulators, IEEE Int. Conf. Intell. Robot. Syst. (2006) 85–90. https://doi.org/10.1109/IROS.2006.281747.

[114] C. Ericson, Real-Time Collision Detection, 2005. https://doi.org/10.1007/s13398-014-0173-7.2.

[115] R. Meziane, P. Li, M.J.D. Otis, H. Ezzaidi, P. Cardou, Safer hybrid workspace using human-robot interaction while sharing production activities, in: ROSE 2014 - 2014 IEEE Int. Symp. Robot. SEnsors Environ. Proc., 2014. https://doi.org/10.1109/ROSE.2014.6952980.

[116] G. Bellusci, F. Dijkstra, P. Slycke, Xsens MTw : Miniature Wireless Inertial Motion Tracker for Highly Accurate 3D Kinematic Applications, Xsens Technol. (2013).

[117] M. Garcia-Salguero, J. Gonzalez-Jimenez, F.A. Moreno, Human 3D pose estimation with a tilting camera for social mobile robot interaction, Sensors (Switzerland). (2019). https://doi.org/10.3390/s19224943.

[118] S. Sankar, C.-Y. Tsai, ROS-Based Human Detection and Tracking from a Wireless Controlled Mobile Robot Using Kinect, Appl. Syst. Innov. (2019). https://doi.org/10.3390/asi2010005.

[119] G. Nagymáté, R.M. Kiss, Application of OptiTrack motion capture systems in human movement analysis A systematic literature review, Recent Innov. Mechatronics. (2018). https://doi.org/10.17667/riim.2018.1/13.

[120] T. Xu, M. Chen, M. Xie, E. Wu, A Skinning Method in Real-time Skeletal Character Animation, Int. J. Virtual Real. (2011). https://doi.org/10.20870/ijvr.2011.10.3.2818.

[121] I. Baran, J. Popović, Automatic rigging and animation of 3D characters, ACM Trans. Graph. (2007). https://doi.org/10.1145/1276377.1276467.

[122] M. Gouttefarde, J.-P. Merlet, D. Daney, Determination of the wrench-closure workspace of 6-DOF parallel cable-driven mechanisms, in: Adv. Robot Kinemat., 2006. https://doi.org/10.1007/978-1-4020-4941-5_34.

[123] X. Diao, M. Ou, Workspace analysis of a 6-DOF cable robot for hardware-in-the-loop dynamic simulation, in: IEEE Int. Conf. Intell. Robot. Syst., 2006. https://doi.org/10.1109/IROS.2006.281876.

[124] J.P. Merlet, Parallel robots, Solid Mech. Its Appl. (2006). https://doi.org/10.1007/978-3-319-72911-4_6.

[125] Q.J. Duan, X. Duan, Workspace classification and quantification calculations of cable-driven parallel robots, Adv. Mech. Eng. (2014). https://doi.org/10.1155/2014/358727.

[126] A.T. Riechel, I. Ebert-Uphoff, Force-Feasible Workspace analysis for underconstrained, point-mass cable robots, in: Proc. - IEEE Int. Conf. Robot. Autom., 2004. https://doi.org/10.1109/robot.2004.1302503.

[127] M. Gouttefarde, C.M. Gosselin, Wrench-closure workspace of six-dof parallel mechanisms driven by 7 cables, in: Trans. Can. Soc. Mech. Eng., 2005.

https://doi.org/10.1139/tcsme-2005-0034.

[128] M. Gouttefarde, J.P. Merlet, D. Daney, Wrench-feasible workspace of parallel cable-driven mechanisms, Proc. - IEEE Int. Conf. Robot. Autom. (2007) 1492–1497. https://doi.org/10.1109/ROBOT.2007.363195.

[129] G. Barrette, C.M. Gosselin, Kinematic analysis and design of planar parallel mechanism actuated with cables, in: ASME Des. Eng. Tech. Conf., 2000.

[130] S. Rezazadeh, S. Behzadipour, Workspace analysis of multibody cable-driven mechanisms, J. Mech. Robot. (2011). https://doi.org/10.1115/1.4003581.

[131] L. Gagliardini, M. Gouttefarde, S. Caro, Determination of a Dynamic Feasible Workspace for Cable-Driven Parallel Robots, in: 2018. https://doi.org/10.1007/978-3-319-56802-7_38.

[132] H. Hong, J. Ali, L. Ren, A review on topological architecture and design methods of cable-driven mechanism, Adv. Mech. Eng. (2018). https://doi.org/10.1177/1687814018774186.

[133] M.A. Carpio-Aleman, R.J. Saltaren-Pasmino, A. Rodriguez, G.A. Portilla, J.S. Cely, N.X. Gonzalez-Alvarez, J.M. Castillo-Guerrero, Collision and tension analysis of cable-driven parallel robot for positioning and orientation, in: 2018 IEEE Int. Autumn Meet. Power, Electron. Comput. ROPEC 2018, 2019. https://doi.org/10.1109/ROPEC.2018.8661464.

[134] W.J. Shiang, D. Cannon, J. Gorman, Dynamic analysis of the cable array robotic crane, Proc. - IEEE Int. Conf. Robot. Autom. (1999).

https://doi.org/10.1109/robot.1999.773972.

[135] H. Jamshidifar, A. Khajepour, B. Fidan, M. Rushton, Kinematically-Constrained Redundant Cable-Driven Parallel Robots: Modeling, Redundancy Analysis, and Stiffness Optimization, IEEE/ASME Trans. Mechatronics. (2017). https://doi.org/10.1109/TMECH.2016.2639053.

[136] S. Perreault, P. Cardou, C. Gosselin, Approximate static balancing of a planar parallel cable-driven mechanism based on four-bar linkages and springs, Mech. Mach. Theory. (2014). https://doi.org/10.1016/j.mechmachtheory.2014.04.008.

[137] S.R. Oh, S.K. Agrawal, Cable suspended planar robots with redundant cables: Controllers with positive tensions, IEEE Trans. Robot. (2005). https://doi.org/10.1109/TRO.2004.838029.

[138] K. Azizian, P. Cardou, The Dimensional Synthesis of Planar Parallel Cable-Driven Mechanisms Through Convex Relaxations, J. Mech. Robot. (2012). https://doi.org/10.1115/1.4006952.

[139] W.J. Shiang, D. Cannon, J. Gorman, Optimal force distribution applied to a robotic crane with flexible cables, in: Proc. - IEEE Int. Conf. Robot. Autom., 2000. https://doi.org/10.1109/robot.2000.844880.

[140] T. Reichenbach, P. Tempel, A. Verl, A. Pott, On Kinetostatics and Workspace Analysis of Multi-platform Cable-Driven Parallel Robots with Unlimited Rotation, in: Mech. Mach. Sci., 2020. https://doi.org/10.1007/978-3-030-30036-4_7.

[141] A. Pott, T. Bruckmann, L. Mikelsons, Closed-form force distribution for parallel

wire robots, in: Proc. 5th Int. Work. Comput. Kinemat., 2009. https://doi.org/10.1007/978-3-642-01947-0_4.

[142] T. Bruckmann, A. Pott, M. Hiller, Calculating force distributions for redundantly actuated tendon-based Stewart platforms, in: Adv. Robot Kinemat., 2006. https://doi.org/10.1007/978-1-4020-4941-5_44.

[143] D.Q. Nguyen, M. Gouttefarde, O. Company, F. Pierrot, On The analysis of large-dimension reconfigurable suspended cable-driven parallel robots, in: Proc. - IEEE Int. Conf. Robot. Autom., 2014. https://doi.org/10.1109/ICRA.2014.6907701.

[144] B. Ouyang, W. Shang, Rapid optimization of tension distribution for cable-driven parallel manipulators with redundant cables, Chinese J. Mech. Eng. (English Ed. (2016). https://doi.org/10.3901/CJME.2015.1120.137.

[145] S. Abdelaziz, L. Barbé, P. Renaud, M. de Mathelin, B. Bayle, Control of cable-driven manipulators in the presence of friction, Mech. Mach. Theory. (2017). https://doi.org/10.1016/j.mechmachtheory.2016.09.014.

[146] R. Verhoeven, Analysis of the Workspace of Tendon-based Stewart Platforms, Thesis. (2004).

[147] Parallel Manipulators, New Developments, 2012. https://doi.org/10.5772/58.

[148] J.T. Bryson, X. Jin, S.K. Agrawal, Optimal design of cable-driven manipulators using particle swarm optimization, J. Mech. Robot. (2016). https://doi.org/10.1115/1.4032103.

[149] D. Song, L. Zhang, F. Xue, Configuration Optimization and a Tension Distribution

Algorithm for Cable-Driven Parallel Robots, IEEE Access. (2018). https://doi.org/10.1109/ACCESS.2018.2841988.

[150] Y. Su, Y. Qiu, P. Liu, The continuity and real-time performance of the cable tension determining for a suspend cable-driven parallel camera robot, Adv. Robot. (2015). https://doi.org/10.1080/01691864.2015.1014417.

[151] C. Passarini, D. Zanotto, G. Boschetti, Dynamic trajectory planning for failure recovery in cable-suspended camera systems, J. Mech. Robot. (2019). https://doi.org/10.1115/1.4041942.

Appendix "A"

For all the trajectories, the height of the end effector's center of mass is 4 m and the three orientation angles are zero.

Circular trajectory:

time	X	Y	time	X	Y	time	X	Y	time	X	Y	time	X	Y
0.1	3	3.5	4.1	3.4	3.99	8.1	3.8	3.9	12.1	3.8	3.1	16.1	3.4	3.01
0.2	3.01	3.599	4.2	3.41	3.992	8.2	3.81	3.892	12.2	3.79	3.093	16.2	3.39	3.012
0.3	3.02	3.64	4.3	3.42	3.994	8.3	3.82	3.884	12.3	3.78	3.086	16.3	3.38	3.015
0.4	3.03	3.671	4.4	3.43	3.995	8.4	3.83	3.876	12.4	3.77	3.079	16.4	3.37	3.017
0.5	3.04	3.696	4.5	3.44	3.996	8.5	3.84	3.867	12.5	3.76	3.073	16.5	3.36	3.02
0.6	3.05	3.718	4.6	3.45	3.997	8.6	3.85	3.857	12.6	3.75	3.067	16.6	3.35	3.023
0.7	3.06	3.737	4.7	3.46	3.998	8.7	3.86	3.847	12.7	3.74	3.061	16.7	3.34	3.026
0.8	3.07	3.755	4.8	3.47	3.999	8.8	3.87	3.836	12.8	3.73	3.056	16.8	3.33	3.03
0.9	3.08	3.771	4.9	3.48	4	8.9	3.88	3.825	12.9	3.72	3.051	16.9	3.32	3.034
1	3.09	3.786	5	3.49	4	9	3.89	3.813	13	3.71	3.046	17	3.31	3.038
1.1	3.1	3.8	5.1	3.5	4	9.1	3.9	3.8	13.1	3.7	3.042	17.1	3.3	3.042
1.2	3.11	3.813	5.2	3.51	4	9.2	3.91	3.786	13.2	3.69	3.038	17.2	3.29	3.046
1.3	3.12	3.825	5.3	3.52	4	9.3	3.92	3.771	13.3	3.68	3.034	17.3	3.28	3.051
1.4	3.13	3.836	5.4	3.53	3.999	9.4	3.93	3.755	13.4	3.67	3.03	17.4	3.27	3.056
1.5	3.14	3.847	5.5	3.54	3.998	9.5	3.94	3.737	13.5	3.66	3.026	17.5	3.26	3.061
1.6	3.15	3.857	5.6	3.55	3.997	9.6	3.95	3.718	13.6	3.65	3.023	17.6	3.25	3.067
1.7	3.16	3.867	5.7	3.56	3.996	9.7	3.96	3.696	13.7	3.64	3.02	17.7	3.24	3.073
1.8	3.17	3.876	5.8	3.57	3.995	9.8	3.97	3.671	13.8	3.63	3.017	17.8	3.23	3.079
1.9	3.18	3.884	5.9	3.58	3.994	9.9	3.98	3.64	13.9	3.62	3.015	17.9	3.22	3.086
2	3.19	3.892	6	3.59	3.992	10	3.99	3.599	14	3.61	3.012	18	3.21	3.093
2.1	3.2	3.9	6.1	3.6	3.99	10.1	4	3.5	14.1	3.6	3.01	18.1	3.2	3.1
2.2	3.21	3.907	6.2	3.61	3.988	10.2	3.99	3.401	14.2	3.59	3.008	18.2	3.19	3.108
2.3	3.22	3.914	6.3	3.62	3.985	10.3	3.98	3.36	14.3	3.58	3.006	18.3	3.18	3.116
2.4	3.23	3.921	6.4	3.63	3.983	10.4	3.97	3.329	14.4	3.57	3.005	18.4	3.17	3.124
2.5	3.24	3.927	6.5	3.64	3.98	10.5	3.96	3.304	14.5	3.56	3.004	18.5	3.16	3.133
2.6	3.25	3.933	6.6	3.65	3.977	10.6	3.95	3.282	14.6	3.55	3.003	18.6	3.15	3.143
2.7	3.26	3.939	6.7	3.66	3.974	10.7	3.94	3.263	14.7	3.54	3.002	18.7	3.14	3.153
2.8	3.27	3.944	6.8	3.67	3.97	10.8	3.93	3.245	14.8	3.53	3.001	18.8	3.13	3.164
2.9	3.28	3.949	6.9	3.68	3.966	10.9	3.92	3.229	14.9	3.52	3	18.9	3.12	3.175
3	3.29	3.954	7	3.69	3.962	11	3.91	3.214	15	3.51	3	19	3.11	3.187
3.1	3.3	3.958	7.1	3.7	3.958	11.1	3.9	3.2	15.1	3.5	3	19.1	3.1	3.2
3.2	3.31	3.962	7.2	3.71	3.954	11.2	3.89	3.187	15.2	3.49	3	19.2	3.09	3.214
3.3	3.32	3.966	7.3	3.72	3.949	11.3	3.88	3.175	15.3	3.48	3	19.3	3.08	3.229
3.4	3.33	3.97	7.4	3.73	3.944	11.4	3.87	3.164	15.4	3.47	3.001	19.4	3.07	3.245
3.5	3.34	3.974	7.5	3.74	3.939	11.5	3.86	3.153	15.5	3.46	3.002	19.5	3.06	3.263
3.6	3.35	3.977	7.6	3.75	3.933	11.6	3.85	3.143	15.6	3.45	3.003	19.6	3.05	3.282
3.7	3.36	3.98	7.7	3.76	3.927	11.7	3.84	3.133	15.7	3.44	3.004	19.7	3.04	3.304
3.8	3.37	3.983	7.8	3.77	3.921	11.8	3.83	3.124	15.8	3.43	3.005	19.8	3.03	3.329
3.9	3.38	3.985	7.9	3.78	3.914	11.9	3.82	3.116	15.9	3.42	3.006	19.9	3.02	3.36
4	3.39	3.988	8	3.79	3.907	12	3.81	3.108	16	3.41	3.008	20	3.01	3.401

Sinusoidal trajectory:

time	X	Y	time	X	Y	time	X	Y	time	X	Y	time	X	Y
0.1	3.5	3	4.1	5.1	4.5	8.1	4.3	3.47	12.1	2.7	4.06	16.1	1.9	3
0.2	3.54	3.19	4.2	5.14	4.48	8.2	4.26	3.49	12.2	2.66	4.08	16.2	1.94	2.83
0.3	3.58	3.4	4.3	5.18	4.41	8.3	4.22	3.5	12.3	2.62	4.09	16.3	1.98	2.69
0.4	3.62	3.6	4.4	5.22	4.31	8.4	4.18	3.52	12.4	2.58	4.11	16.4	2.02	2.59
0.5	3.66	3.81	4.5	5.26	4.17	8.5	4.14	3.53	12.5	2.54	4.12	16.5	2.06	2.52
0.6	3.7	4	4.6	5.3	4	8.6	4.1	3.55	12.6	2.5	4.14	16.6	2.1	2.5
0.7	3.74	4.17	4.7	5.34	3.81	8.7	4.06	3.56	12.7	2.46	4.15	16.7	2.14	2.52
0.8	3.78	4.31	4.8	5.38	3.6	8.8	4.02	3.58	12.8	2.42	4.17	16.8	2.18	2.59
0.9	3.82	4.41	4.9	5.42	3.4	8.9	3.98	3.59	12.9	2.38	4.18	16.9	2.22	2.69
1	3.86	4.48	5	5.46	3.19	9	3.94	3.6	13	2.34	4.2	17	2.26	2.83
1.1	3.9	4.5	5.1	5.5	3	9.1	3.9	3.62	13.1	2.3	4.21	17.1	2.3	3
1.2	3.94	4.48	5.2	5.46	3.04	9.2	3.86	3.63	13.2	2.26	4.23	17.2	2.34	3.19
1.3	3.98	4.41	5.3	5.42	3.06	9.3	3.82	3.65	13.3	2.22	4.24	17.3	2.38	3.4
1.4	4.02	4.31	5.4	5.38	3.07	9.4	3.78	3.66	13.4	2.18	4.26	17.4	2.42	3.6
1.5	4.06	4.17	5.5	5.34	3.09	9.5	3.74	3.68	13.5	2.14	4.27	17.5	2.46	3.81
1.6	4.1	4	5.6	5.3	3.1	9.6	3.7	3.69	13.6	2.1	4.29	17.6	2.5	4
1.7	4.14	3.81	5.7	5.26	3.12	9.7	3.66	3.71	13.7	2.06	4.3	17.7	2.54	4.17
1.8	4.18	3.6	5.8	5.22	3.13	9.8	3.62	3.72	13.8	2.02	4.32	17.8	2.58	4.31
1.9	4.22	3.4	5.9	5.18	3.15	9.9	3.58	3.74	13.9	1.98	4.33	17.9	2.62	4.41
2	4.26	3.19	6	5.14	3.16	10	3.54	3.75	14	1.94	4.34	18	2.66	4.48
2.1	4.3	3	6.1	5.1	3.18	10.1	3.5	3.77	14.1	1.9	4.36	18.1	2.7	4.5
2.2	4.34	2.83	6.2	5.06	3.19	10.2	3.46	3.78	14.2	1.86	4.37	18.2	2.74	4.48
2.3	4.38	2.69	6.3	5.02	3.21	10.3	3.42	3.8	14.3	1.82	4.39	18.3	2.78	4.41
2.4	4.42	2.59	6.4	4.98	3.22	10.4	3.38	3.81	14.4	1.78	4.4	18.4	2.82	4.31
2.5	4.46	2.52	6.5	4.94	3.23	10.5	3.34	3.83	14.5	1.74	4.42	18.5	2.86	4.17
2.6	4.5	2.5	6.6	4.9	3.25	10.6	3.3	3.84	14.6	1.7	4.43	18.6	2.9	4
2.7	4.54	2.52	6.7	4.86	3.26	10.7	3.26	3.86	14.7	1.66	4.45	18.7	2.94	3.81
2.8	4.58	2.59	6.8	4.82	3.28	10.8	3.22	3.87	14.8	1.62	4.46	18.8	2.98	3.6
2.9	4.62	2.69	6.9	4.78	3.29	10.9	3.18	3.89	14.9	1.58	4.48	18.9	3.02	3.4
3	4.66	2.83	7	4.74	3.31	11	3.14	3.9	15	1.54	4.49	19	3.06	3.19
3.1	4.7	3	7.1	4.7	3.32	11.1	3.1	3.92	15.1	1.5	4.51	19.1	3.1	3
3.2	4.74	3.19	7.2	4.66	3.34	11.2	3.06	3.93	15.2	1.54	4.48	19.2	3.14	2.83
3.3	4.78	3.4	7.3	4.62	3.35	11.3	3.02	3.95	15.3	1.58	4.41	19.3	3.18	2.69
3.4	4.82	3.6	7.4	4.58	3.37	11.4	2.98	3.96	15.4	1.62	4.31	19.4	3.22	2.59
3.5	4.86	3.81	7.5	4.54	3.38	11.5	2.94	3.97	15.5	1.66	4.17	19.5	3.26	2.52
3.6	4.9	4	7.6	4.5	3.4	11.6	2.9	3.99	15.6	1.7	4	19.6	3.3	2.5
3.7	4.94	4.17	7.7	4.46	3.41	11.7	2.86	4	15.7	1.74	3.81	19.7	3.34	2.52
3.8	4.98	4.31	7.8	4.42	3.43	11.8	2.82	4.02	15.8	1.78	3.6	19.8	3.38	2.59
3.9	5.02	4.41	7.9	4.38	3.44	11.9	2.78	4.03	15.9	1.82	3.4	19.9	3.42	2.69
4	5.06	4.48	8	4.34	3.46	12	2.74	4.05	16	1.86	3.19	20	3.46	2.83

Random trajectory:

time	X	Y	time	X	Y	time	X	Y	time	X	Y	time	X	Y
0.1	4.56	4.3	4.1	3.28	2.05	8.1	2.6	2.52	12.1	1.98	2.9	16.1	3.84	3.39
0.2	4.58	4.38	4.2	3.37	2.06	8.2	2.78	2.77	12.2	2.14	2.83	16.2	3.68	3.34
0.3	4.59	4.47	4.3	3.46	2.06	8.3	2.96	3.01	12.3	2.31	2.76	16.3	3.52	3.29
0.4	4.6	4.55	4.4	3.55	2.07	8.4	3.14	3.26	12.4	2.48	2.7	16.4	3.36	3.23
0.5	4.61	4.64	4.5	3.64	2.07	8.5	3.32	3.51	12.5	2.65	2.63	16.5	3.2	3.18
0.6	4.63	4.72	4.6	3.73	2.08	8.6	3.5	3.76	12.6	2.82	2.56	16.6	3.04	3.12
0.7	4.64	4.81	4.7	3.82	2.08	8.7	3.68	4.01	12.7	2.99	2.49	16.7	2.88	3.07
0.8	4.65	4.89	4.8	3.91	2.09	8.8	3.86	4.26	12.8	3.16	2.42	16.8	2.72	3.01
0.9	4.67	4.98	4.9	4	2.09	8.9	4.04	4.51	12.9	3.32	2.35	16.9	2.56	2.96
1	4.68	5.06	5	4.09	2.1	9	4.22	4.76	13	3.49	2.29	17	2.4	2.91
1.1	4.68	5.06	5.1	4.09	2.1	9.1	4.22	4.76	13.1	3.49	2.29	17.1	2.4	2.91
1.2	4.41	5.09	5.2	4.11	2.15	9.2	4.21	4.5	13.2	3.7	2.31	17.2	2.63	3.12
1.3	4.14	5.12	5.3	4.14	2.19	9.3	4.2	4.25	13.3	3.9	2.33	17.3	2.86	3.33
1.4	3.87	5.15	5.4	4.17	2.24	9.4	4.19	4	13.4	4.11	2.36	17.4	3.1	3.55
1.5	3.6	5.19	5.5	4.2	2.29	9.5	4.18	3.74	13.5	4.31	2.38	17.5	3.33	3.76
1.6	3.33	5.22	5.6	4.23	2.34	9.6	4.16	3.49	13.6	4.52	2.41	17.6	3.57	3.97
1.7	3.06	5.25	5.7	4.25	2.39	9.7	4.15	3.24	13.7	4.72	2.43	17.7	3.8	4.18
1.8	2.79	5.28	5.8	4.28	2.43	9.8	4.14	2.98	13.8	4.93	2.46	17.8	4.04	4.4
1.9	2.52	5.31	5.9	4.31	2.48	9.9	4.13	2.73	13.9	5.13	2.48	17.9	4.27	4.61
2	2.25	5.34	6	4.34	2.53	10	4.12	2.47	14	5.34	2.5	18	4.51	4.82
2.1	2.25	5.34	6.1	4.34	2.53	10.1	4.12	2.47	14.1	5.34	2.5	18.1	4.51	4.82
2.2	2.38	5.15	6.2	4.36	2.79	10.2	3.9	2.78	14.2	5.06	2.67	18.2	4.28	4.71
2.3	2.52	4.97	6.3	4.38	3.05	10.3	3.68	3.08	14.3	4.79	2.83	18.3	4.06	4.61
2.4	2.65	4.79	6.4	4.4	3.31	10.4	3.46	3.39	14.4	4.51	2.99	18.4	3.84	4.5
2.5	2.79	4.6	6.5	4.42	3.57	10.5	3.24	3.69	14.5	4.24	3.15	18.5	3.62	4.39
2.6	2.92	4.42	6.6	4.44	3.83	10.6	3.03	4	14.6	3.96	3.32	18.6	3.4	4.28
2.7	3.06	4.24	6.7	4.46	4.09	10.7	2.81	4.3	14.7	3.69	3.48	18.7	3.18	4.17
2.8	3.19	4.06	6.8	4.48	4.34	10.8	2.59	4.61	14.8	3.41	3.64	18.8	2.96	4.06
2.9	3.32	3.87	6.9	4.5	4.6	10.9	2.37	4.91	14.9	3.14	3.8	18.9	2.74	3.95
3	3.46	3.69	7	4.52	4.86	11	2.15	5.22	15	2.86	3.96	19	2.52	3.84
3.1	3.46	3.69	7.1	4.52	4.86	11.1	2.15	5.22	15.1	2.86	3.96	19.1	2.52	3.84
3.2	3.44	3.51	7.2	4.31	4.6	11.2	2.13	4.96	15.2	2.97	3.9	19.2	2.63	3.83
3.3	3.42	3.33	7.3	4.09	4.34	11.3	2.11	4.7	15.3	3.08	3.84	19.3	2.74	3.81
3.4	3.4	3.14	7.4	3.88	4.08	11.4	2.09	4.44	15.4	3.19	3.77	19.4	2.85	3.79
3.5	3.38	2.96	7.5	3.67	3.82	11.5	2.07	4.19	15.5	3.3	3.71	19.5	2.97	3.78
3.6	3.36	2.78	7.6	3.46	3.56	11.6	2.05	3.93	15.6	3.41	3.65	19.6	3.08	3.76
3.7	3.34	2.6	7.7	3.24	3.3	11.7	2.03	3.67	15.7	3.51	3.58	19.7	3.19	3.75
3.8	3.32	2.42	7.8	3.03	3.04	11.8	2.01	3.41	15.8	3.62	3.52	19.8	3.3	3.73
3.9	3.3	2.24	7.9	2.82	2.78	11.9	2	3.16	15.9	3.73	3.46	19.9	3.41	3.71
4	3.28	2.05	8	2.6	2.52	12	1.98	2.9	16	3.84	3.39	20	3.52	3.7

Appendix “B”

Photo permissions:

[1] Figure 2:

Dear Khaled,

thank you for your email. You may use the picture in your these with proper reference in the caption, e.g. "Courtesy of Andreas Pott" followed by a citation to my book with your reference style.

I really acknowledge your efforts to make proper citation of other works. I found a large number of copies of my figures without reference and permission.

Best regards

Andreas

-----Ursprüngliche Nachricht-----
Von: Khaled Mohamed Youssef [mailto:khaled-mohamed.youssef1@uqac.ca]
Gesendet: Montag, 24. Februar 2020 20:07
An: Pott, Andreas <andreas.pott@isw.uni-stuttgart.de>
Betreff: CDPR photo permission

Dear Prof. Pott,

My name is Khaled Youssef. I am a ph.D candidate in the deprtament of applied science at university of Quebec in Chicoutimi (Canada) under the supervision of Prof. Martin Otis.
I would like to ask you if it is possible that I include the attached photo where i quaoted from your book "Cable-driven parallel robots: Theory and application" in my ph.D thesis . Of course, the proper citation will be be added to the reffrences.

In case you agree, please let me know the appropriate citation for the photo.

Thank you very much

Khaled

[2] Figure 4:

Hi Khaled,

Sure, no problem!

- Philippe

-----Original Message-----
From: Khaled Mohamed Youssef <khaled-mohamed.youssef1@uqac.ca>
Sent: February 7, 2020 12:13 PM
To: Philippe Cardou <Philippe.Cardou@gmc.ulaval.ca>
Subject: CDPM at ulaval

[Externe UL*]

Hello Prof. Philippe,

i am just wondering if I can take a photo for the cable driven robot at Ulaval to include it in my phD thesis as an example for real application?

Thanks

Khaled
*ATTENTION : L'émetteur de ce courriel est externe à l'Université Laval.
Évitez de cliquer sur un hyperlien, d'ouvrir une pièce jointe ou de transmettre des informations si vous ne connaissez pas l'expéditeur du courriel. En cas de doute, contactez l'équipe de soutien informatique de votre unité ou hameconnage@ulaval.ca.
_____

[3] Figure 5:

Dear Khaled,

Yes, I agree, thank you for your interest in this research work.

Please, cite the following two papers:

T. Dallej, *M. Gouttefarde*, N. Andreff, P.-E. Hervé, P. Martinet, "Modeling and vision-based control of large-dimension cable-driven parallel robots using a multiple-camera setup," Mechatronics, Vol. 61, pp. 20-36, 2019.

M. Gouttefarde, J. F. Collard, N. Riehl, C. Baradat, "Geometry Selection of a Redundantly Actuated Cable-Suspended Parallel Robot," IEEE Transactions on Robotics, Vol. 31, No. 2, pp. 501-510, 2015.

Best regards

Marc

Le 13/02/2020 à 21:52, Khaled Mohamed Youssef a écrit :

Dear Prof. Marc,

My name is Khaled Youssef. I am a ph.D candidate in the deprtament of applied science at university of Quebec in Chicoutimi under the supervision of Prof. Martin Otis.

I would like to ask you if it is possible that I include the attached photo in my ph.D thesis as a real application of cable driven mechanism. Of course, the proper citation will be be added to the reffrences.

In case you agree, please let me know the appropriate citation for the photo.

Thank you very much

Khaled
--
.....
Marc Gouttefarde
CNRS - LIRMM Robotics Dpt
tel: +33 4 67 41 85 59
fax: +33 4 67 41 85 00
https://www.lirmm.fr/users/utilisateurs-lirmm/marc-gouttefarde

[4] Figure 6:

Dear Khaled,

Thank you very much asking!

This photo has essentially been in public domain, so it is only subjected to similar restriction as those from NASA or NRAO of US, i.e., most of non-commercial usage are allowed. So a simple statement like "produced by the FAST team" would suffice.

That being said, I'd really appreciate if you can cite the following two papers

Li, D.*, Wang, Pei, Qian, Lei, Krco, Marko, Dunning, Alex, Jiang, Peng, Yue, Youling, Jin, Chenjin, Zhu, Yan, Pan, Zhichen, Nan, Rendong 2018, “FAST in Space: Considerations for a Multi-beam Multi-purpose Survey with FAST”, IEEE Microwave, Vol. 19, Issue 3, p112-119 (arxiv:1802.03709)

Nan, R, Li, D., Jin, C., Wang, Q., Zhu, L., Zhu, W., Zhang, H., Yue, Y. & Qian, L. 2011, “THE FIVE-HUNDRED-METER APERTURE SPHERICAL RADIO TELESCOPE (FAST) PROJECT”, International Journal of Modern Physics D, Volume No.20, Issue No. 6 (arXiv:1105.3794)

They contain overall project description and similar but not identical images.

Good luck with your dissertation!

best,
Di

--

此致
敬礼！

李菂

==========
Chief Scientist, Radio Division
National Astronomical Observatories of China;
FAST Operation Center
==========

> -----Original Messages-----

> From: "Khaled Mohamed Youssef" <khaled-mohamed.youssef1@uqac.ca>
> Sent Time: 2020-02-14 05:09:28 (Friday)
> To: "dili@nao.cas.cn" <dili@nao.cas.cn>
> Cc:
> Subject: FW: Cogiro photo permission
>
> Dear Prof. Dili,
>
> My name is Khaled Youssef. I am a ph.D candidate in the deprtament of applied science at university of Quebec in Chicoutimi under the supervision of Prof. Martin Otis.
>
> I would like to ask you if it is possible that I include the attached photo in my ph.D thesis as a real application of cable driven mechanism. Of course, the proper citation will be be added to the reffrences.
>
> In case you agree, please let me know the appropriate citation for the photo.
>
> Thank you very much
>
> Khaled